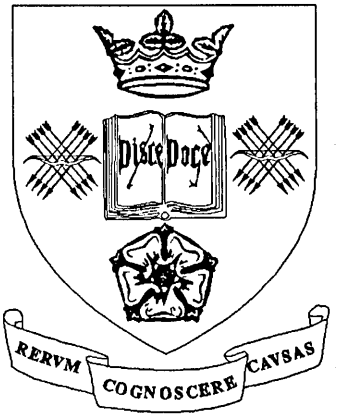

Modelling and Control of a Twin Rotor MIMO System

by

Sarvat Mushtaq Ahmad B

A thesis submitted to the University of Sheffield for the degree of
Doctor of Philosophy

Department of Automatic Control and Systems Engineering
The University of Sheffield
Mappin Street
Sheffield, S1 3JD
UK

February 2001

Department of
AUTOMATIC
CONTROL
and SYSTEMS
ENGINEERING
UNIVERSITY of SHEFFIELD

ABSTRACT

In this research, a laboratory platform which has 2 degrees of freedom (DOF), the Twin Rotor MIMO System (TRMS), is investigated. Although, the TRMS does not fly, it has a striking similarity with a helicopter, such as system nonlinearities and cross-coupled modes. Therefore, the TRMS can be perceived as an unconventional and complex "air vehicle" that poses formidable challenges in modelling, control design and analysis and implementation. These issues are the subject of this work.

The linear models for 1 and 2 DOFs are obtained via system identification techniques. Such a black-box modelling approach yields input-output models with neither *a priori* defined model *structure* nor specific *parameter* settings reflecting any physical attributes. Further, a nonlinear model using Radial Basis Function networks is obtained. Such a high fidelity nonlinear model is often required for nonlinear system simulation studies and is commonly employed in the aerospace industry. Modelling exercises were conducted that included rigid as well as flexible modes of the system. The approach presented here is shown to be suitable for modelling complex new generation air vehicles.

Modelling of the TRMS revealed the presence of resonant system modes which are responsible for inducing unwanted vibrations. In this research, open-loop, closed-loop and combined open and closed-loop control strategies are investigated to address this problem. Initially, open-loop control techniques based on "input shaping control" are employed. Digital filters are then developed to shape the command signals such that the resonance modes are not overly excited. The effectiveness of this concept is then demonstrated on the TRMS rig for both 1 and 2 DOF motion, with a significant reduction in vibration.

The linear model for the 1 DOF (SISO) TRMS was found to have the non-minimum phase characteristics and have 4 states with only pitch angle output. This behaviour imposes certain limitations on the type of control topologies one can adopt. The LQG approach, which has an elegant structure with an embedded Kalman filter to estimate the unmeasured states, is adopted in this study.

The identified linear model is employed in the design of a feedback LQG compensator for the TRMS with 1 DOF. This is shown to have good tracking capability but requires high control effort and has inadequate authority over residual vibration of the system. These problems are resolved by further augmenting the system with a command path prefilter. The combined feedforward and feedback compensator satisfies the performance objectives and obeys the constraint on the actuator. Finally, 1 DOF controller is implemented on the laboratory platform.

Acknowledgements

I gratefully acknowledges the financial support of the University of Sheffield and the Department of Automatic Control and Systems Engineering, which made this study feasible.

This thesis was made possible because of few people who command acknowledgement foremost, they are, my family, Prof. P. Fleming, Andy (my supervisor) and Dr. O. Tokhi. I thank all of them for their support, advice, supervision and patience. Special thanks goes to Prof. Fleming for his timely support, encouragement and continual expert advises on research matters, from which I benefited immensely. I appreciate and thank Andy for his excellent supervision and friendly approach. His guidance and help at every stage of my work, kept me motivated and focused on my research objectives. I was fortunate to indulge in lengthy technical discussions with Dr. Tokhi, which ultimately culminated into realisation of research ideas. I am obliged to him for his patience, compassion and help in publishing research papers.

I would also like to thank Dr. H. A. Thompson, Manager, Rolls-Royce (UTC, the University of Sheffield), for many valuable comments on helicopter dynamics. Thanks are also due to Prof. S. Billings and Dr. Zi-Qiang Lang for useful discussions on linear and nonlinear system identification.

Craig Bacon provided technical support for the rig along with Stan and Roger. The departmental staff - Mr. Alex Price, Ms. A. Kisby, Mrs. C. A. Spurr and Mrs. A. N. Meah helped much in planning my visits to various conferences, again with the generous support of the Department, Andy and Dr. Tokhi. Not to be missed are Mike Bluet, Tony and Ian Durkaz for their help with the MATLAB. A big thanks to all of them.

I also benefited from many academic discussions, presentation and lively time with my friends and colleagues in A14, B20 and C13: Val, Katya, Wael, Steve, Daniela (all PhD holders now), Edin, Hasan, Othman, Yudi, Dong, Beatrice, Hisham, Sadaat, Dr. M. Abbod, Zahruddin, Ibrahim, Anjan and Siddique. Thanks to all of them for creating a serious yet relaxed research environment.

Now, the ones who kept me ticking, my nephew and niece. The memories of their sweet talk and innocent charm would often boost my sagging energy supplies.

Finally, a very-very deep thanks to my brothers, sisters and brother-in-law for their unflinching and unswerving support during my stay in the UK, while they braved countless upheavals back home. They were equal partners in my father's prolonged battle against cancer, to which he succumbed ultimately. This work, therefore, truly belongs to them and my parents.

to my family

Contents

Chapter 5 Nonlinear modelling of a 1 DOF TRMS using radial basis function networks

Chapter 6 Control law development for a 1 DOF TRMS

Chapter 1

Introduction

1.1 Background

In recent years there has been a phenomenal interest in unmanned aerial vehicles or UAVs. "Unmanned" simply means that a human is not aboard actively piloting or directing the aircraft. The control functions are either indigenous (on board computer), or off-board (computer or remote pilot). There are a broad spectrum of UAVs, differing in size, type, capabilities and complexity. They range from the piezo electrically actuated flying insect work at the Vanderbilt University [1] that attempts to mechanically emulate the flapping wing motion of an insect and Micro-UAVs which are as small as 15 cm and weigh just 90 grams [2], to the USAF Unmanned Combat Aircraft (UCAV) and Global Hawk [3]. The impetus this field has received can partly be attributed to the limitations of conventional air vehicles in achieving ever increasing demands on their operational capabilities. UAVs are currently being designed and researched and to perform an array of tasks, such as :

- close-up inspection of power lines and bridges,
- terrain surveying, cinematography and aerial mapping,
- surveillance , law enforcement and border patrol, and
- oceanography and meteorological data collection

Carnegie-Mellon University have tested an unmanned helicopter in the Arctic to examine Haughton Crater's rock and conducted other experiments to asses the crater and its environs. This UAV was designed to create three dimensional maps using lasers and satellite data for further geological studies [4]. Aerosonde's robotic aircraft was developed primarily for meteorological and environmental reconnaissance over oceanic and remote areas and in harsh environments [5]. It has been flight tested across the Atlantic ocean and Alaska for use in environment related research. In short, they are

expected to carry out difficult and dangerous tasks. The advantages outlined above have led to a burst of activity in this arena. It is important to note that there are few operational UAVs and fewer still available for academic research-most current UAVs have been developed for military applications.

The vast majority of modern systems incorporate the latest light-weight material, smart sensors and complex control paradigms, in order to facilitate characteristics such as greater payload capability for a given structure, high manoeuvrability and a fast speed of response. Therefore, design, control and analysis of such systems are non trivial and entail multi-disciplinary expertise from domains such as aerodynamics (modelling), control, structures, sensors and elctronic hardware. Thus, challenges associated with contemporary systems can be categorised as that of:

- System (UAV, aircraft, plant etc.) design and requirement definition.
- Modelling and model analysis.
- Control design.
- Control analysis.
- Control implementation.

each of these aspects are discussed next and shown in Figure 1.1.

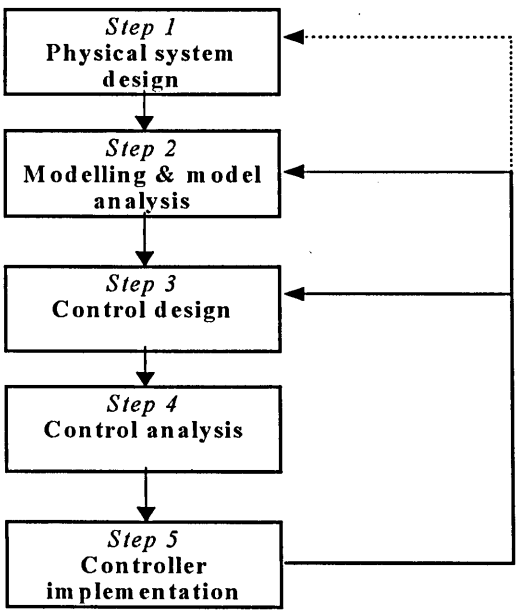

Figure 1.1. Steps in system design.

System design and requirement: Traditionally, application-specific engineers design the system or plant. After completing the design, control engineers inherit two products from the designer: i) the system itself and ii) physical requirements that the system must achieve after control design. Requirements define the problem, that is what is expected from the system. A good example is the ultra-agile military aircraft, in order to induce agility, canards or fore wings were appended to the aircraft. Another one is the need of light weight flexible space observatories so that they can carry a greater payload or on board equipments. Such high performance systems are no longer crafted in isolation but with increasing participation of control experts from an early stage. A cohesive mechanism requires control engineers to be involved early in the design phase of these systems, to provide input into how a particular plant design may affect controller design and vice-versa. Agile aircraft and flexible structures are prime examples where the role of control specialist is evident from the embryonic system design stage. It is only in the design stage that significant changes can be made. Thus, requirements feed the control design steps for modelling, design, analyses and implementation.

Modelling: Suitable plant models are required for the ensuing control design and analyses steps. After the design process, the most daunting task is to develop a working model. In fact an old saying in the control field is that *"most of the work in a control design is in developing the model"* [6]. Modern control techniques can achieve extraordinary results using state-space models. However, not even the most robust controller can compensate for a poor model. The model obtained either via mathematical modelling or the system identification route must be checked, analysed (i.e. determine its properties), and refined throughout the course of the control law development. Simplified rigid body models may be employed initially and if necessary more complex flexible or elastic modes may be included. This two stage procedure is commonly practised for flexible space craft appendages, helicopter rotor or agile air vehicle modelling and subsequent control. The control design model forms the basis for all designs and analyses. Generally, models for flight control imply a high-fidelity linear model for controller design and a nonlinear model for the closed system evaluation in a simulation environment.

Control design: Control design step begins with the selection of operating conditions at which the control design is to be accomplished. Then, a particular design methodology is selected. The designer has an impressive list of control paradigms from which to

choose, using either classical or modern state-space approaches. Much would depend upon the type of plant i.e. single input single output (SISO) or multi-input multi-ouptut (MIMO). Classical frequency domain methods have been very successful in handling SISO systems. On the other hand, modern control techniques are more amenable for MIMO systems. Also, factors like past history of successful application of certain control mechanism for a specific type of plant play an important role. For instance, to date PID controller is the most successful control paradigm in the process industry. Although alternative and more advanced paradigms exist for the process industry, such as Model Predictive Control, the industry is wary of changing practice that already works well. It could be said that there are many factors which decides a fate of a particular control option.

Control Analysis: Closely related to the control design step is the control analysis in the design process. For a requirement to be valid, it must be verifiable. Thus, as a requirement is included into a design, the control analysis test provides an immediate check on whether the requirement is met. If the resulting controlled system analysis is unsatisfactory then the specification/requirements could be modified or the type of controller or system design itself could be altered. As such, the analysis test forms the basis for the design iteration decision.

Control implementation: Once the design has passed all of its analysis assessments, considerable effort is still required to take the algorithm to a plant operational state. A simulated operational environment will never be a perfect representation of the real thing. Real systems are built from real imperfect (not mathematical) components and must operate under real (non ideal) conditions. Therefore, factors such as noise, quantization, nonlinearities, saturation (rate or amplitude), delays, model errors, sensors/actuator dynamics and disturbances can adversely affect control system operation.

Therefore, the controller implementation stage is regarded as the ultimate test for the validity of the whole design process i.e. step 1 to 5 of Figure 1.1. Generally, design steps 2 to 5 are carried out in an iterative manner until the design and operational requirements are satisfied. If this is unachievable then the plant itself may be modified and the design process repeated. This is indicated by the dotted line in Figure 1.1.

1.2 Problems and challenges of modern systems

Research interest in unconventional aircraft, such as tilt rotor, tilt wing, delta-wing, canard or talieron control surfaces, X-wing, tilt body, different types of light, micro, hand held unmanned aerial vehicles etc., have assumed increased importance in recent years. Two examples are shown in Figure 1.2. Figure 1.2 (a) shows the traffic surveillance drone being developed at Georgia Tech [7], and Figure 1.2 (b), is the Freewing Inc.[8] tilt-body UAV, to be employed for remote sensing applications.

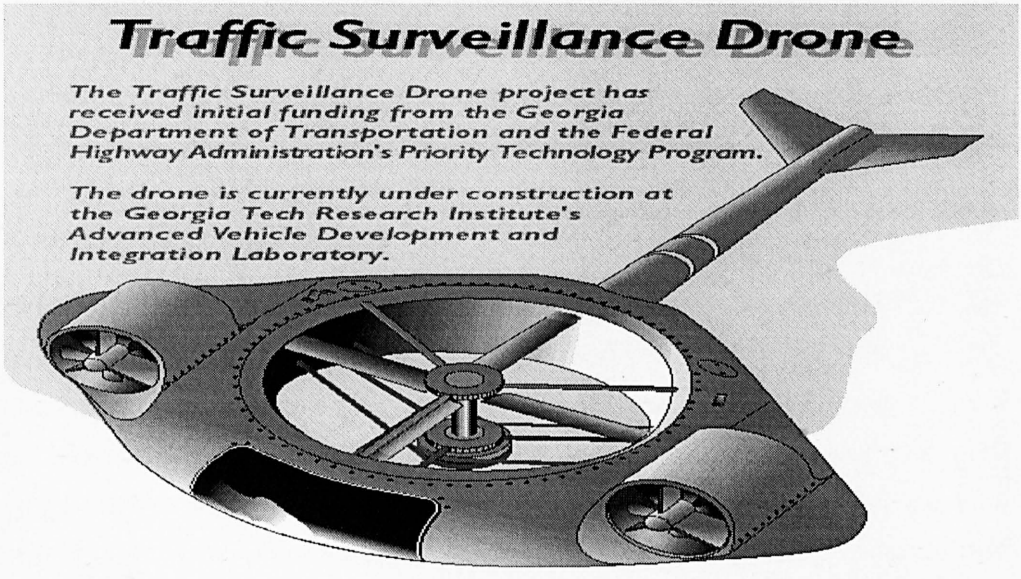

(a)

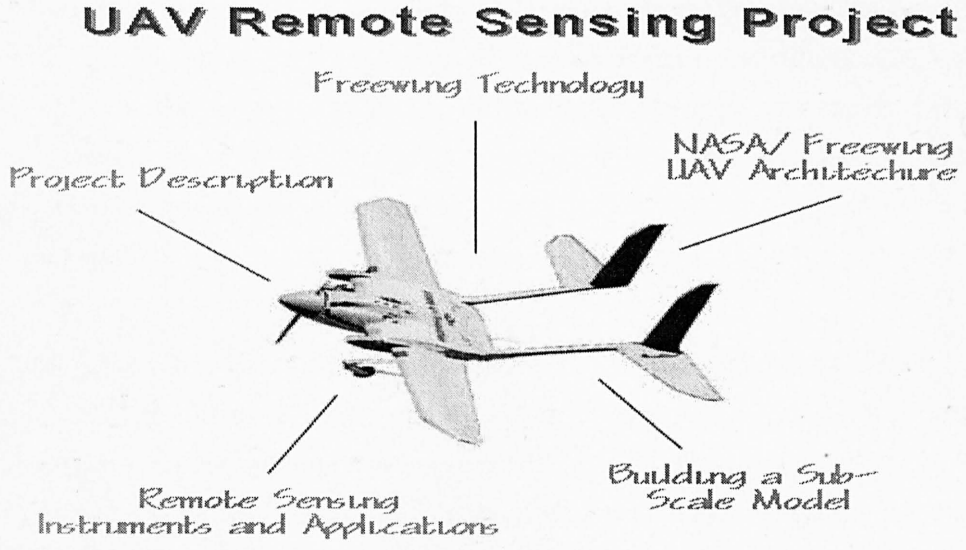

(b)

Figure 1.2. Illustrations of small UAVs.

The latter's hinged mid-body feature allows it to take-off and land like a bird. The importance of UAVs can be attributed to the increasing emphasis on the aircraft to be stealthy, agile, multi-purpose, autonomous etc., for varied civilian and military operations. However, modelling details of these vehicles are not reported due to classified nature of such projects. Moreover, the flight mechanics equations are not always easy to establish from first principles for a non-standard aircraft configuration. A case in point is the UAV Pegasus XL, which crashed due to the poor modelling procedure adopted [9]. However, these equations are imperative for subsequent control law development. A high fidelity nonlinear model is also often required to study controlled system performance in a simulation environment. Modelling of such vehicles is non-trivial and therefore, presents considerable challenges The modelling task is further complicated if coupling exists between different axis (plane) of motion, as for example in the case of a helicopter.

The last decade has witnessed a phenomenal growth in numerous fields, including robotics, space structures/space telerobotics, and unconventional air vehicles. The significant features of these endeavours have included the introduction of innovative design, fascinating structural materials and sophisticated control paradigms. This is a striking departure from the classical systems engineering philosophy. The assimilation of the above in systems development has led to systems which are sophisticated, accurate and robust. For instance, Artificial Intelligence (AI) techniques, such as neural networks, fuzzy-logic, and genetic algorithms, have been employed to address a range of engineering issues, such as modelling, optimisation, control, guidance, and fault-diagnosis. Flexible structures, an area of intense interest in robotics [10-12] and spacecraft with flexible appendages [13-15] research, are attractive mainly because of their lightweight and strength. In aerospace vehicles [16,17] too, a flexible airframe is adopted due to its light weight, thereby improving the thrust to weight ratio for a given propulsion system.

However, these advances have come at a cost, and the penalties imposed are complex systems with little historical data, no exhaustive literature or proven track record. An unconventional system configuration means considerable efforts are required to develop new mathematical models, especially in case of air vehicles. AI based control paradigms are complex and have not yet gained the confidence of the industry. In flexible or elastic structures the added complexity of the control problem is due to the inherently lightly

damped nature of the structure which causes vibration in the system. Control of modern system with flexible modes is a rather daunting and necessitates knowledge of a braod range of control methodologies.

In spite of the increased difficulties most of the control problems can be addressed using open loop, closed loop or a combined open and closed loop strategy. The open loop control technique of shaped command methods [10-12] have been particularly attractive. This method involves development of a suitable forcing function so that the vibrations at the resonance modes are reduced. Open-loop control topologies are particularly suitable for systems with slow dynamics, for instance flexible manipulators or similar plants.

On the other hand, fast manoeuvring systems, such as high speed robots [18], large flexible space structures [19], flexible aircraft [16,17] as well as the flexible missile [20] invariably incorporate feedback control mechanisms. With a variety of feedback control methods available, such as LQR/LQG, LQG-LTR, H-∞, eigenstructure assignments, dynamic inversion, classical method and including AI based control methods mentioned above, it is unclear which control scheme provides the best all round solution for a complex systems. Highly agile system such as combat aircraft are generally non minimum phase in nature. As some of the modern control techniques have limitations dealing with non minimum phase plants, control method selection becomes problamatic. Perhaps, the optimum approach is to evaluate different paradigms or rely on past experiences of researchers who have addressed analogous problems.

Thus, it is apparent from the above discussion that there are various issue connected with these sophisticated contemporary systems. These issues invariably fall under the broad guidelines described earlier in Section 1.1.

1.3 Motivation

Although, the twin rotor MIMO system (TRMS) shown in Figure 1.3 does not fly, it has a striking similarity with a helicopter, such as system nonlinearityies and cross-coupled modes. The TRMS, therefore, can be perceived as an unconventional and complex "air vehicle" with a flexible main body. These system characteristics present formidable challenges in modelling, control design, control analysis and implementation.

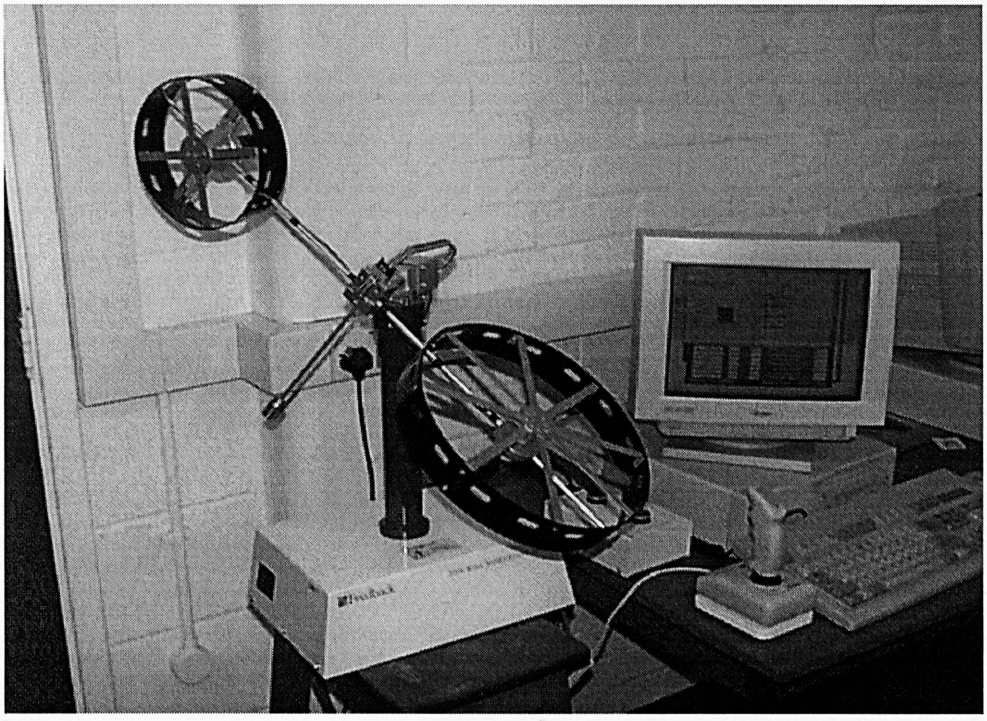

Figure 1.3. The twin rotor MIMO system (TRMS).

The motivation for this work stems from the fact that the TRMS behaviour in certain aspects resembles that of a helicopter. The TRMS is a laboratory set-up designed for control experiments by Feedback Instruments Ltd [21]. From the control point of view it typifies a high order non-linear system with significant cross-coupling. The main differences between the helicopter and the TRMS are

- In a single main rotor helicopter the pivot point is located at the main rotor head, whereas in case of the TRMS pivot point is at midway between the two rotors.
- In a helicopter, lift is generated via *collective pitch control,* i.e. pitch angles of all the blades of the main rotor are changed by an identical amount at every point in azimuth, but at constant rotor speed. However, in the case of the TRMS, pitch angles of all the blades are fixed and speed control of the main rotor is employed to achieve vertical control.
- Similarly, yaw is controlled in a helicopter by changing, by the same amount, the pitch angle of all the blades of the tail rotor. In the TRMS, yawing is affected by varying the tail rotor speed.

- There are no *cyclical controls* in the TRMS, *cyclic* is used for directional control in a helicopter.

However, like a helicopter there is strong cross-coupling between the collective (main rotor) and the tail rotor.

The hovering property of helicopter/TRMS is the main area of interest in this work. Station keeping, or hovering, is vital for variety of flight missions such as load delivery, air-sea rescue etc. Yet maintaining a station is one of the most difficult problems in helicopter flight because in this mode the dynamically unstable helicopter is flying at near zero forward speed. Although the TRMS rig reference point is fixed, it still resembles a helicopter by being highly non-linear with strongly coupled modes. Such a plant is thus a good benchmark problem to test and explore modern identification and control methodologies. The experimental set-up simulates similar problems and challenges encountered in real systems. These include complex dynamics leading to both parametric and dynamic uncertainty, unmeasurable states, sensor and actuator noise, saturation and quantization, bandwidth limitations and delays.

The presence of flexible dynamics in the TRMS is an additional motivating factor for this research. There is an immense interest in design, development, modelling and control of flexible systems, due to its utility in a multitude of applications, as discussed briefly in Section 1.2.

1.4 Aims of this research

From the foregoing discussion it is evident that the fundamental issues regarding the TRMS are: modelling, control design, analysis and implementation. These problems are systematically investigated in this work.

1.4.1 Contributions

The main contributions of this thesis are:

- Dynamic modelling of a 1 degree of freedom (DOF) TRMS using linear black box system identification techniques. The concept is extended to model a 2 DOF TRMS, which has cross-coupled dynamic modes. Cross-coupling renders MIMO modelling rather daunting. Helicopters too exhibit coupling between different axes and this is

an area of active research [22]. The extracted model is to be employed to detect system resonance modes for subsequent control design. It has been demonstrated that the black-box modelling approach presented is suitable to model a class of unconventional air platforms, whose flight dynamics are not well understood or difficult to model from first principles.

- Nonlinear modelling of a 1 DOF TRMS utilising radial basis function networks (RBF). The modelling concept provides an attractive alternative to model new generation UAVs with significant nonlinearities. Such a high fidelity nonlinear model is often required for gauging the performance of control design and analyses. The linear and nonlinear modelling exercise is carried out to include rigid as well as flexible modes of the system. The presence of high frequency modes in flexible systems have profound impact on the ensuing control design.
- Development and real-time realisation of open-loop vibration control for the 1 and 2 DOF TRMS. This concept is particularly useful in addressing vibration problems in MIMO systems, if modal coupling exists.
- Control law development and evaluation in the MATLAB/Simulink simulation environment for the 1 DOF TRMS to achieve vibration attenuation as well robust tracking performance. Investigation of feedback and combined feedforward and feedback techniques. Demonstration of the suitability of integrated feedforward and feedback method to tackle the dual problem of vibration reduction and command tracking in the system.
- Real-time realisation of the developed control strategies for the TRMS application.

1.5 Thesis outline

The organisation of the thesis reflects the sequence of steps involved in the development of a complete systems solution for the TRMS. A brief outline of the thesis contents is as follows:

Chapter 2 describes the experimental test bed, the Twin Rotor MIMO System, developed by Feedback Instruments Ltd. [21], designed for control experiments. A brief description of the rig, necessary instrumentation, hardware and software is presented. The TRMS is used as a test bed throughout this work.

Chapter 3 presents the development of linear models of both 1 and 2 DOF TRMS using the linear system identification techniques. Rigid and flexible modes are accounted for in the modelling procedure. Identification of 1 and 2 DOF discrete time linear models are presented in detail. The identification process for a MIMO system is non-trivial and a systematic approached is explained. Rigorous time and frequency domain test are employed to validate the identified models.

Chapter 4 explains the development of open-loop control strategies on the basis of the system's identified resonance modes. Command signals are preshaped using low-pass and a band-stop filter. For the 2 DOF case, due to coupling between horizontal and vertical planes as well as presence of vibrational modes in different channels poses significant difficulties in filter design. The filtered inputs are thus employed for both 1 and 2 DOF TRMS in the open-loop configuration. Their performance in suppressing structural vibrations of the TRMS is evaluated in comparison to a doublet signal. A comparative study of the low-pass and band-stop shaped inputs in suppressing the system's vibrations is also presented.

Chapter 5 describes the nonlinear system identification technique for modelling the 1 DOF TRMS using the radial basis function networks (RBF). The extracted models are verified using several time and frequency domain tests including model predicted output, correlation tests and time domain cross validation tests. The rationale for obtaining a high fidelity nonlinear model is that such a model is often required for assessing the performance of control design and system analysis.

Chapter 6 utilises the 1 DOF linear model obtained in Chapter 3 to design a feedback control mechanism. The LQG method is initially investigated within the simulation environment. The controller is shown to exhibit good tracking capabilities, but requires high control effort and has inadequate authority over residual vibration of the system. These problems are resolved by further augmenting the system with a command path prefilter. The combined feedforward and feedback compensator satisfies the performance objectives and obeys the actuator constraint.

Chapter 7 presents the implementation and realisation of the proposed control strategies of Chapter 6 on the TRMS test bed. Several additional designs are tested to improve the systems performance. The system's performance for various LQG weighting matrices are assessed and discussed from practical perspective.

Chapter 8 concludes the thesis with notable remarks. Future probable research directions are also outlined in this chapter.

1.6 Publications

Technical papers arising from this research, which are either published or under review, are listed below.

a) Journal Papers:

[1] S. M. Ahmad, A. J. Chipperfield and M. O. Tokhi. "Parametric Modelling and Dynamic Characterisation of a 2-DOF Twin Rotor MIMO System", *IMechE, Part G, Journal of Aerospace Engineering* (to appear).

[2] S. M. Ahmad, A. J. Chipperfield and M. O. Tokhi. "Dynamic modelling and open loop control of a twin rotor mimo system", (submitted to *IFAC Journal of Control Engineering Practice*).

b) Conference Papers:

[1] S. M. Ahmad, A. J. Chipperfield and M. O. Tokhi (2000). "Modelling and Control of a Twin Rotor Multi-Input Multi-output System", *Proc. American Control Conference (ACC' 2000)*, Chicago, IL, USA, 28-30 June, pp 1720-1724.

[2] S. M. Ahmad, A. J. Chipperfield and M. O. Tokhi (2000). "Dynamic Modelling of a Two Degree-of-Freedom Twin Rotor Multi-Input Multi-output System", *Proc. IEE United Kingdom Automatic Control Conference (UKACC' 2000)*, 4-7 Sept., Cambridge, UK.

[3] S. M. Ahmad, A. J. Chipperfield and M. O. Tokhi (2000). "Dynamic Modelling and Control of a 2 DOF Twin Rotor Multi-Input Multi-Output System", *Proc. IEEE Industrial Electronics, Control and Instrumentation Conference (IECON' 2000)*, *Nagoya*, Japan, 22-28 Oct., pp 1451-1456.

[4] S. M. Ahmad, A. J. Chipperfield and M. O. Tokhi (2000). "Dynamic modelling and Optimal Control of a Twin Rotor MIMO System", *Proc. IEEE National Aerospace and Electronics Conference (NAECON' 2000)*, Dayton, Ohio, USA, 10-12 Oct., pp 391-398.

[5] S. M. Ahmad, M. H. Shaheed, A. J. Chipperfield and M. O. Tokhi (2000). "Nonlinear Modelling of a Twin Rotor MIMO System using Radial Basis Function Networks", *Proc. IEEE National Aerospace and Electronics Conference (NAECON' 2000)*, Dayton, Ohio, USA, 10-12 Oct., pp 313-320.

[6] S. M. Ahmad, A. J. Chipperfield, and M. O. Tokhi. (1999). "System Identification of a One Degree-of-Freedom Twin Rotor Multi-Input Multi-Output System", *In International Conference on Computer and Information Technology (ICCIT' 99)*. SUST, Sylhet, Bangladesh, 3-5 Dec., pp 94-98.

Chapter 2

The twin rotor MIMO system description

This Chapter presents the general description of the TRMS. The physical as well as the hardware and software aspects of the TRMS are explained. Important considerations essential for conducting the experiments have been highlighted.

2.1 Introduction

The Twin Rotor MIMO System (TRMS) is a laboratory platform designed for control experiments by Feedback Instruments Ltd [21]. In certain aspects, its behaviour resembles that of a helicopter. For example, like a helicopter there is a strong cross-coupling between the *collective (main rotor)* and the tail rotor. The main differences between a helicopter and the TRMS are described in Section 1.3. As such it can considered a static test rig for an air vehicle. There is a small, but growing, literature on laboratory platforms simulating complex aircraft manoeuvre and problems. These platforms are often employed to test the suitability of different control methods for these systems. Some specific laboratory rigs used by researchers are described in Section 6.1.1. The remainder of this Chapter will describe the TRMS, a schematic diagram of which is shown in Figure 2.1.

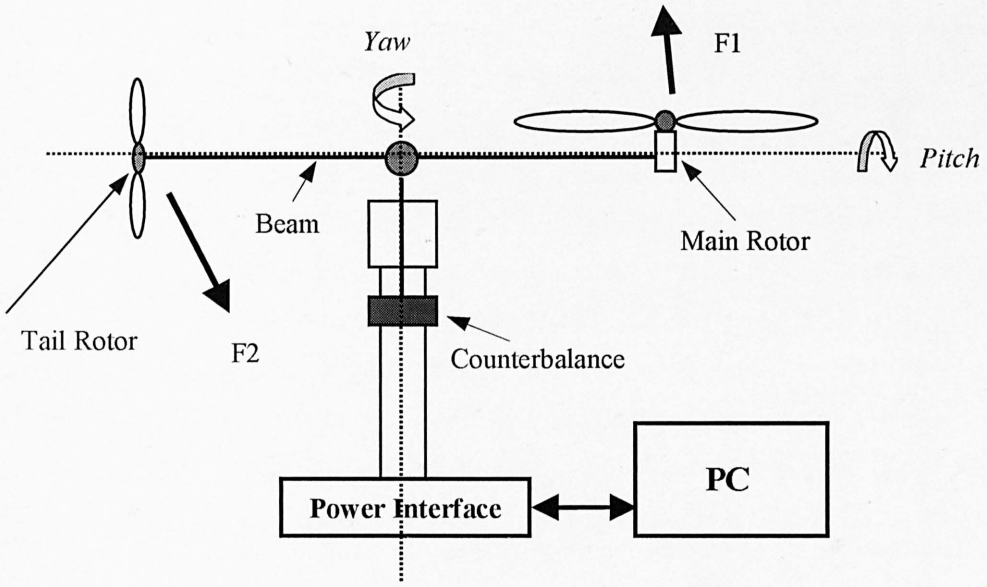

Figure 2.1. The twin rotor MIMO system.

The TRMS consists of a beam pivoted on its base in such a way that it can rotate freely in both its horizontal and vertical planes. There are rotors (the main and tail rotors), driven by DC motors, at each end of the beam. The input voltage is limited to the range +/- 10 volts. A counterbalance arm with a weight at its end is fixed to the beam at the pivot. The state of the beam is described by four process variables: horizontal and vertical angles measured by position sensors fitted at the pivot, and two corresponding angular velocities. Two additional state variables are the angular velocities of the rotors, measured by tachogenerators coupled with the driving DC motors. When not in use, either or both axes of rotation can be locked by means of the two locking screws provided for physically restricting the horizontal or vertical plane TRMS rotation. Thus, the system permits both 1 and 2 DOF experiments.

In a typical helicopter, the aerodynamic force is controlled by changing the angle of attack of the blades. The laboratory set-up is constructed such that the angle of attack of the blades is fixed. The aerodynamic force is controlled by varying the speed of the motors. Therefore, the control inputs are supply voltages of the DC motors. A change in the voltage value results in a change of the rotational speed of the propeller, which in turn results in a change of the corresponding position of the beam [21]. F1 and F2 in Figure 2.1 represents the thrust generated by the rotors in the vertical and horizontal planes respectively.

Rotation of a propeller produces an angular momentum which, according to the law of conservation of angular momentum, must be compensated by the remaining body of the TRMS. This results in the interaction between two planes of motion. This interaction directly influences the velocity of the beam in both planes. The coupling effect between the two channels may be accounted for by representing the dynamics of the TRMS by the multivariable transfer-function model as given in Figure 2.2. In Figure 2.2, the input signals *u1* and *u2* represent voltage inputs to the main rotor and tail rotor respectively. The outputs *y1* and *y2* represent pitch and yaw angles respectively. Note that, a similar coupling also exist in helicopters. The coupling between various channels or planes of motion therefore makes the modelling and control problems challenging for such systems.

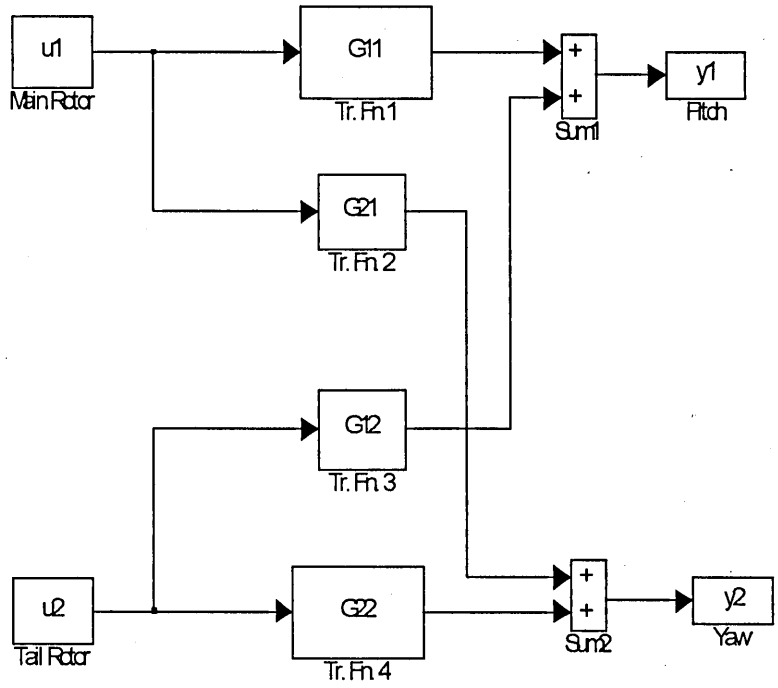

Figure 2.2. Coupled MIMO transfer function model.

2.2 The TRMS hardware and software description

A PC can be used for real-time control of the TRMS. The computer is supplied with an interface board-PCL-812. The PCL-812PG is a high performance, high speed, multi-function data acquisition card for IBM PC/XT/AT and compatible computers from Advantech Co. Ltd. Figure 2.3 shows details of the hardware and software configuration of the control system for the TRMS.

The control software for the TRMS consists of:

- Real-time kernel (RTK).
- The TRMS toolbox.

2.2.1 Real-time kernel

The real-time kernel (RTK) provides a mechanism of real-time measurements and control of the TRMS in the WINDOWS environment. It is implemented by dynamic linked library (DLL) and contains measurement procedures, digital filters, a data acquisition buffer, built-in control algorithms, software to control system actuators and a MATLAB-to-RTK interface. The RTK controls flow of all signals to and from the TRMS. It contains functions for performing analogue-to-digital and digital-to-analogue conversions. The RTK DLL library is excited by time interrupts. The main part of the RTK is executed during interrupt time. In summary, the RTK contains all the functions that are required for feedback control and data acquisition in real time. A typical TRMS Simulink block diagram is shown in Figure 2.4.

Example control algorithms are embedded in the real-time-kernel, including open-loop, PID and state-space controller. It is possible to tune the parameters of the controller without emphasis on analytical model. Such an approach to the control problem seems to be reasonable, if a well defined model of the TRMS is not available. These controller parameters are functions of error signals, that is the difference between the desired and actual TRMS beam positions and angular velocities. Selection of control algorithms and tuning of their parameters is done by means of the communication software (Figure 2.3) from the MATLAB environment. Since the focus of this research is on model-based control law development therefore, these controllers were of no use to this work. The interested reader can refer to the TRMS manual [21] for further details of these controllers.

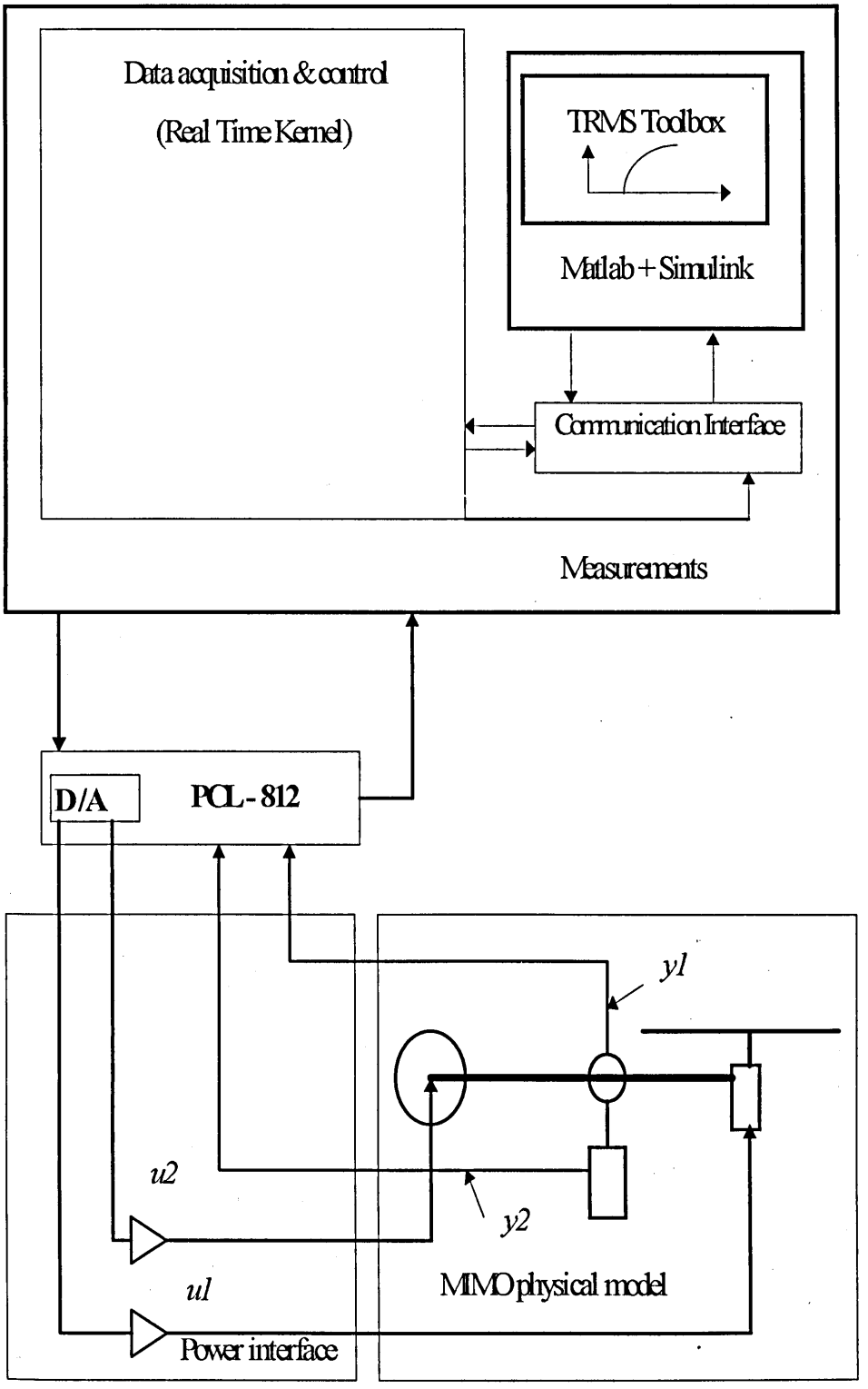

Figure 2.3. Hardware and software configuration of the TRMS.

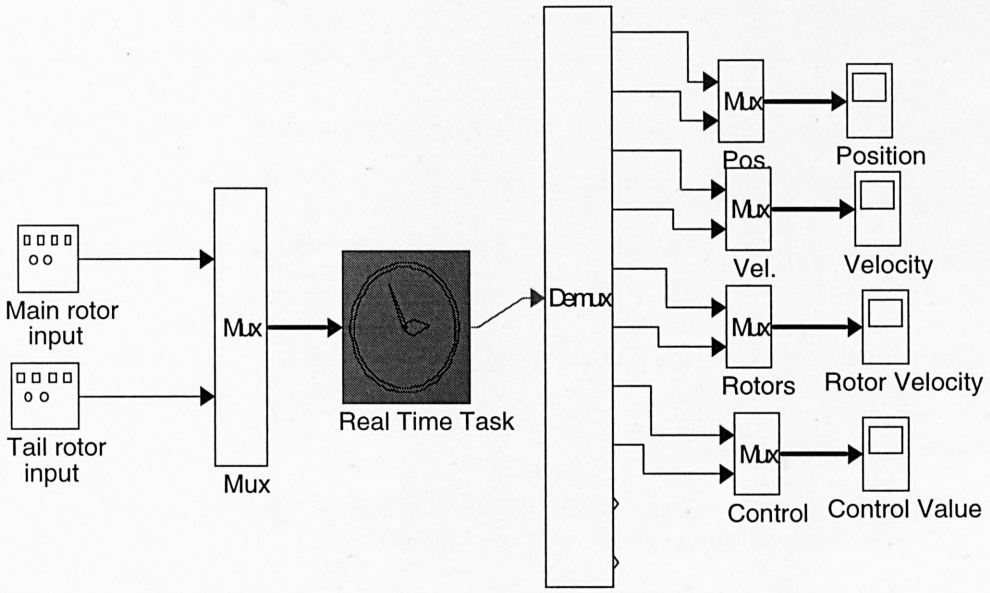

Figure 2.4. The TRMS Simulink diagram.

The communication interface is also used for configuration of real-time kernel parameters, e.g. setting of the sampling period for experiments or encoder resetting at the beginning of each new experiment. Time history of experiments is collected in a cyclic buffer. The data can be transferred to the MATLAB workspace using the communication interface.

2.2.2 The TRMS toolbox

The TRMS toolbox is a collection of m-functions and C-coded DLL-files that extend the MATLAB environment in order to address TRMS modelling and real-time control problems. On-line data flow between the RTK and toolbox functions is performed by the communication interface. The TRMS toolbox, using MATLAB matrix functions and Simulink utilities, provides the user with functions specialised for real-time control of the twin rotor system. This toolbox is an open system. This approach by its nature makes basic functions of the toolbox available to the user. It empowers the user to create a system of his own, add new control algorithms to it, or further customise it to satisfy his requirements better.

There are 34 toolbox functions. The functions are divided into the four following categories according to the specific roles performed:

hardware: the functions in this category is used to obtain and set the base address of PCL-812 interface board. A function is also available to reset the encoders at the beginning of each experiment.

data acquisition: the functions in this category is employed to set the sampling time, acquire the sampling interval and retrieves the time histories of various measurements.

software: the loading and the unloading of the RTK to and from the memory is carried out by functions in this category.

control: the job of assigning different control parameters for various in-built control algorithms are mainly achieved by invoking functions in this category.

The important ones used during this research are described in Appendix 1.

2.3 TRMS experimentation

Important consideration for carrying out the experiments with the TRMS are level of input signals, sampling time and environmental conditions. Each of these are explained next.

The level of input signals have been selected in this research so that these signals no not drive the TRMS out of its linear operating range. The range of operation is the slight deviation from the steady-state "hover" mode. Throughout this research the experimentation was carried out with the TRMS beam in a flat horizontal position representing the "hover" mode. The TRMS in this position is shown in Figure 2.5. The hovering property of the TRMS is the main area of interest in this work. Station keeping or hovering is vital for a variety of flight missions such as load delivery and air-sea rescue.

For the identification of the discrete time models, the sampling time has to be selected before starting the experiments. The sampling time depends on the final application and the intended accuracy of the resulting model. The model can easily exhibit high order behaviour if the sampling period is chosen too short. On the other hand, if the sampling period is too large, the model looks like a constant or multiple integrators and its dynamics representation would be inaccurate. Some useful guidelines for sampling period selection are given in Section 3.2.4.

Figure 2.5. The TRMS in "hover" mode.

It has been observed that, the TRMS is very sensitive to the atmospheric disturbances. A slight gust of wind can affects it dynamical behaviour. Therefore, care has been taken to conduct experiments with minimal environmental influence. If necessary experiments have been repeated until "true" responses are obtained.

2.4 Concluding remarks

A general description of the TRMS considered for this research has been presented in this Chapter. The system consists of a main beam and measuring devices. The beam is pivoted on its base such that it can rotate freely in horizontal and vertical planes. Details of hardware and software configuration have also been presented. The PC communicates with the TRMS rig via MATLAB-Simulink environment. Important considerations while conducting experiments with the TRMS have been highlighted.

Chapter 3

Dynamic modelling of the twin rotor MIMO system

Mathematical models for the dynamic characterisation of one and two-degree-of-freedom twin rotor multi-input multi-output system (TRMS) in hover, are determined using a black-box system identification technique. Identification for 1 and 2-DOF rigid-body, discrete-time linear models are presented in detail. The extracted model is shown to have a good degree of prediction capability. The modelling approach presented is suitable for complex new generation air vehicles.

3.1 Introduction

Mathematical modelling is perhaps the best known analytical method of describing the dynamics of a physical system. The parameters associated with such a model have a direct link and influence on the physical and dynamical properties of the system. An important feature of such characterisation of a system is that it helps in observing the "cause" and "effect" phenomena clearly, that is, which parameter has what effect on the system behaviour. The approach is generally best suited to *simple* systems. However, with the increasingly complex nature of systems, which may constitute many subsystems, modelling of such a system is often a formidable task. Furthermore, mechanical systems in general have electro-mechanical components and mathematical modelling would entail specialist knowledge of these areas. Mathematical models are derived from first principles and, in the process, employ many simplifications and assumptions. Such methods will thereby ignore less important dynamics and disturbances acting on the system. These factors, if not accounted for, would yield a poor system model. Thus, the utility of mathematical modelling to fairly complex plants is limited. *System identification*, on the other hand, is an experimental technique, and has proven to be an excellent tool to model *complex* processes where it is not possible to obtain reasonable models using only physical insight. Important applications of system identification are visible in areas that require higher accuracy of the mathematical

model for simulation, validation, control system design and handling qualities, in aerospace applications for example. It provides an accurate, rapid and reliable approach for defining design specifications and for validating control systems.

In aircraft applications, the typical role of system identification is to estimate the parameters of the linearized 6 degree-of-freedom equation of motion from flight or wind tunnel data. Here, the model structure is *known* and the parameters of the model have some physical meaning, and are often called stability and control derivatives. These derivatives are functions of altitude and Mach number of the aircraft and therefore would change at different operating conditions. This holds true for most classical fixed and rotary wing aircraft. There are a vast number of papers addressing parameter estimation techniques for conventional aircraft for example, [23,24]. However, with many new innovative experimental aircraft designs or those which are inherently more complex such as the tilt rotor, tilt wing, delta-wing, canard or talieron control surfaces, X-wing and tilt body, flight mechanics equations are not always easy to establish from first-principles. Yet, these equations are essential for designing and studying flight control systems. System identification is a viable alternative for modelling unconventional aircraft, where both model structure and model parameters are *unknown* and need to be identified. Modelling of such vehicles is the subject matter of this Chapter.

A number of unmanned aerial vehicles (UAVs) such as Bluebird [25], Frog [26], Solus [27]. Raven-2 [28], have been reported recently. These are based on *conventional* aircraft aerodynamic design philosophy and are often scaled versions of contemporary aircraft. The dynamic models of these aircraft have been derived from first-principles through determination of the aerodynamic stability and control derivatives, with usual decoupling of longitudinal and lateral dynamics. Many other *unconventional* but fascinating experimental air vehicles have also been reported in the literature, some of these are briefly discussed below. These innovative platforms or *"next generation air vehicles"* are designed for specific applications, and differ significantly from their *classical* counterparts. Recently, a considerable amount of research effort has been devoted to different modelling and control aspects of these *unconventional* vehicles. A free wing [8] UAV is modelled using conventional mathematical modelling techniques. The Caltech ducted fan laboratory aircraft [29] has been developed to demonstrate control techniques for hover to forward flight transition for thrust-vectored aircraft.

Modelling and control of a radio controlled (RC) laboratory helicopter has been reported by Morris *et al* [30] where modern identification and robust control techniques have been investigated for the hover mode. Identification of an autogyro (gyroplane), a popular sport and recreational flying machine, has been documented by Houston [31]. Werner and Meister [32] have developed a mathematical model, from first-principles, for a 2 DOF laboratory aircraft. This plant was developed primarily to model the behaviour of a vertical-take-off plane. Nonlinear system identification techniques such as neural networks have been applied in modelling of an *Ariel* UAV [33]. Neural networks were also employed for characterising the wind-tunnel wing model at NASA [34]. It is evident from the above cases that the plant is modelled using *mathematical modelling* based on the analysis of plant aerodynamics i.e. using laws of physics. Furthermore, the parameters of the model are either known or obtained using linear or nonlinear system identification techniques.

However, the modelling technique presented in this Chapter is suitable for a wide range of *new generation* air vehicles whose flight dynamics are either difficult to obtain via mathematical modelling or not easily understood. The modelling is done assuming no prior knowledge of the model *structure* or *parameters* relating to physical phenomena, i.e. black-box modelling. Such an approach yields input-output transfer function models with neither prior defined model structure nor specific parameter settings reflecting any physical aspects. It is then the responsibility of the systems engineer to examine the resultant black-box model and interpret the extracted model parameters in relation to the plant dynamics. This is discussed in more detail in Section 3.6 of this Chapter. System identification is a powerful interim solution for such systems. The designer can use these models to build an initial understanding of the whole system and develop general solutions. If more rigorous analytical models become available, they can then be used to fine-tune the general solutions, if they prove to be more accurate.

The work in this Chapter addresses modelling of an experimental test rig, representing a complex TRMS using system identification techniques. In this Chapter, attention is first focused on the identification and verification of longitudinal dynamics of a 1 DOF TRMS with its main beam (body) in a flat horizontal position representing the hover mode. Although the system permits multi-input multi-output (MIMO) experiments, initially single-input single-output (SISO) set-up will be discussed. The concept is then extended for modelling a 2 DOF MIMO twin rotor plant. The objective is to get

satisfactory models of the pitch and the yaw plane dynamics, including the cross-coupled dynamics that may exist between different channels.The primary interest lies in the identification of low frequency (0-3 Hz) dynamic modes corresponding to the rigid-body dynamics of the TRMS. This range is assumed to be good enough for high fidelity modelling of the TRMS. The extracted model can be used for many purpose such as dynamic simulation of the system, model validation, vibration suppression and control design. These areas are investigated in Chapters 4, 6 and 7 respectively. Hence, the issue of sampling rate and accurate identification of resonance modes is also addressed.

The remainder of the Chapter is split into two main parts. The first part deals with the 1 DOF TRMS modelling. The experimentation and data analysis is given in Section 3.2 and the results of the system identification are presented in Section 3.3. The second part investigates the 2 DOF modelling. Similar to 1 DOF, the MIMO experimentation procedure is described in Section 3.4, while the results are delineated in Section 3.5. A physical interpretation of the 1 DOF black-box model is given in Section 3.6 and the Chapter is concluded in Section 3.7.

3.2 One DOF modelling

In this Section a 1 DOF modelling procedure is described in detail and the following Section will present the results.

3.2.1 Experimentation

The objective of the identification experiments is to estimate a linear time-invariant (LTI) model of the 1 DOF TRMS in hover without any prior system knowledge pertaining to the exact mathematical model structure. No model structure is assumed *a priori* unlike aircraft system identification wherein the identification procedure is reduced to estimating the coefficients of a set of differential equations describing the aircraft dynamics. The differential equations describe the external forces and moments in terms of accelerations, state and control variables, where the coefficients are the stability and control derivatives. The extracted model is to be utilised for low frequency vibration control (Chapter 4) and design of a suitable feedback control law for disturbance rejection and reference tracking (Chapter 6 and 7 respectively). Hence, accurate identification of the rigid body dynamics is imperative. This would also facilitate understanding of the dominant modes of the TRMS. Since no mathematical

model is available, a level of confidence has to be established in the identified model through rigorous frequency and time domain analyses and cross-validation tests.

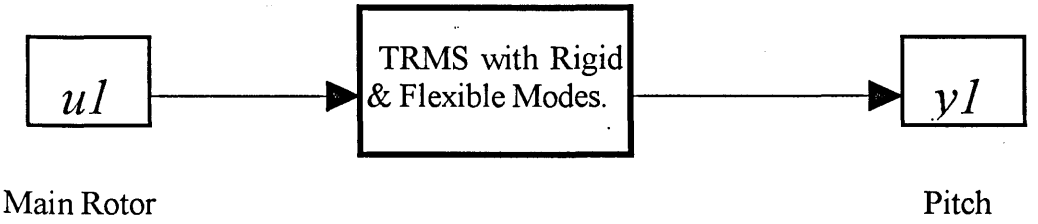

Figure 3.1. SISO transfer function model.

It is intuitively assumed that the body resonance modes of the TRMS lie in a low frequency range of 0-3 Hz, while the main rotor dynamics are at significantly higher frequencies. The rig configuration is such that it permits open-loop system identification, unlike a helicopter which is open-loop unstable in hover mode. In Figure 3.1, the input signal *u1* represents voltage input to the main rotor and the output *y1* represents pitch angle in radians. During experimentation, yaw plane movement is physically locked, thereby allowing only pitch plane motion.

3.2.2 Flight test data base

The TRMS has been upgraded, and a joy stick control analogous to that of a helicopter pilot stick has been provided. Test signals could be applied using the stick. However, only a very simple signal sequence is feasible, which is not sufficient for adequacy of spectral content and repeatability. Moreover, the system is very sensitive, and precise control cannot be exercised. Hence, the test signal is designed separately and read from the workspace in the MATLAB\Simulink environment, instead of using the stick. This is analogous to automation of the test signal, which ensures the experiments to be sufficiently controlled, be repeatable, and guarantees the desired spectral content.

Trim configuration for this identification experiments was steady-state horizontal position of the beam of the TRMS. Since the TRMS is very sensitive to the atmospheric disturbances, it was ensured that the tests were conducted in calm air. The system was excited with pseudo random binary sequence (PRBS) signals of different bandwidths (2-

20 Hz), so as to ensure that all resonance modes are captured both in the range of interest, i.e. 0-3 Hz, and out of curiosity to find out if any modes exist beyond this range. Finally, a PRBS of 5 Hz bandwidth and duration of 60 seconds was deemed fit for this study. The spectral plot of the PRBS is shown in Figure 3.2(a).

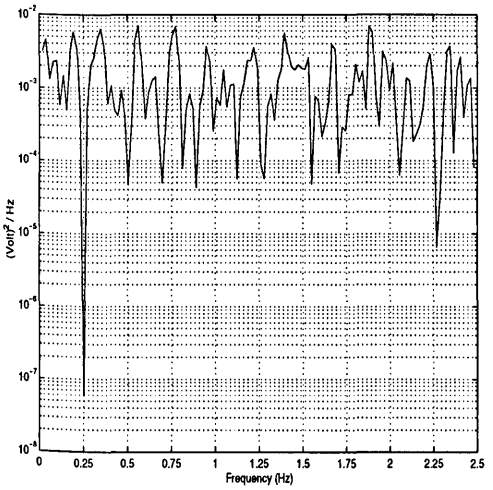

(a) PRBS.

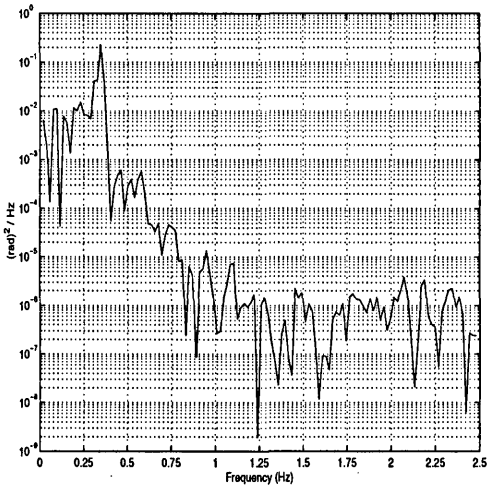

(b) Pitch response.

Figure 3.2. Power spectral density (a) PRBS signal. (b) Pitch response.

The PRBS magnitude was selected so that it does not drive the TRMS out of its linear operating range. Good excitation was achieved from 0-2.5 Hz which includes all the important rigid body and flexible modes-see Figure 3.2(b). It is noted, that the significant system modes lie in the 0-1 Hz bandwidth.

3.2.3 Data reliability analysis

Measurements used for system identification were pitch position, *y1*, in radians and control, *u1*, in volts. The measured data was sampled and recorded on a PC using the real-time kernel (RTK) software (Chapter 2). Data quality and consistency are critical to the identification. Excessively noisy or kinematically inconsistent data may lead to identification of an incorrect model. Preliminary checks of data quality and consistency can ensure that these sources of error are minimised. The TRMS is very sensitive to the atmospheric disturbances and in order to ensure accurate identification each signal was repeated many times until a response, undisturbed by gust, was obtained.

3.2.4 Sampling Rate

One of the important considerations in discrete-time systems is the sampling rate. A low sampling rate would yield data with little information about the process dynamics. A high sampling rate, on the other hand, will lead to poor signal to noise ratio (SNR). Low SNR means less informative data and the estimation would be biased. A good choice of sampling rate thus is a trade-off between noise reduction and relevance for the process dynamics.

Since the intended use of the system model is for control purposes, certain other aspects need to be considered. It is recommended that the sampling interval for which the model is built should be the same for the control application [35]. There are, however, some useful guidelines, which relate the sample interval to the response of the system to be identified. Certain symptoms will appear in the estimated model if a wrong sample interval is selected. This can be done by observing the position of all poles of the obtained model in the z-plane. If the poles and zeros are found clustered tightly around $|z|=1$, this indicates that the system has been sampled too rapidly. If the poles and zeros are found clustered tightly around the origin of the z-plane, this indicates that the system has been sampled too slowly. The ideal aim is for a set of estimated model parameters, which correspond to a reasonable spread of pole-zero positions in the z-plane [36].

There are some useful rules of thumb for setting the initial sampling rate, based on the dominant time constant (i.e. from the step response), process settling time and guessed bandwidth of the system. For instance, one could choose i) sampling rate of 1/5 of time constant or 10 times the guessed system bandwidth [35], ii) four times the guessed system bandwidth [36], and iii) 10 % of settling time [37], with optimal choice lying around the time constant of the system. The step response of the plant is given in Figure 3.3. It is noted that the dynamics of the system are not simple, with highly oscillatory poles. The dominating time constant is around 1.2 seconds and there is a pure time delay of about 0.6~0.7 seconds.

Using the above guidelines a sampling rate of 5 Hz was chosen iteratively. At this rate only the marginally stable system poles were close to the unit circle and the rest well within the unit circle see Figure 3.4. Hence, a sampling rate of 5 Hz was found to be appropriate for this case study. In retrospect, the sampling rate is close to 10 times the

identified system bandwidth (refer to section 3.2.2). It can also be deduced from Figure 3.4, that the system is non-minimum phase, with zeros outside the unit circle. Note, that the pole-zero plot of the identified TRMS model is presented here for illustrating the effect of sampling period. However, the identified model parameters are given in Section 3.6.

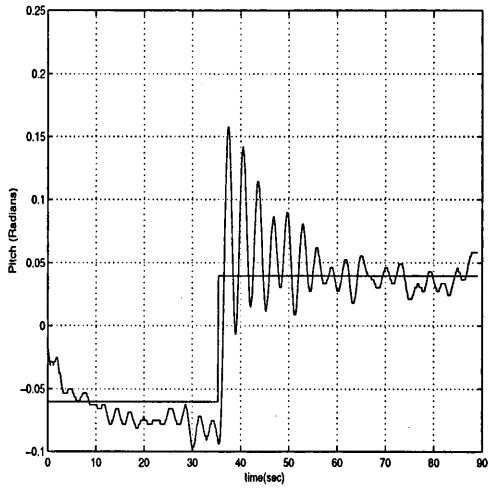

Figure 3.3. Step response of the process.

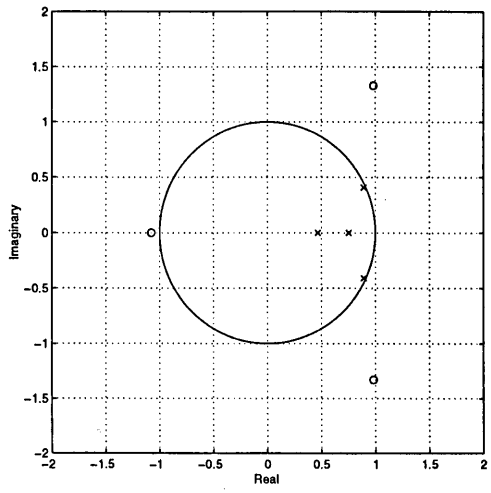

Figure 3.4. Pole-zero plot.

3.2.5 Coherence test for linearity

It is important in linear system identification to keep the effects of non-linearities to a minimum. The coherence is a measure of linear dependence of the output on the input, defined in spectral terms, i.e. it expresses the degree of linear correlation in the

frequency domain between the input and the output signal. An important use of the coherence spectrum is its application as a test of signal-to-noise ratio and linearity between one or more input variables and an output variable. The coherence function $\gamma^2_{xy}(f)$ is given by:

$$\gamma^2_{xy}(f) = \frac{|S_{xy}(f)|^2}{S_{xx}(f)S_{yy}(f)} \tag{3.1}$$

where S_{xx} and S_{yy} are the auto-spectral densities of the input and output signals respectively and S_{xy} is the cross-spectral density between the input and output signals. By definition, the coherence function lies between 0 and 1 for all frequencies f;

$$0 \leq \gamma^2_{xy}(f) \leq 1$$

If x(t) and y(t) are completely unrelated, the coherence function will be zero. While a totally noise-free linear system would yield $\gamma^2_{xy}(f) = 1$. The coherence function may thus be viewed as a type of correlation function in the frequency domain where a coherence function not equal to 1 indicates the presence of one or more of the following [38].

- Extraneous noise is present in the input and the output measurements.
- The system relating $x(t)$ and $y(t)$ is not linear.
- The output $y(t)$ is due to an input $x(t)$ as well as other inputs such as external disturbances.
- Resolution bias errors are present in the spectral estimates.

When a system is noisy or nonlinear, the coherence function indicates the accuracy of a linear identification as a function of frequency. The closer it is to unity at a given frequency, the more reliance can be placed on an accompanying frequency response estimate, at that frequency. For a real-world application, which will be nonlinear and affected, to some extent by noise, a plot of the coherence function against frequency will indicate the way in which the disturbances change across the frequency band. Coherence testing is employed on the input-output data channel and is discussed next.

The linearity of the operating region is confirmed by a flat coherence of unity between the input PRBS signal and the output pitch response. The coherence spectra with 5 Hz

sampling rate is shown in Figure 3.5(a). The poor quality is suspected to be due to resolution bias errors.

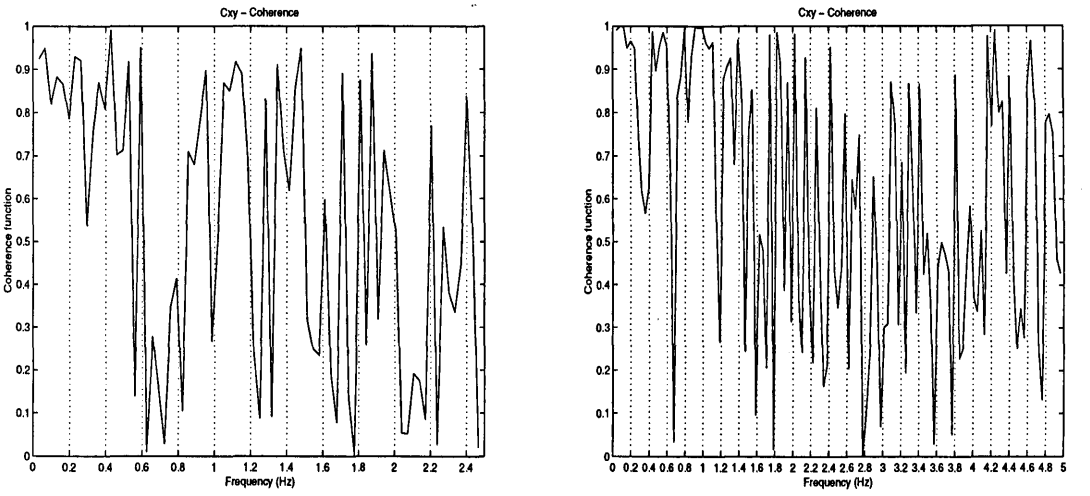

(a) Data sampled at 5 Hz.

(b) Data sampled at 10 Hz.

Figure 3.5. Coherence test.

Hence, the input-output data were re-sampled at a rate of 10 Hz, and the corresponding coherence function is depicted in Figure 3.5(b). This has an improved resolution, but as with Figure 3.5(a), there is a notch in the proximity of 0.4 Hz, which could be due to the nonlinear behaviour of the system at that frequency.

3.3 Results: 1 DOF

This section discusses the identification of the TRMS which involves three steps.

- The first step is qualitative operation, which defines the structure of the system for example, type and order of the differential equation relating the input to the output; it is known as *characterization*. This means selection of a suitable model structure, e.g. auto-regressive with exogenous input (ARX), auto-regressive moving average with exogenous input (ARMAX) or Box-Jenkins.
- The second step is *identification/estimation*. This consists of determining the numerical values of the structural parameters which minimize a error between the system to be identified and its model. Common estimation methods are least-squares (LS), instrumental-variable (IV), maximum-likelihood (MLE) and the prediction-error method (PEM). This is, in simple terms, a curve fitting exercise.

- The third step, *verification,* consists of relating the system to the identified model responses in time or frequency domain to instil confidence in the obtained model. Residual test, bode plots and cross-validation tests are generally employed for model validation.

These main features of system identification are symbolically indicated in Figure 3.6. The objective of identification is to minimize the sum squared errors or residuals $\varepsilon(t)$. More details on the general aspects of identification theory can be found in Ljung [35] and Soderstrom and Stoica [37].

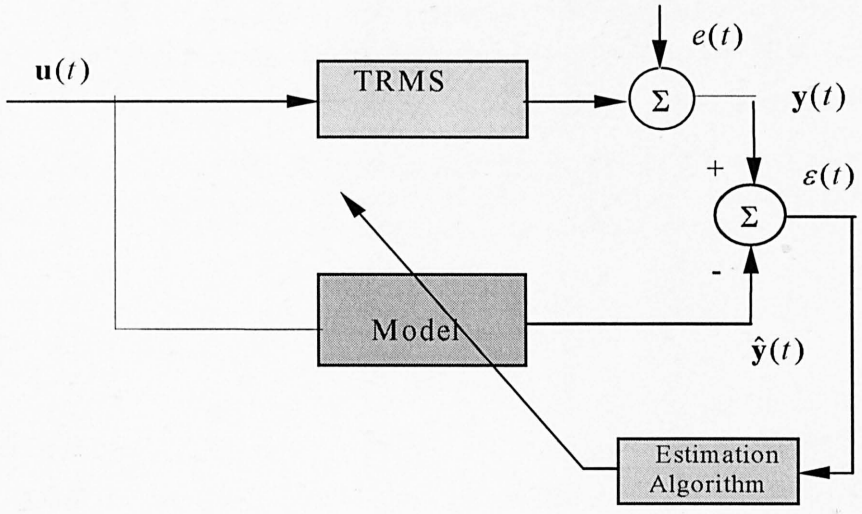

Figure 3.6. The identification procedure.

3.3.1 Mode or structure determination

To identify an unknown process, some knowledge or engineering judgement of the process and type of excitation signal is required. The parameters of the physical systems are generally distributed in space. Hence, the systems will have more than one frequency of resonance. The primary interest in this work lies in locating these *resonance* or *normal modes*, which ultimately dictate the behaviour of the system. Theoretically, the TRMS will have an infinite number of such *normal modes* with associated frequencies. It is observed from the power spectral density in Figure 3.2(b), that the significant system modes lie in the 0-1 Hz bandwidth, with a main resonance mode at 0.34 Hz

which can be attributed to the main body dynamics. A model order of 2, 4 or 6 corresponding to prominent normal modes at 0.25, 0.34 and 0.46 Hz and a rigid body *pitch* mode is thus anticipated.

3.3.2 Parametric modelling

Equipped with the insight mentioned above, attention is focused on selecting *parameters* in the model to obtain a satisfactory system description. A parametric method can be characterised as a mapping from the experimental data to the estimated parameter vector. Such models are often required for control application purposes. With no prior knowledge of sensor or instrument noise, a preliminary second order ARX model was assumed for the *u1* → *y1* channel. The auto-correlation of residuals revealed negative correlation at lag 1, indicating the presence of non-white, sensor or external noise. This necessitates estimating the noise statistics. Therefore, the ARMAX model structure:

$$y(t)+a_1y(t-1)+.....+a_{n_a}y(t-n_a)=b_1u(t-1)+.....+b_{n_b}u(t-n_b)+ e(t)+c_1e(t-1)+....+c_{n_c}e(t-n_c) \tag{3.2}$$

was selected for further analysis, where, a_i, b_i, c_i, are the parameters to be identified, and, $e(t)$ is a zero mean white noise. This structure takes into account both the true system and noise models.

The predictor for equation (3.2) is given by

$$\hat{y}(t|\theta)=\frac{\mathrm{B}(q)}{\mathrm{C}(q)}\mathrm{u}(t)+\left[1-\frac{\mathrm{A}(q)}{\mathrm{C}(q)}\right]y(t) \tag{3.3}$$

where

$\hat{y}(t|\theta)=$ is the predicted output according to model parameter θ.

$$\mathrm{A}(q)=1+a_1q^{-1}+.....+a_{n_a}q^{-n_a}$$

$$\mathrm{B}(q)=b_1q^{-1}+.....+b_{n_b}q^{-n_b}$$

$$C(q) = 1 + c_1 q^{-1} + \ldots\ldots + c_{n_c} q^{-n_c}$$

This means that the prediction is obtained by filtering u and y through a filter with denominator dynamics determined by $C(q)$ [35].

The predictor (3.3) can be rewritten as follows. Adding $[1 - C(q)]\hat{y}(t|\theta)$ to both sides of equation (3.3) gives

$$\hat{y}(t|\theta) = B(q)u(t) + [1 - A(q)]y(t) + [C(q) - 1][y(t) - \hat{y}(t|\theta)] \quad (3.4)$$

Introducing the prediction error

$$\varepsilon(t,\theta) = y(t) - \hat{y}(t|\theta) \quad (3.5)$$

and the vector

$$\varphi(t,\theta) = [-y(t-1)\ldots - y(t-n_a)\ \ u(t-1)\ldots - u(t-n_b)\ \ \varepsilon(t-1,\theta)\ldots\varepsilon(t-n_c,\theta)]^T \quad (3.6)$$

Then equation (3.4) can be expressed as

$$\hat{y}(t|\theta) = \varphi(t,\theta)\,\theta \quad (3.7)$$

The equation (3.7) is referred as a *pseudolinear regression* due to the nonlinear effect of θ in the vector $\varphi(t,\theta)$.

In the time-domain identification, prediction errors or residuals $\varepsilon(t)$ (this form is used for notational simplicity instead of $\varepsilon(t,\theta)$) are analysed for determining an appropriate model structure. Residuals are the errors observed between the model response and the actual response of the plant to the same excitation. A model structure can be found, iteratively, that minimises the absolute sum of the residuals. Ideally, the residuals $\varepsilon(t)$ should be reduced to an uncorrelated sequence denoted by $e(t)$ with zero mean and finite variance. Correlation based model validity tests are employed to verify if

$$e(t) \approx \varepsilon(t) \quad (3.8)$$

This can be achieved by verifying if all the correlation functions are within the confidence intervals. When equation (3.8) is true then,

$$\phi_{\varepsilon\varepsilon}(\tau) = E[\varepsilon(t-\tau)\varepsilon(t)] = \delta(\tau) \qquad (3.9a)$$

$$\phi_{u\varepsilon}(\tau) = E[u(t-\tau)\varepsilon(t)] = 0 \qquad \forall\tau \qquad (3.9b)$$

where $\phi_{\varepsilon\varepsilon}(\tau)$ and $\phi_{u\varepsilon}(\tau)$ are the estimated auto-correlation function of the residuals and the cross-correlation function between $u(t)$ and $\varepsilon(t)$, respectively. $\delta(\tau)$ is an impulse function. These two tests can be used to check the deficiencies of both the plant and the noise model. The expression (3.9b) implies that the plant model is correct and the residuals are uncorrelated with the input. But if $\phi_{\varepsilon\varepsilon}(\tau) \neq \delta(t)$, then it is an indication that although the plant model is correct, the noise model is incorrect and therefore, the residuals are autocorreleted. On the other hand, if the noise model is correct and the plant model is biased, then the residuals are both autocorrelated such that $\phi_{\varepsilon\varepsilon}(\tau) \neq \delta(t)$ and correlated with the input $\phi_{u\varepsilon}(\tau) \neq 0$.

3.3.3 Identification

Having selected a model structure, it is next desired to estimate the parameter vector θ. The search for the best model within the set then becomes a problem of determining or estimating θ. Once the model and the predictor are given, the prediction errors are computed as in (3.5). The parameter estimate $\hat{\theta}_N$ is then chosen to make the prediction error $\varepsilon(1,\theta),.....\varepsilon(N,\theta)$ small. One of the common method to obtain $\hat{\theta}_N$ is to minimise a quadratic *cost-function* $V_N(\theta)$ defined as,

$$V_N(\theta) = \frac{1}{2}\sum_{t=1}^{N}\varepsilon^2(t,\theta) \qquad (3.10)$$

where N denotes the number of data points.

This problem is known as "the nonlinear least-squares problem" in numerical analysis. However, since $\hat{y}(t|\theta)$ in equation (3.7) is a nonlinear function of θ, and therefore, the function $V_N(\theta)$ cannot be minimised analytically. Instead, some numerical minimisation routines such as the gradient or steepest-descent and Gauss-Newton can be used to

determine $\hat{\theta}_N$. This approach to estimation of parameter vector $\hat{\theta}_N$ is referred as the *prediction error method* (PEM).

Thus, the system identification process using the PEM can be summarised as follows:

(i) Choose a model structure and a predictor of the form in equations (3.2) and (3.3) respectively.

(ii) Select a *cost-function*, equation (3.10).

(iii) Form an initial estimate of $\hat{\theta}^{(1)}{}_N$ by a procedure outlined in [35]. The recommended approach leads to faster convergence of $\hat{\theta}_N$ and therefore, shorter computing time.

(iv) Then minimise $V_N(\theta)$ iteratively by one of the numerical methods, e.g. Gauss-Newton, until $\hat{\theta}_N$ converges.

(v) Substitute $\hat{\theta}_N$ in equation (3.3) and find the prediction errors $\varepsilon(t,\theta)$.

(vi) Carry out the residual tests of (3.9). If satisfactory go to model validation Section 3.3.4. If not change the model order and go to step (iii), iterate until equations (3.9a and 3.9b) are satisfied.

The PRBS signal was used for excitation and a multi-step input (3211) and a doublet were used for cross-validation. These signals along with their corresponding outputs are shown in Figures 3.7, 3.8, and 3.9 respectively. Initially a second-order ARMAX model with 9 time delay terms was investigated. This satisfied the residual tests criterion as well as described the dynamics reasonably well. However, a fourth-order model was employed, which gave better representation of system dynamics than the second-order model. The fourth-order model response can be seen in Figure 3.10. These results are discussed in more detail in the next section. Hence, subsequent investigations are based on the 4th order ARMAX model, using the MATLAB System Identification Toolbox [39]. The toolbox, utilises the prediction error method (PEM) to estimate the model parameters and incorporates IV method for the initial estimate of $\hat{\theta}^{(1)}{}_N$.

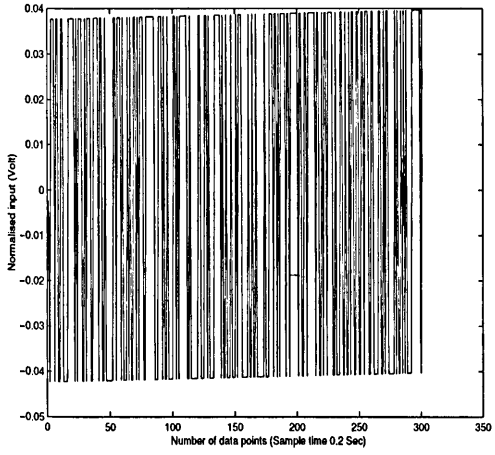

(a) PRBS input for system identification.

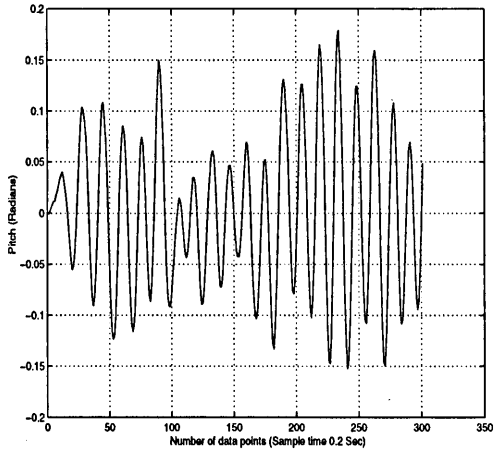

(b) System response to a PRBS input.

Figure 3.7. Input and output signals used for modelling.

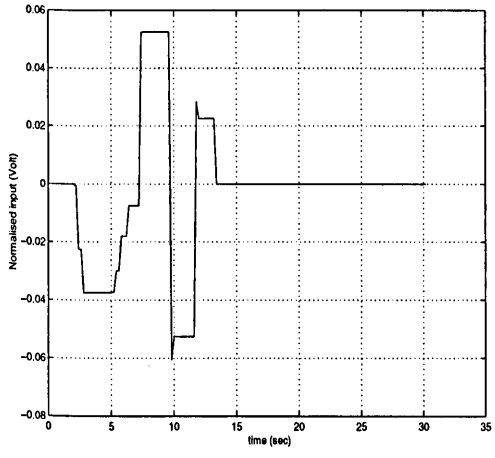

(a) Multi-step input (3211).

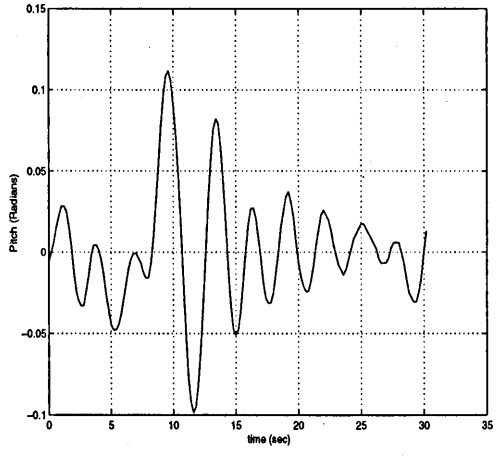

(b) System response to a multi-step input.

Figure 3.8. Input and output signals used for model cross validation.

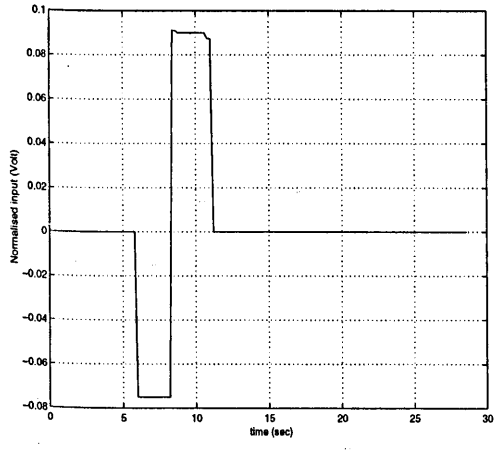

(a) Doublet input.

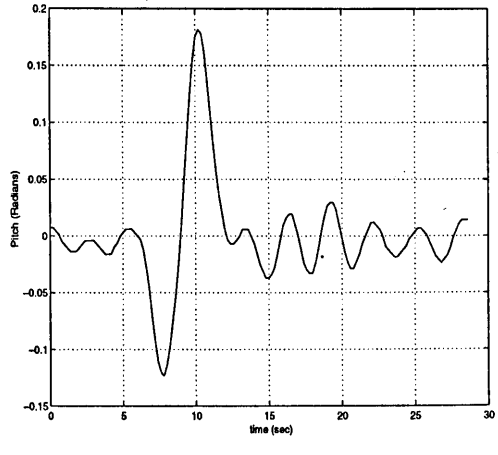

(b) System response to a doublet.

Figure 3.9. Input and output signals used for model cross validation.

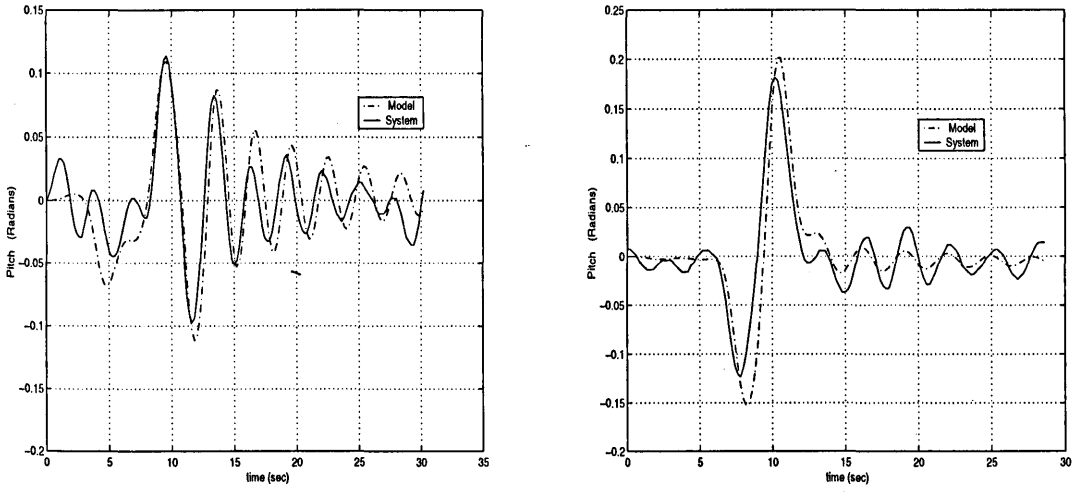

(a) with a 3211 input.

(b) with a doublet input.

Figure 3.10. The system and model response.

Figure 3.11(a) depicts the auto-correlation test of residuals, signifying that the noise has been modelled adequately as well as that the model order is appropriate. The cross-correlation function between the residuals and the input is shown in Figure 3.11(b), which is well within the 95% confidence band, marked by the dotted lines. Independence between residuals and past inputs is imperative and this is a measure of proper estimation of time delays. This model gives a reliable representation of the TRMS dynamics and, as will be shown next, has a high predictive capability.

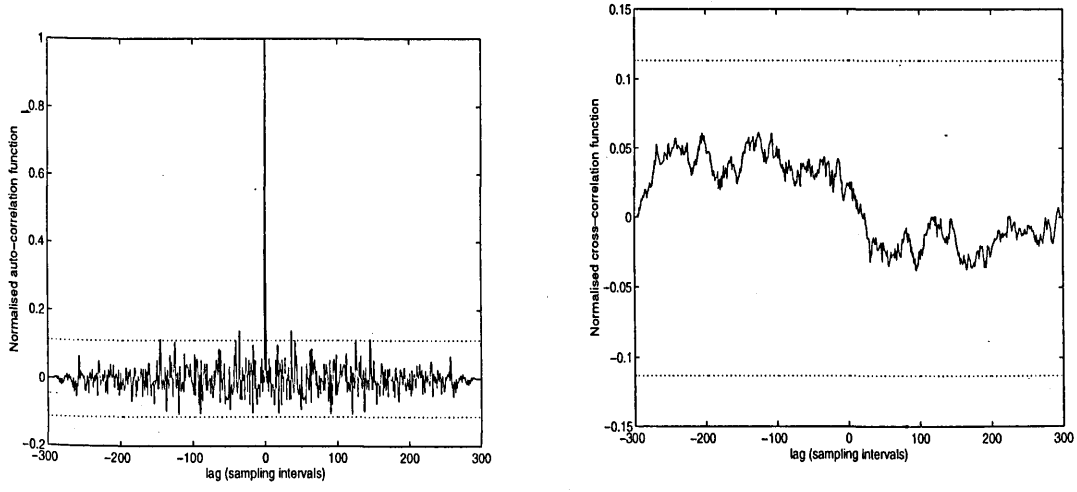

(a) Auto-correlation of residuals.

(b) Cross-correlation of input and residuals.

Figure 3.11. Residual test.

3.3.4 Time-domain validation

Verification is a key final step in a system identification process, which assesses the predictive quality of the extracted model. Data not used in the estimation is selected in order to ensure that the model is not tuned to specific data records or input forms. Major deficiencies in model structure and parameter estimates would give rise to obvious errors in the model output sequence. The excitation signal used in the comparison could be the same as was used to identify the model. In practice, it is desirable to obtain further plant responses to an excitation signal that has slightly different frequency components. In this cross-validation study, the model is tested against two different sets of input records, (i) multi-step input and (ii) doublet. In Figure 3.10 the simulated model output and the experimental outputs are compared. Figure 3.10(a) depicts the responses for a multi-step input and Figure 3.10(b) for a doublet. Overall, the predictive capability of the model is quite good, especially considering the sensitive nature of the TRMS to ambient disturbances. Although there are still some discrepancies, the overall agreement is satisfactory. These discrepancies can be attributed to i) mild oscillatory nature of the TRMS even in steady-state as well as being ii) very sensitive to the slightest atmospheric disturbance. The combined effect is reflected in these figures with the occasional rising peaks due to slight wind, even when the input signals have ceased to exist.

A few differences are worth noting. On the whole, the faster dynamics of the model do correspond well with the system results but the slower more dominant dynamics do not respond as well. However, it is presumed that the resulting model is suitable for further control analysis, as evident from the time domain cross-validation test (Figure 3.10).

3.3.5 Frequency domain validation

In frequency domain cross-validation tests, emphasis is placed on the ability of the model to predict system *modes*. Power spectral density plots of the plant and model outputs are superimposed and compared in Figure 3.12. It is noted that the dominant modes of the model and the plant coincide with one another quite well implying good model predicting capability of the important system dynamics. Thus, from the foregoing analysis it can be concluded that the model has captured the important plant dynamics quite well.

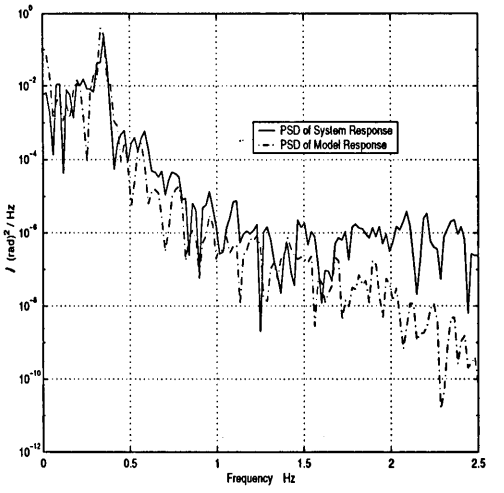

Figure 3.12. Frequency domain validation.

3.4 Two DOF modelling

Having successfully accomplished SISO modelling the same concept is applied for the MIMO plant.

3.4.1 Experimentation

The objective of the identification experiments in this Section is to estimate a LTI model of the 2 DOF TRMS. The yaw plane mechanical lock is released, allowing unrestricted 2 DOF movement in the pitch and the yaw plane. In Figure 3.13, the input signals *u1* and *u2* represent voltage inputs to the main rotor and tail rotor respectively. The outputs *y1* and *y2* represent pitch and yaw angles respectively. Strong coupling exists between the two channels, and this may be accounted for by representing the dynamics of the TRMS by the multivariable transfer-function model as given in Figure 3.13.

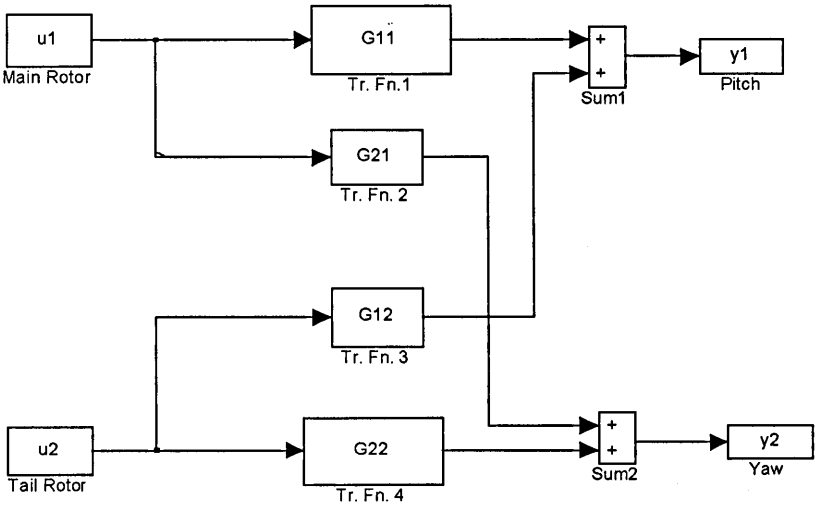

Figure 3.13. MIMO transfer function model.

3.4.2 Flight test data base

Having established trim, a predesigned input signal is given to one control input at a time. Note, that the pitch plane has faster dynamics than the yaw plane. Also, from the SISO modelling, it is evident that the significant plant dynamics lie between 0-1 Hz. Therefore, in order to excite the system within the dynamic range of interest i.e. up to 1 Hz, a pseudo-random binary sequence (PRBS) signal of 2 Hz band limit, instead of 5 Hz as in SISO case, and of smaller amplitude is applied to the controls so that the system remains in its linear operating region around the selected equilibrium (trim) point. The PRBS signal used in this work is shown in Figure 3.19(a). A simple approach is adopted, wherein the first channel is excited using the PRBS while the input to the second channel is held constant and responses are measured for the two outputs. The steady-state effects of the 2nd constant input signal on the 1st and 2nd output, via the transfer functions G12 and G22, are removed prior to fitting the model between *u1* → *y1*, and *u1* → *y2* channels. The experiments were then repeated for the second channel by keeping the first input constant. Similarly, the 1st input's steady state influence on the 1st and 2nd outputs, through the transfer functions G11 and G21, are removed prior to fitting the model between *u2* → *y1* and *u2* → y2 channels. This is accomplished by subtracting the mean values from the corresponding output signals. As described in

Chapter 2, the flow of signals to and from the system is via the MATLAB/Simulink interface.

3.4.3 Data reliability

Measurements used for system identification were pitch position *y1*, azimuth or yaw position *y2* in radians and controls *u1* and *u2* in volts. Input-output data quality is maintained by following a procedure similar to that adopted with the SISO case.

3.4.4 Sampling rate

The duration of the test signal was 120 seconds and a sampling interval of 10 Hz was chosen as a sampling frequency; 10 times the estimated bandwidth is found a good choice in most cases [35]. Although it has been shown in the SISO case, that 5 Hz sampling is good enough to capture the main system dynamics, a sampling period of 10 Hz is employed in this case. The reason for this is that, the frequency domain data analysis as carried out in this work, in particular the coherence function calculation, requires a large number of data points in order to avoid resolution bias error [38].

3.4.5 Coherence test for linearity

The linearity of the operating region is confirmed by a flat coherence of unity between the input PRBS signal and the output responses. Coherence spectra for the four channels are shown in Figure 3.14. Good excitation was achieved from 0-1 Hz, which includes all the important rigid body and main rotor dynamic modes. Strong interaction was observed among the channels *u1* → *y1*, *u1* → *y2* and *u2* → *y2*, but not the *u2* → *y1* channel. Non-interaction between *u2* → *y1* is clearly visible from Figure 3.15, as there is negligible pitch movement *y1* due to the PRBS input *u2*. Strong coupling is manifest from the coherence spectrum of near unity for *u1* → *y1*, *u1* → *y2* and *u2* → *y2* routes, at most frequencies of interest, i.e. 0-1 Hz. Since no strong coherence exists between the *u2* → *y1* channel, this channel was not investigated further for model fitting.

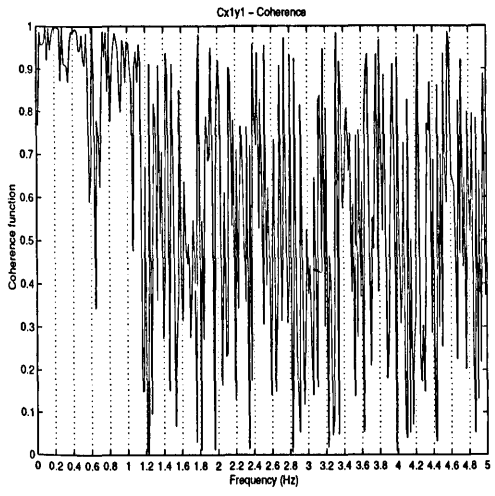

(a) Channel *u1* → *y1*.

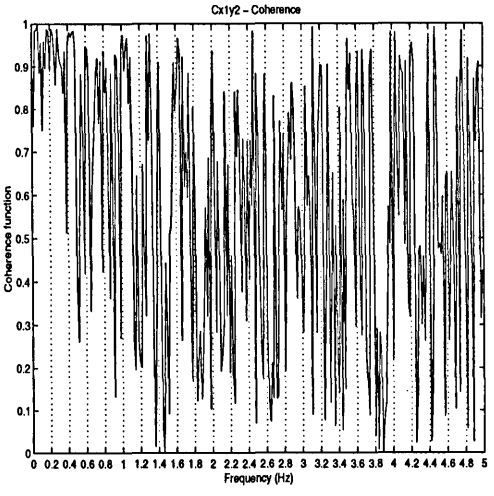

(b) Channel *u1* → *y2*.

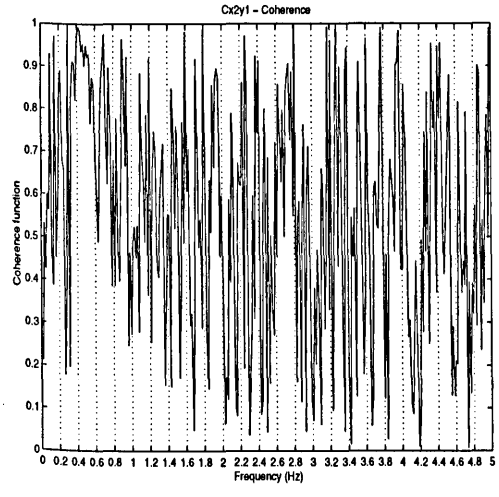

(c) Channel *u2* → *y1*.

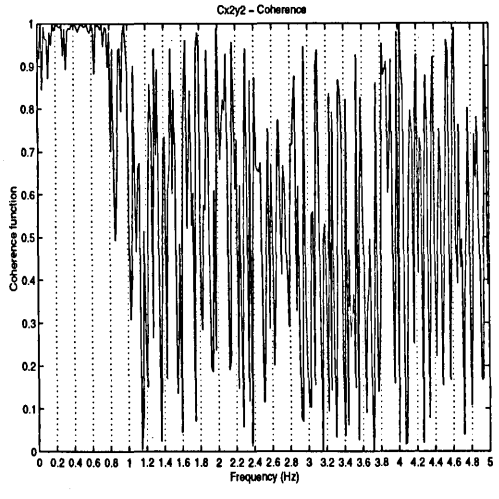

(d) Channel *u2* → *y2*.

Figure 3.14. Coherence spectrum.

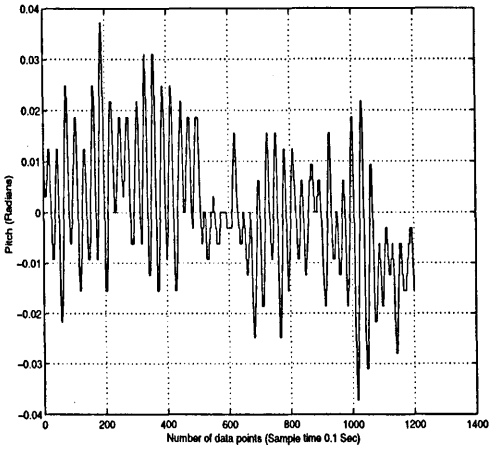

Figure 3.15. Pitch response for Channel *u2* → *y1*.

3.5 Results: 2 DOF

This section discusses the identification of the TRMS, which involves the three steps *characterisation*, *identification* and *verification*, as described in Section 3.3.

3.5.1 Mode or structure determination

The coherence spectra in Figure 3.14 and spectral density analyses of the system revealed that the information is good for most frequencies up to 1 Hz i.e. the bandwidth containing the dominant system modes. The power spectral density plot of the *pitch* (*y1*) and the *yaw* (*y2*) responses, Figure 3.16, to the PRBS input (*u1*) signal, shown in Figure 3.17, indicates that the dominant resonance modes of the system are located within 0-1 Hz, as expected. The pitch channel (*u1* → *y1*) has a main resonant mode at 0.34 Hz, and the yaw (*u1* → *y2*) channel at around 0.1 Hz. Hence, a 4th order model is expected, corresponding to one *resonance mode* at 0.34 Hz and one rigid body *pitch mode*, for the *u1* → *y1* channel. Similarly, a model order of 2 or 4 is anticipated for the *u1* → *y2* channel due to the presence of one *resonance mode* at 0.1 Hz and the *yaw rigid body mode.*

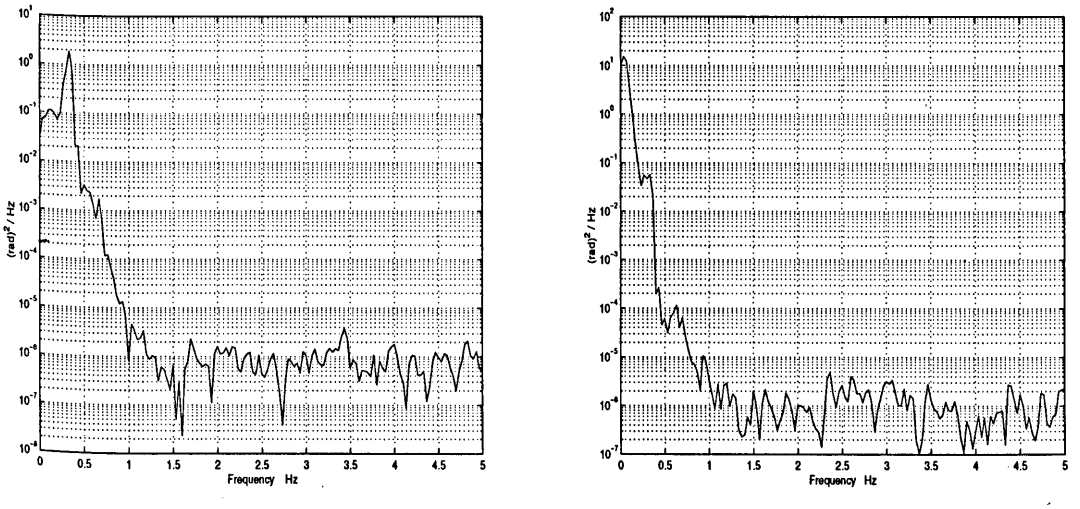

(a) Pitch response, *u1* → *y1*.

(b) Yaw response, *u1* → *y2*.

Figure 3.16. Power spectral density.

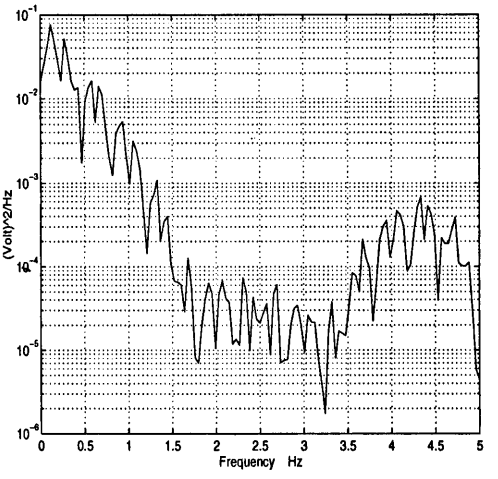

Figure 3.17. Spectral density of the PRBS input.

Again, for the 2nd input *u2* and 2nd output *y2* a model order of 2 or 4 is expected corresponding to the normal mode at 0.1 Hz, and a rigid body *yaw mode*, see Figure 3.18. The results of identification of system modes are summarised in Table 3.1.

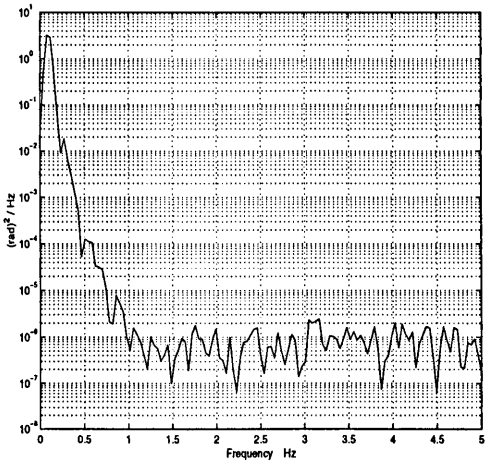

Yaw response *u2* → *y2*.

Figure 3.18. Power spectral density.

Channel	Identified system modes
u1 → *y1*	0.1 Hz and 0.34 Hz
u1 → *y2*	0.1 Hz
u2 → *y2*	0.1 Hz
u2→ *y1*	No cross coupling

Table 3.1. Identified natural frequencies.

3.5.2 Parametric modelling

Analogous to the SISO modelling procedure, each individual channel of the MIMO plant is considered at a time and parameters identified. The iterative parametric fitting exercise is terminated when the auto and the cross-correlation residual tests are satisfied.

3.5.3 Identification

The input signals utilised for identification and cross-validation are depicted in Figure 3.19. The corresponding ouput responses for the different channels are shown in Figures 3.20, 3.21 and 3.22. Referring to Figures 3.19 and 3.20, only 600 input-output data points were used for estimation of parameters, while the doublet signal was used for model cross-validation test for the input *u1* and the output *y1*. A 4^{th} order ARMAX model was found iteratively.

Figure 3.23(a) depicts the auto-correlation test of the residuals, signifying that the noise has been modelled adequately as well as that the model order is appropriate. The cross-correlation function between the residuals and the input is shown in Figure 3.23(b), which is well within the 95% confidence band, marked by the dotted lines. Independence between the residuals and past input is imperative, and this is a measure of proper estimation of time delays.

An analogous procedure was repeated for channels *u1* → *y2* and *u2* → y2. The test data used for identification and model cross-validation is that shown in Figures 3.19, 3.21 and 3.22. Finally, the residual test for the identified models is illustrated in Figures 3.24 and 3.25 respectively, for these two channels.

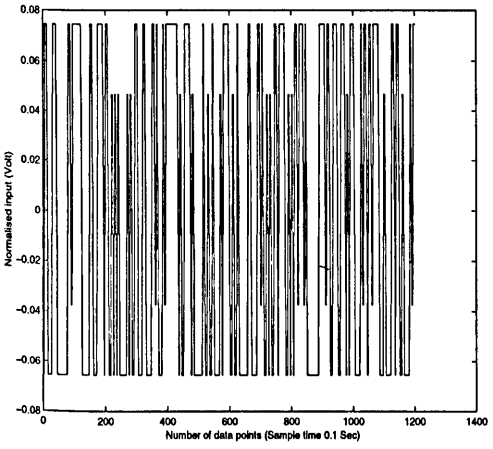

(a) PRBS input for system identification.

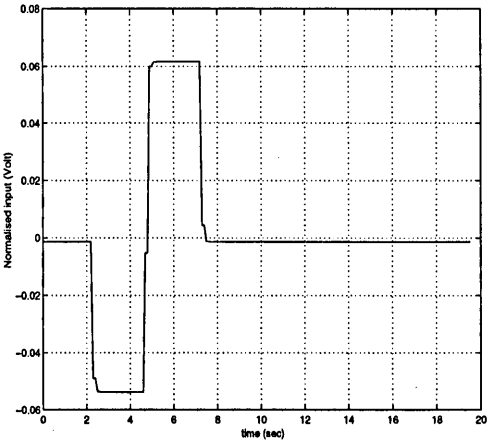

(b) Doublet input for cross- validation.

Figure 3.19. Input signals used for modelling

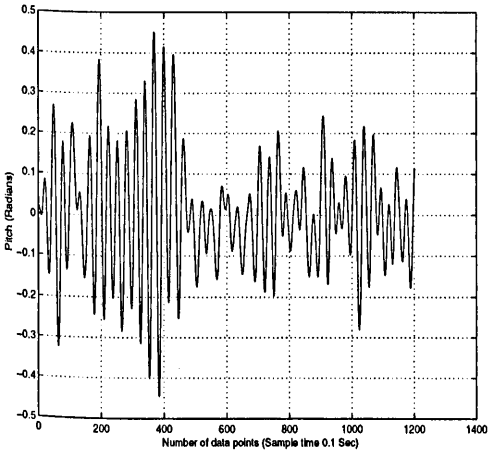

(a) System response to a PRBS input.

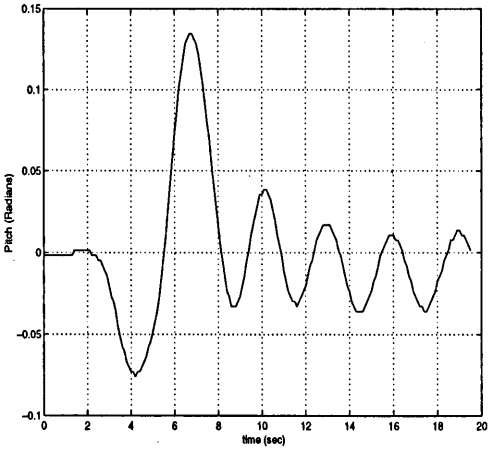

(b) System response to a doublet.

Figure 3.20. Output test data for channel *u1* → *y1*.

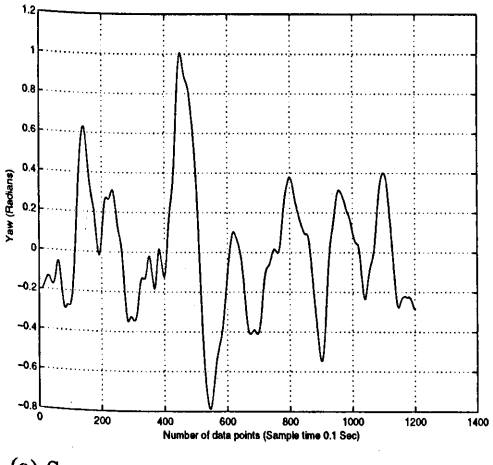

(a) System response to a PRBS input.

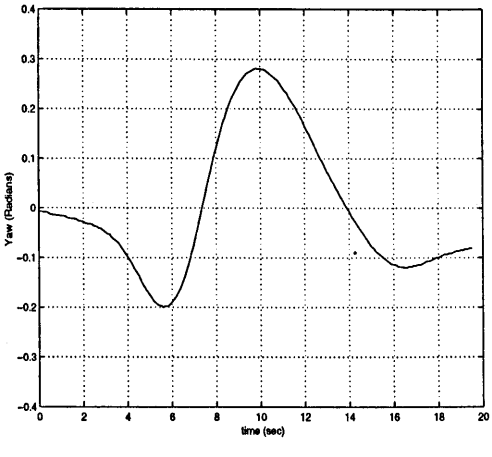

(b) System response to a doublet.

Figure 3.21. Output test data for channel *u1* → *y2*.

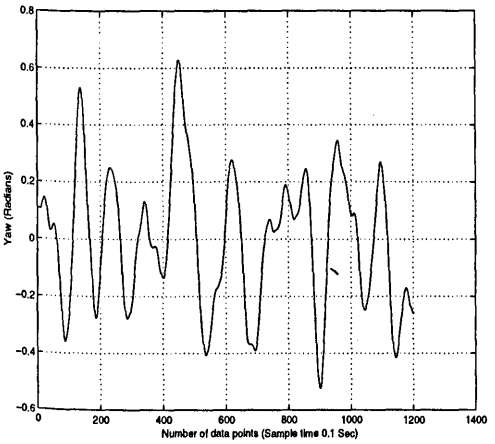

(a) System response to a PRBS input.

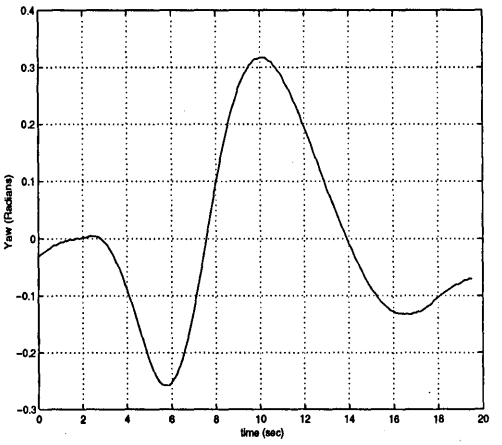

(b) System response to a doublet.

Figure 3.22. Output test data for channel *u2* → *y2*.

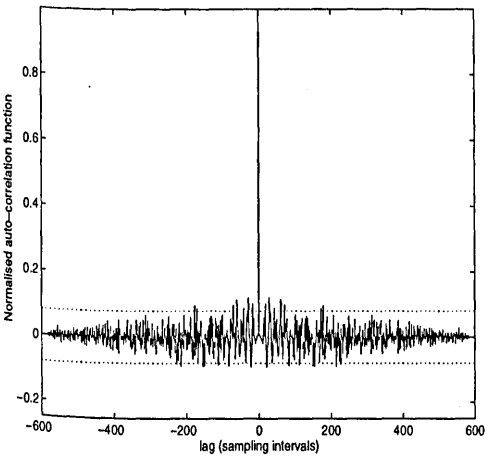

(a) Auto-correlation of residuals.

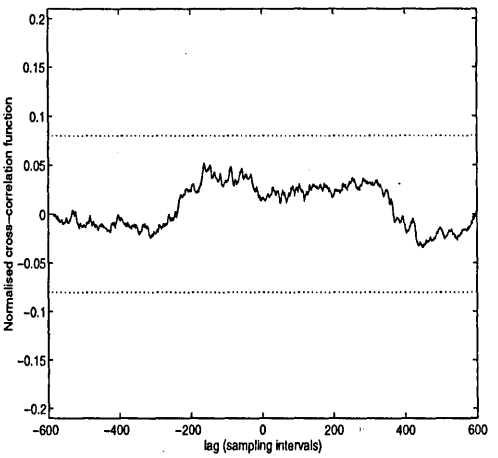

(b) Cross-correlation of residuals.

Figure 3.23. Residual test for Channel *u1* → *y1*.

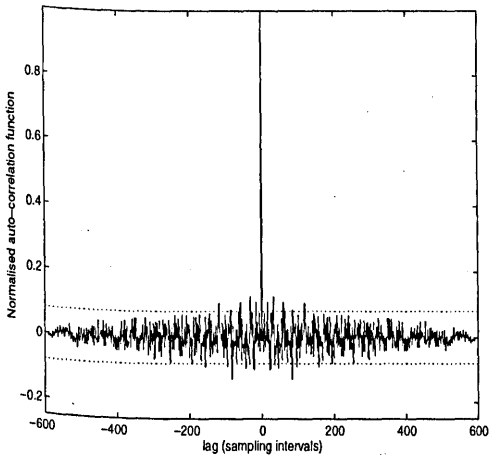

(a) Auto-correlation of residuals.

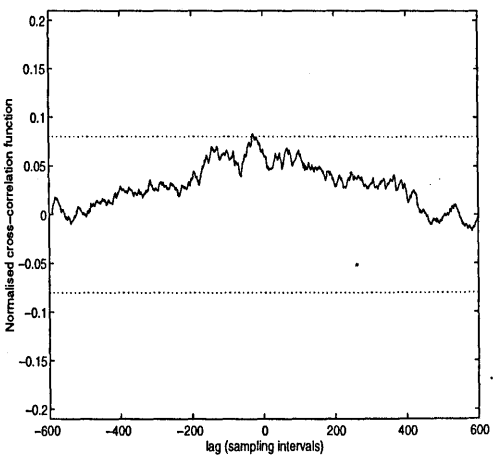

(b) Cross-correlation of residuals.

Figure 3.24. Residual test for channel *u1* → *y2*.

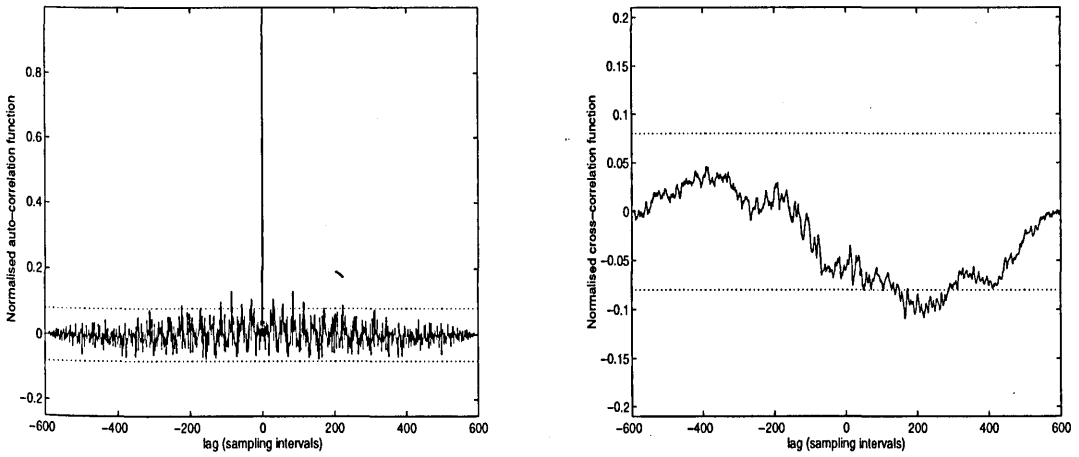

(a) Auto-correlation of residuals. (b) Cross-correlation of residuals.

Figure 3.25. Residual test for channel *u2* → *y2*.

3.5.4 Time-domain validation

In this cross-validation study, the model is tested against a doublet and shown in Figure 3.19(b). In Figure 3.26, the simulated model output and the experimental output are compared for the *u1* → *y1* channel. It is clearly noticed that, the predictive capability of the model is quite good, as the model closely follows the plant output. As is evident from the latter half of the dynamic response, i.e. between 10-20 seconds region, it is noted that even the slower dynamics of the plant are captured quite well by the model.

However as evident from Figure 3.27, the model response for *u1* → *y2* is not so good. This is most likely due to the unrestricted movement in the yaw plane, leading to nonlinearity. This will be discussed further in Section 3.5.5. Excellent model response was obtained for the *u2* → *y2* channel, as illustrated in Figure 3.28. The model response in Figure 3.28 clearly demonstrates the superior predictive capability of this model.

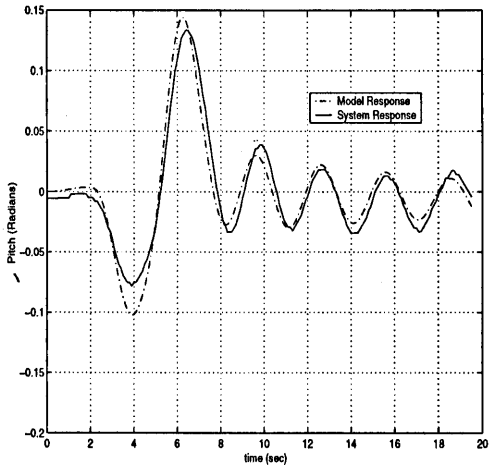

Figure 3.26. Response to a doublet, *u1* → *y1*.

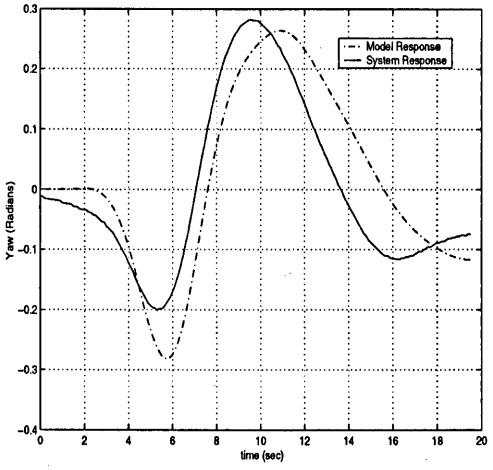

Figure 3.27. Response to a doublet, *u1* → *y2*.

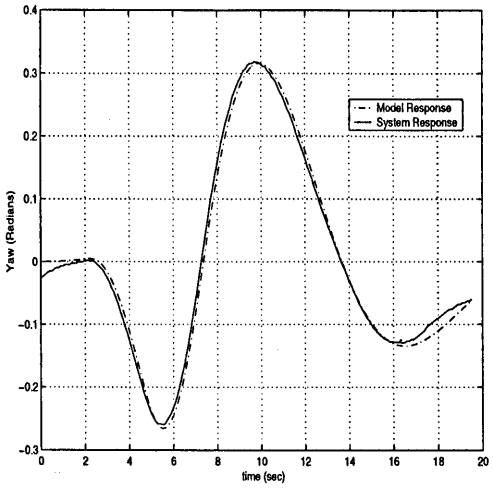

Figure 3.28. Response to a doublet, *u2* → *y2*.

3.5.5 Frequency domain validation

Power spectral density plots of the plant and model outputs are superimposed in Figure 3.29 for the *u1* → *y1*, *u1* → *y2* channels and in Figure 3.30 for the *u2* → *y2* channel. Note the presence of one common mode at 0.1 Hz in the *u1* → *y2* and *u2* → *y2* channels. This is because both channels describe the yaw motion although excited by different inputs. It is noted that the dominant modes of the model and the plant coincide quite well for the *u1* → *y1* channel, implying good model predicting capability of the important system dynamics. However, the spectral plot of the model indicates slightly higher magnitude for the *u1* → *y2* channel, Figure 3.29(b). The coherence spectrum shown in Figure 3.14(b), indicates a coherence lower than 1 in the proximity of the dominant mode i.e. 0.1 Hz. This could well be due to one or combination of reasons discussed in Section 3.2.5. Extraneous noise cannot be suspected as the coherence functions of the other channels are close to unity. At sharply peaked system resonance modes, the coherence functions - $\gamma^2_{xy}(f)$ will usually peak sharply corresponding to these resonance frequencies, because the signal-to-noise is highest at these frequencies. If $\gamma^2_{xy}(f)$ at such frequencies does not peak sharply, or worse yet notches, then system nonlinearities and resolution bias errors might be suspected [38]. Bias error is an unlikely candidate, as enough data points were used for coherence calculation. Thus, from the analysis, this test, indicates that there is a slightly nonlinear relationship between *u1* and *y2*, which may be the cause of poor model fit. However, the affect of external disturbances is not ruled out either.

The spectral plot in Figure 3.30 for the *u2* → *y2* channel also illustrates excellent agreement between the plant and the model modes, in the frequency range of interest i.e. 0-1 Hz. Thus, from the foregoing analysis it can be concluded that models have captured the important plant dynamics quite well.

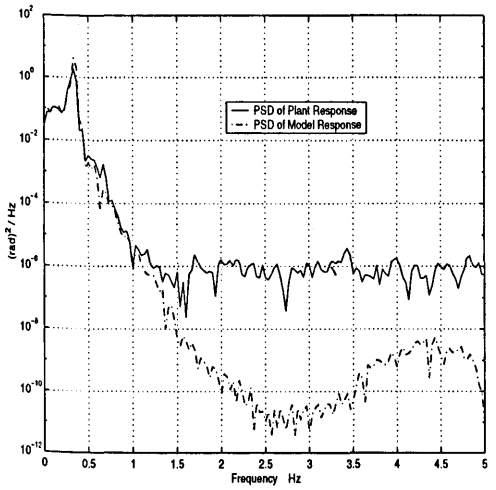

(a) Pitch response, *u1* → *y1*

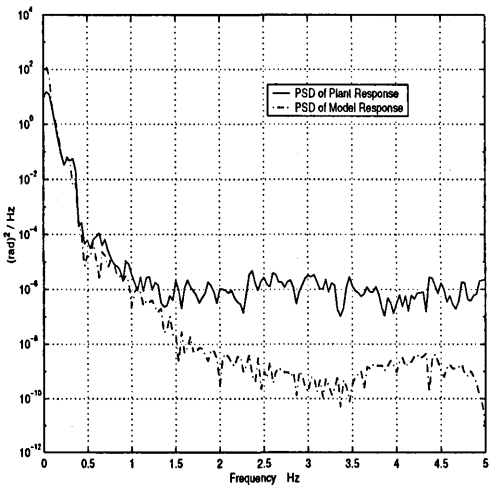

(b) Yaw response, *u1* → *y2*.

Figure 3.29. Power spectral density.

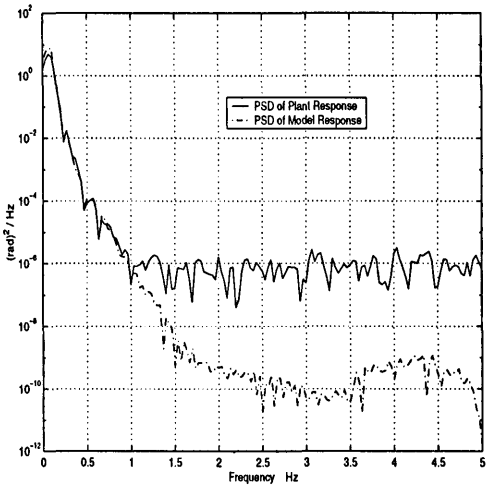

Yaw response, *u2* → *y2*.

Figure 3.30. Power spectral density.

3.6 Interpreting the 1 DOF black-box model

In this work, a black-box approach is adopted instead of conventional mathematical modelling process. However, it may be desirable to give physical meaning to the model coefficients and undertstand their influence on the vehicle motion. Such an understanding would aid in the system analysis, controller design and even redesigning or modifying the vehicle component(s) to achieve the desired system dynamic characteristics. Therefore, in this section an attempt is made to interpret the extracted black-box model, that is, to relate the parameters of the model to the actual system

dynamic behaviour. If one is only interested in an input-output representation of the pitch axis of the TRMS, a discrete-time transfer function can be obtained from the identified 1 DOF parametric model as:

$$\frac{y1}{u1} = \frac{0.0097z^3 - 0.0086z^2 + 0.006z + 0.0284}{z^4 - 3.0077z^3 + 3.5001z^2 - 1.8096z + 0.3407} \tag{3.11}$$

where, $y1$ = pitch angle, radians ; and
$u1$ = main rotor input, volts.

The coefficients of the transfer function in equation (3.11) have no physical meaning, but the dynamic characteristics of the system depend directly upon them, and it would be interesting to make it evident in the structure. Factoring the numerator and the denominator polynomials of equation (3.11) yields

$$\frac{y1}{u1} = \frac{(z - 9805 + 1.3281i)(z - 9805 - 1.3281i)(z + 1.0743)}{(z - 0.8926 - 0.4095i)(z - 0.8926 + 0.4095i)(z - 0.7541)(z - 0.4685)} \tag{3.12}$$

implying that the system has complex poles, refer Figure 3.4. Thus, bringing into evidence the (almost) unstable oscillatory mode, which is a significant dynamic characteristic of the TRMS and also of a helicopter in hover. The *oscillatory* or *vibrational* motion is imparted to the system due to flexible structural component(s). The complex poles in the characteristic equation are therefore, directly related to the physical properties of the structural material.

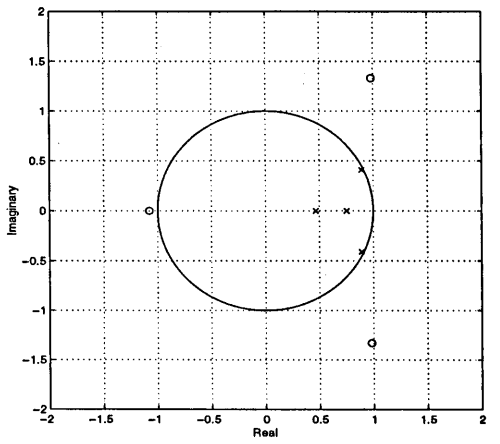

Figure 3.4. Pole-zero plot.

For a 1 DOF purely rigid body, it takes two state variables (one position and one velocity) to describe the motion of the body. Thus, the real poles in equation (3.12) represent two state variables which describe the *rigid body* motion, namely *pitch* angle (position) and *pitch* velocity. Note that the system is non-minimum phase, with zeros outside the unit circle. Interpretation of the black box model thus brings to the fore similar information as one would obtain from the mathematical modelling process.

Similar rational can be employed to seek physical reasoning for a 2 DOF model.

3.7 Concluding remarks

System identification is an ideal tool to model non-standard aircraft configurations, whose flight mechanics are not well understood. Linear system identification techniques have been investigated for modelling a 1 and a 2-DOF MIMO TRMS in hover, whose dynamics resemble those of a helicopter. Time domain linear system identification has been employed to obtain the parametric system models. These transfer functions are to be used for control applications. Both time and frequency domain analyses have been utilised to investigate and develop confidence in the models obtained. The frequency domain verification method is a useful tool in the validation of extracted parametric models. It allows high-fidelity verification of dynamic characteristics over a frequency range of interest. The extracted models have predicted the system behaviour well. The TRMS has a strong coupling between $u1 \rightarrow y1$, $u1 \rightarrow y2$ and $u2 \rightarrow y2$ channels. But there is a weak interaction between the $u2 \rightarrow y1$ channel, hence this path was omitted and no attempt was made to fit the model for this route. Moreover, identification of $u1 \rightarrow y2$ was imperfect which may be due to nonlinearity, external disturbances or combination of both. It is presumed that the resulting model is suitable for controller design, and accordingly the modelling approach presented is suitable for a certain class of new generation air vehicles.

An attempt was also made to relate the black-box model parameters to the actual plant dynamics, thus bringing into evidence the critically stable oscillatory mode, which is a significant dynamic characteristic of the TRMS. Similar interpretation can be easily extended to a 2 DOF TRMS model or any other higher DOF system using the black-box modelling approach presented here.

Chapter 4

Open-loop control design for vibration suppression

In Chapter 3, linear models of the TRMS were developed and found to have vibrational modes. The presence of resonance frequencies are undesirable in many engineering applications. An active vibration control paradigm is employed in this Chapter for attenuating the unwanted structural elastic modes. The TRMS residual oscillations are substantially reduced using the open-loop control technique, which utilises digital filters for shaping the command inputs. Open-loop study is often necessary for designing more complex feedback control laws.

4.1 Introduction

The successful completion of the modelling exercise leads to Step 2 of Figure 1.1 in the overall control system design process. The model analysis reveals the presence of flexible structural modes in both 1 and 2 DOF models as seen from the spectral plots of the TRMS output (pitch and yaw) responses of Figures 3.2(b), 3.16 and 3.18. The lightly damped natural frequency of oscillation of the TRMS arising from the structural (main beam) elasticity, induces undesirable residual vibration. In general, the residual motion (vibration) is induced in flexible structures primarily as a result of faster motion commands. The occurrence of any vibration after the commanded position has reached will necessitate additional settling time before a new manoeuvres may be initiated. Therefore, in order to achieve fast system response to command input signals, it is imperative to reduce this vibration. Although, vibrations are undesirable, light weight yet strong flexible structures along with other associated advantages like low energy consumption and smaller actuator requirements, are highly desirable in a number of modern systems such as spacecraft with flexible appendages [13-15], robotics [10-12], flexible aircraft [16,17] and flexible missile and launch vehicle [20].

Fast speed of response is another important characteristics imparted to the system due to flexible material. Essentially, the choice of the physical parameters, for example mass, stiffness and damping factor of the material, determine the response of the system. The choice of these parameters can be thought of as *passive control.* For example, adding mass to the TRMS main beam would lower its natural frequency. If adding the mass is not practical, such as in the case of most aerospace structures, a common and and very effective way to reduce transient and steady-state vibration is to increase the amount of damping in the structure so that there is greater energy dissipation. A damping treatment consists of adding a layer of visco-elastic material, such as rubber, to an existing structure. The combined system often has a higher damping level and thus reduces unwanted vibration. Thus, passive control in essence involves changing the physical parameters of the material to attenuate structural vibrations. Hybrid approaches involving passive and active (discussed next) control techniques have been found to be ideal for damping the vibration modes of civil structures such as high rise buildings [40,41].

If the materials are fixed for a given system, such as the TRMS, it is difficult to change the mass and stiffness of the system by more than a few percent. Despite this constraint, it is often possible that the desired system response can be achieved with *active control.* Active control employes external adjustable or *active* devices, *actuator* (for e.g, electric motors, hydrulic pistons, piezo-electric devices etc.,) to provide a force to the structure, machine or the device whose vibration properties are to be altered. In this work, active control option is considered without resorting to changing the physical properties of the TRMS. Active control can be broadly categorise as open-loop (feedforward), closed-loop (feedback) or combination of feedforward and feedback methods. Open-loop control is the subject matter of this Chapter, feedback and combined feedforward and feedback topologies are presented in Chapter 6. The feedback and combined feedforward and feedback controllers are implemented on the TRMS rig and results described in Chapter 7.

Vibration control by open-loop or feedforward methods, essentially consists of manipulating the input signal to the plant by investigating the physical and vibrational properties of the flexible system. The goal of this input shaping control is to avoid excitation of the residual vibration at the end of the manoeuvre. Early papers on input shaping considers feedforward control defined by a finite expansion, e.g. trignometric

[42], that minimises the frequency content over a wide range of frequencies, but requires longer time to complete the motion. More recently, Suk *et al* [43] designed and implemented an optimal shaped input torque based on a trignometric series expansion for simultaneous slewing and vibration suppression of flexible structures. They also incorporated a feedback loop to achieve the desired set-point tracking. Another approach based on trignometric series expansion is the work of Meck *et al* [44]. Later, a version of the same approach using a pulse sequence expansion was proposed by Singer and Seering [45]. It is well known that when two signals are convolved the resulting signal will have a spectra which will produce a zero excitation at frequencies where one or the other of the original signal spectra is zero. Singer and Seering[45], Watkins and Yurkovich [46] and Tzes and Yurkovich [47], made use of this fact in their work by convolving the command signal with a pulse sequence. The result of the convolution is used to drive the system. Therefore, the computation of the appropriate pulse sequence can be considered as the design of a notch filter to remove the resonance excitation from the command signal. In a relatively recent paper, Banerjee and Singhose [48] applied the same technique for end point tracking of a two link flexible robot with a feedback control. They showed that the input shaping of closed-loop control modes gave a robust performance and improved tracking.

Tzse and Yurkovich [47] investigated an adaptive input shaping strategy for vibration attenuation in a slewing flexible structure. In the case of a change in payload or modelling errors, the proposed scheme integrates a frequency domain identification technique along with the input shaping, in order to adjust parameters of the input shapers. The problem of active noise control of multi-degree-of-freedom high rise buildings is considered by [41], who employed direct model reference adaptive control (DMRAC) on a spring-mass-damper system representing a building. The adaptive scheme was shown to yield good disturbance rejection to earthquake and wind effects. Note, that the above frequency-based input shaping methods are only applicable to linear systems. For nonlinear flexible systems, Gorinvesky and Vukovich [49], trained a neural network to obtain the desired system's output trajectory. More recently, Tokhi *et al* [50] employed Multi Layer Perceptron (MLP) to model the inverse plant dyanmics, which in turn is used to cancel out the dominant plant vibrational frequency from the input signal. An adaptive feedback mechanism is also incorporated to address changing plant parameters at different payloads. However, the simplest method to achieve the resonance suppression is via classical digital filters, such as the Butterworth, elliptic and Chebyshev. This concept was demonstrated by [10,11] on a single-link flexible

manipulator.

The remainder of this Chapter develops and applies a feedforward control technique which is related to a number of approaches known as "input shaping control", discussed above. The goal of the open-loop control is to shape the input signal so as to avoid excitation of residual vibrations during and at the end of the plant manoeuvre. The fundamental concept for this type of control is based on the well established theory of digital filters. In these method, a feedforward input signal is shaped so that it does not contain spectral components at the system's resonant eigen-frequencies. The approach requires that the natural resonant frequencies, such as those used in Chapter 3, of the system be determined through suitable identification and modelling techniques. Investigation of SISO and MIMO open-loop control is a prelude to subsequent development of more complex multivariable feedback control laws.

The Chapter is organised as follows: Section 4.2 analyses the TRMS vibrational modes. Section 4.3 discusses digital filters used for command shaping. Section 4.4 and 4.6 discusses filter design, implementation and results. A 2 DOF coupling anaysis is presented in Section 4.5 prior to 2 DOF experiments. Finally, Section 4.8 concludes the work.

4.2 The TRMS vibration mode analysis

In general, for flexible structures/aircraft the parameters which have an influence on the flexible modes are the mass distribution, which may change the frequencies of the modes, the accuracy of the model. For an aircraft, altitude and Mach number also have an influence on the system modes. This is relevant to the TRMS which can be interpreted as a centrally supported cantilever beam with loads (rotors) at both ends. The non-uniform mass distribution due to the rotors and the rotor torque at normal operating conditions are the main causes of beam deflection, which in turn causes vibration. A schematic of a flexible system is illustrated in Figure 4.1. In this Figure u is the rotor input and y is the combined output due to rigid-body as well as elastic motion.

In conventional resonance, a dynamic system is excited by a fluctuating input, the frequency of which is equal to the natural frequency of the dynamic system. The TRMS could oscillate and become unstable if its natural frequency of oscillation is close or

within the frequency range of the disturbance/excitation due to the rotor.

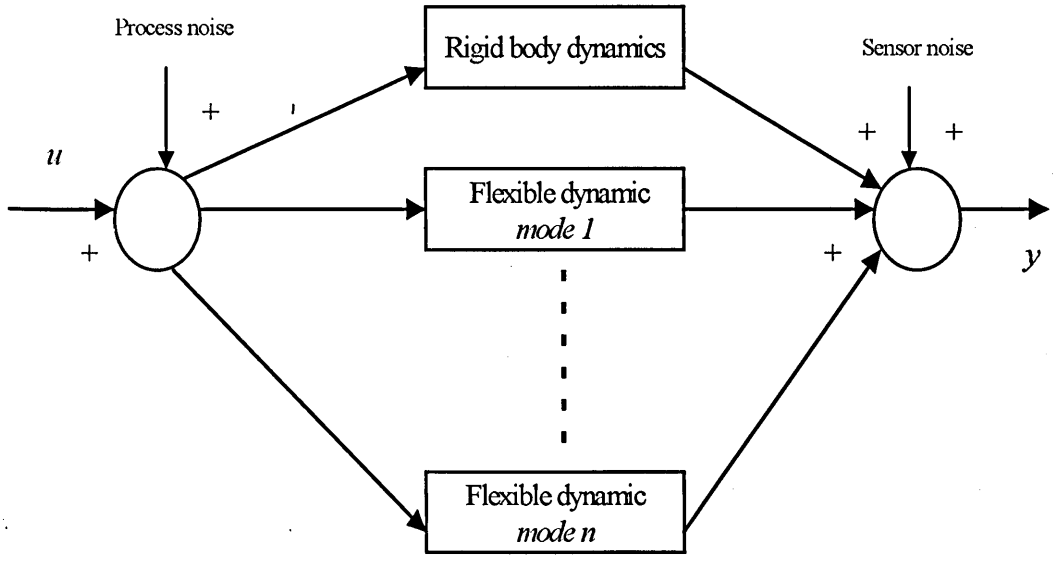

Figure 4.1. A generic schematic of a flexible system.

A system or a structure will oscillate, and could become unstable, due to the excitation of the *resonance modes* by an input signal or disturbance that is rich in system's eigenfrequencies. Hence, accurate identification and subsequent processing of these modes is important from a systems engineering perspective. In particular, this is important for designing control laws to ensure that structural component limits and fatigue loads are not exceeded for the full operating range of aircraft/TRMS manoeuvres. Moreover, this will be useful for minimizing structural damage via resonant modes suppression, reduction in pilot workload and passenger comfort in the case of an aircraft. Similar advantages will result for other systems with elastic modes.

4.3 Digital filters for command shaping

In order to filter out the input energy at the system's natural frequencies two different mechanism can be adopted. The first approach is to pass the command signal through a low-pass filter. This will attenuate input energy at all frequencies above the filter cut-off

frequency. The important consideration is to achieve a steep roll-off rate at the cut-off frequency so that the input energy can be passed for frequencies close to the lowest natural frequency of the TRMS. Another approach that can be employed to attenuate input energy at plant natural frequencies is to use band-stop filters with centre frequencies at selected significant resonance modes of the TRMS. The block diagram of Figure 4.2 shows this approach, where the input is passsed through a filter, resulting in an output which has predominantly rigid-body dynamics y_f.

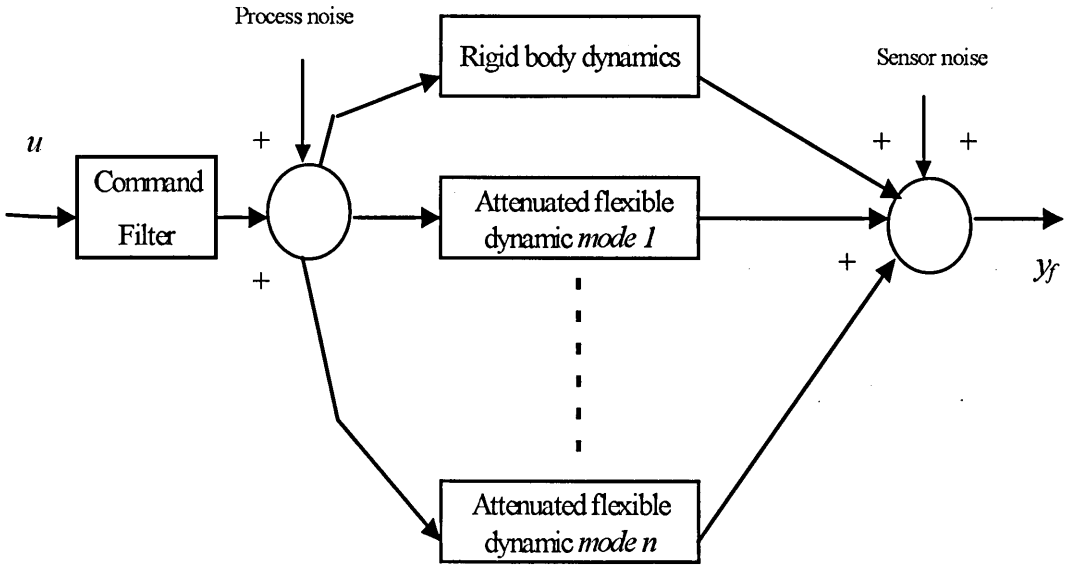

Figure 4.2. Open-loop control scheme.

Different types of filters, such as Butterworth, elliptic and Chebyshev can be used. In this study mainly Butterworth type filter is employed because of its simple design and in particular as its pass-band and stop-band are without ripples. The elliptic type filter is also employed as a band-stop filter in the latter part of this work, primarily because it has a short transition region from pass-band to stop-band.

4.3.1 Butterworth filter

The Butterworth filter is popular because its passband and stopband are without ripples. The Butterworth is called the *maximally flat filter* because of this lack of rippling. However, the Butterworth filter achieves its flatness at the expense of a realtively wide

transition region. This filter has only two design parameters: the order of the filter and the filter's cut-off frequency, ω_C. The order of the filter is also the number of poles for the filter and it determines its complexity. The Butterworth filter is defined by the following squared transfer function, where, n is the order of the filter and ω_C, is the filter cut-off frequency.

$$|H_B(s)|^2 = H_B(s)H^*_B = H_B(j\omega)H_B(-j\omega) = \frac{1}{1+\left(\frac{s}{j\omega_C}\right)^{2n}} \tag{4.1}$$

The magnitude-squared of the Butterworth's frequency response is its squared transfer function, equation 4.1 with s replaced by $j\omega$.

$$|H_B(j\omega)|^2 = \frac{1}{1+\left(\frac{\omega}{\omega_C}\right)^{2n}} \tag{4.2}$$

4.3.2 Elliptic filter

The elliptic filter has the shortest transition region from pass-band to stop-band of any filter with the same order and ripple heights. The elliptic design is optimum in this sense. Therefore, the elliptic filter is ideal for those applications where ripples can be tolerated and short transition regions are demanded.

The magnitude squared transfer function of the elliptic filter is as follows:

$$|H_E(j\omega)|^2 = \frac{1}{1+\varepsilon^2\left[R_n\left(\frac{\omega}{\omega_C}, L\right)\right]^2} \tag{4.3}$$

Where, the parameter ε controls the height of ripples and ω_C controls the frequency breakpoint. R_n is a rational function, the parameter L controls the width of the

transition region, the ripple height in the stop-band, and interacts with ω_c to affect the breakpoint [51]. The design of elliptic filters is much more complex than the Butterworth and Chebyshev types. This is because the designer must select the order of the filter, the cut-off frequency, and the parameter L . The design is further complicated because ω_c and L interact in determining the filter's breakpoint. For this reason, elliptic filters are designed via design tables as given in most standard textbooks [52].

In carrying out experimental investigation for open-loop control, an approach similar to that used for modelling is adopted. Initially, a 1 DOF configuration is considered by physically locking the other degree-of-freedom, thereby restricting the horizontal direction yaw movement. Subsequently, experiments are conducted for a 2 DOF TRMS, allowing movement in both the horizontal and vertical planes. Note, that the significant modes of the TRMS identified in Chapter 3 that need attenuation are given in Table 4.1 for 1 and 2 DOF plant respectively. Also, anologous to modelling, the sampling interval of 5 Hz is employed for 1 DOF and 10 Hz for 2 DOF control experiments. In both these experiments, the TRMS operating point is the flat horizontal position of the beam.

DOF	Channel	Identified system modes
One	*u1* → *y1*	0.25 and 0.34 Hz.
Two	*u1* → *y1*	0.1 Hz and 0.34 Hz
	u1 → *y2*	0.1 Hz
	u2 → *y2*	0.1 Hz
	u2→ *y1*	No cross coupling

Table 4.1. Identified natural frequencies.

4.4 Filter implementation and results: 1 DOF TRMS

To initially study system performance, an unshaped doublet input is used, and the corresponding pitch response is measured. The main objective of this section is to suppress the system vibrations at the first few dominant resonance modes. Note, in this case the yaw plane is clamped and is therefore not considered. The input is the voltage to the main rotor and output is the vertical pitch motion.

4.4.1 Low-pass shaped input

A low-pass Butterworth filter of order three with a cut-off frequency at 0.1 Hz was designed and employed for processing the doublet input. The motive behind selecting the cut-off frequency at 0.1 Hz lies in the fact that the lowest vibrational mode of the system is found to be at 0.25 Hz. Hence, to attenuate resonance of the system the cut-off frequency must be selected lower than the lowest vibrational mode. The shaped doublet input is then injected to the TRMS and the pitch response is measured. The low-pass Butterworth filtered doublet is shown in Figure 4.3(a). It is observed from the power spectral density (PSD) plot 4.3(b), that the spectral energy input at the first (0.25 Hz) and higher resonance frequencies of the system is reduced significantly with the low-pass Butterworth filter doublet input as compared to the unshaped doublet. Removal of high frequency components is clearly visible from the time domain plot of the doublet. Note the disappearance of high frequency sharp edges of the input signal. From the corresponding pitch response in Figure 4.4, it is noticed that the final steady state of response has reached approximately 10 seconds early, in contrast to the unshaped input response. Vibrations in the pitch response of the system, however, have significantly been reduced, specially at higher modes. It is noted that the attenuation in the level of vibration at the first and second resonance modes of the system are 5.83 dB and 7 dB respectively, (see Figure 4.4), with the shaped input in comparison to the unshaped doublet.

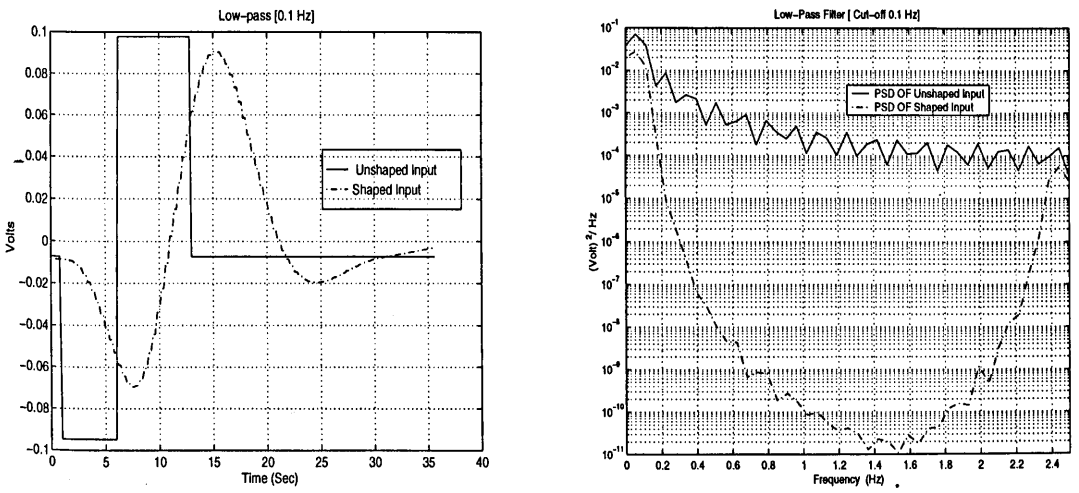

(a) Time domain. (b) Power spectral density.

Figure 4.3. Doublet input using a low-pass filter.

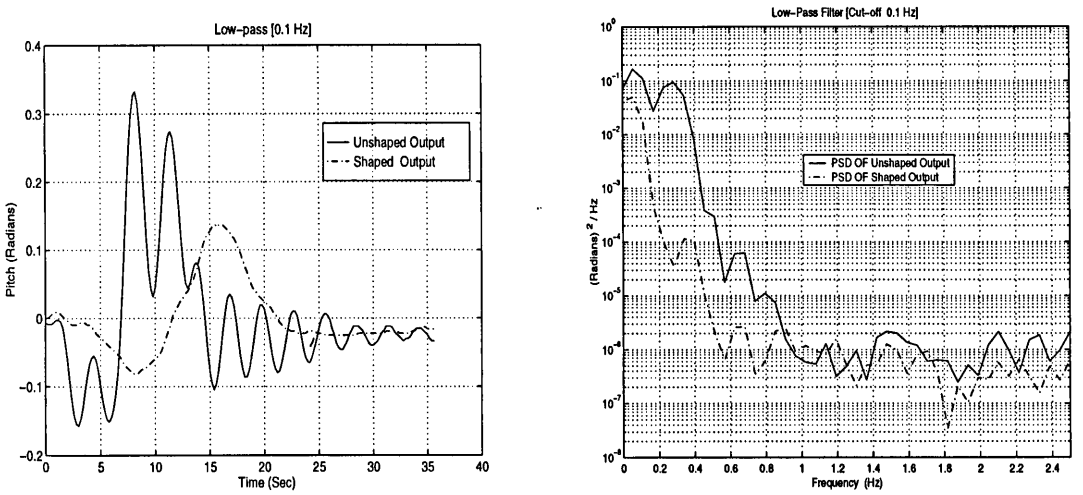

(a) Time domain. (b) Power spectral density.

Figure 4.4. Pitch Response to a low-pass doublet input.

4.4.2 Band-stop shaped input

As above, a third order digital Butterworth filter is used to study the TRMS performance with a band-stop shaped input. For effective suppression of the vibrations of the system, the centre frequency of the band-stop filter has to be at exactly the same frequency or as close as possible to the resonant modes. From the modelling study of the last Chapter (Section 3.2, Figure 3.2(b)) it is observed that the main resonant mode lies at 0.34 Hz, with additional clustered modes in a close proximity to the main mode. Thus, a band-stop frequency range of 0.2 to 0.4 Hz was selected for the filter design. The filter is then used for pre-processing the doublet input, and the result is fed to the plant. The dashed lines in Figure 4.5 represents the generated doublet input using band-stop Butterworth filter. Analogous to low-pass filtered input, the high frequency components are replaced by smoother input profile. The corresponding pitch response is measured and shown in Figure 4.6. It is noted that the spectral attenuation in the level of system vibration at the first and second mode are 0.83 dB and 1.8 dB, respectively as can be observed from Figure 4.6. The speed of pitch response is faster than the Butterworth low-pass filtered doublet in Figure 4.4. However, the final settling time is almost identical in the two cases. The results are tabulated in Table 4.2.

Channel	Modes-Hz	Band-stop Filter Attenuation	Low-Pass Filter
		Filter [0.2-0.4] Hz	Cut-off [0.1] Hz
u1→ y1	0.25	0.83 dB	5.83 dB
	0.34	1.83 dB	7 dB

Table 4.2: SISO open-loop control: mode attenuation.

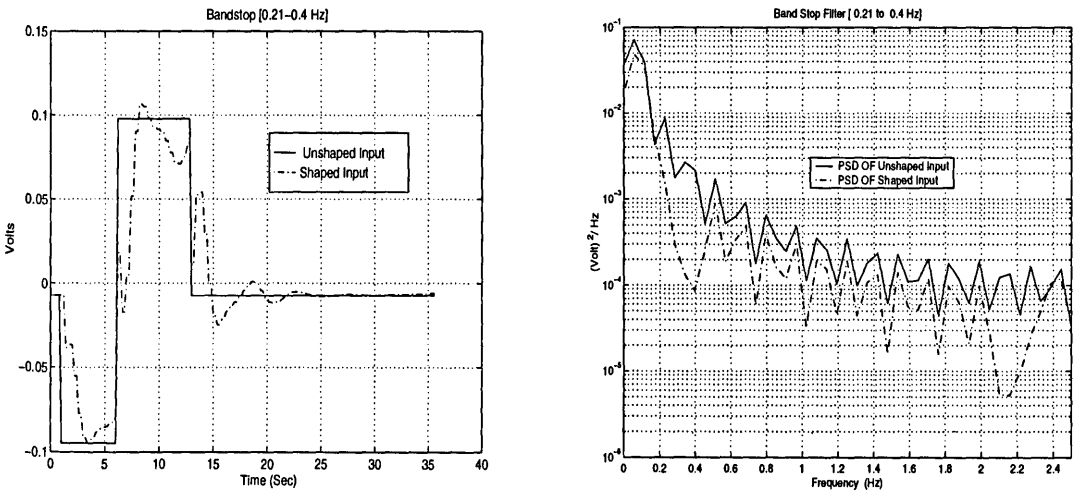

(a) Time domain. (b) Power spectral density.

Figure 4.5. Doublet input using bandstop filter.

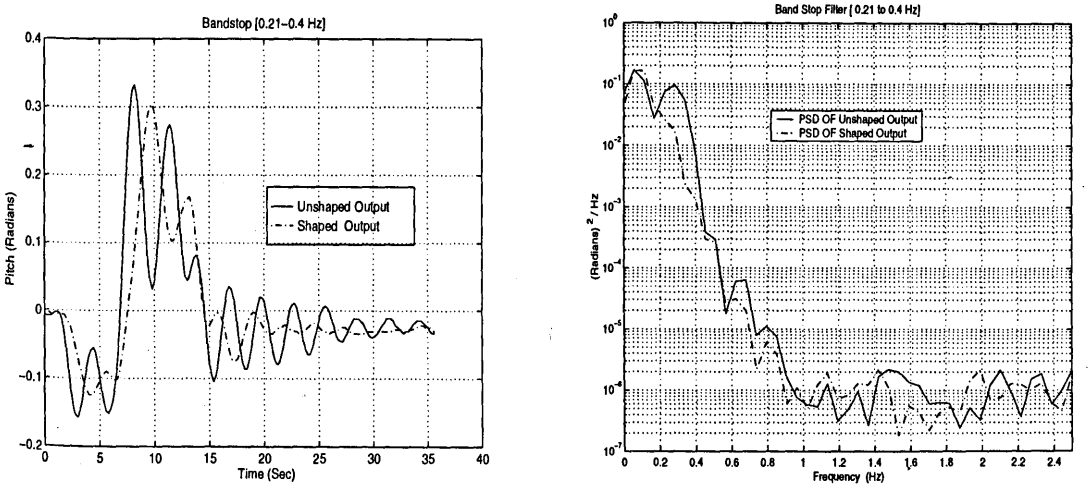

(a) Time domain. (b) Power spectral density.

Figure 4.6 . Pitch Response to a band-stop filtered doublet input.

4.5 Coupling analysis for a 2-DOF TRMS

The two modes of operation of the TRMS i.e. rotation in the vertical plane (*pitch*) and rotation in the horizontal plane (*yaw*), exhibit strong modal coupling. This coupling directly influences the velocities of the TRMS in both planes. The cross-coupling between the *u1* → *y2* channel exists in the frequency range of interest i.e. 0-1 Hz, and is evident from the coherence spectrum of Figure 4.7. The coherence of one indicates (coupled) a linear relationship between the two signals. If the coherence function is equal to zero, it implies that the two signals are completely unrelated.

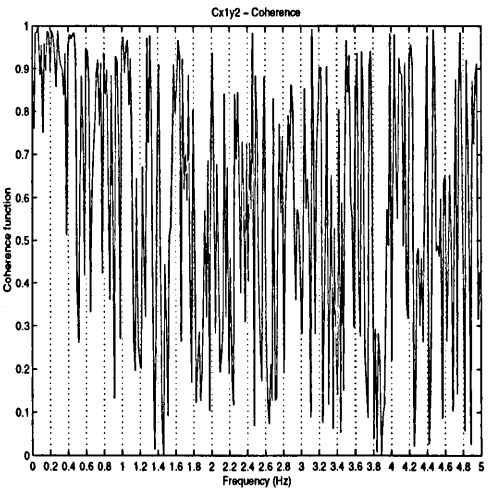

Figure 4.7. Coherence spectrum, *u1* → *y2* channel.

The implication of this coupling is that if motion in one direction contains energy at frequencies corresponding to mode shapes in another direction, then that motion will produce vibration in the other direction and could lead to instability. Hence, accurate identification and subsequent processing of these modes is important from a systems engineering perspective. As indicated in the previous Chapter, there is no strong coupling between the *u2* → *y1* channel therefore it will not be considered for control here.

4.6 Filter implementation and results: 2 DOF TRMS

To study the 2 DOF system performance, like the 1 DOF experiments, initially an unshaped doublet input shown in Figure 4.8 is used to drive the main rotor (*u1*), while input to the tail rotor (*u2*) is kept constant. The corresponding system responses *y1* and *y2* are measured and shown by the solid lines of Figures 4.9 and 4.10 respectively. The

responses overshoots and shows considerable residual vibration, with dominating modes at 0.1 Hz and 0.34 Hz. The procedure is then repeated, exciting the tail rotor (*u2*), using the same input, as above, while maintaining (*u1*) constant. The response *y2* is shown in Figure 4. 11 by solid lines. Even here the response overshoots, however with mild residual vibration. The dominant mode in this axis lies at 0.1 Hz. The main objective of this section is to suppress the system vibrations at the first few dominant resonance modes in both axes simultaneously.

4.6.1 Low-pass shaped input

A low-pass Butterworth filter of order three with a cut-off frequency at 0.05 Hz was designed and employed for off-line processing the doublet input. The motive behind selecting the cut-off frequency at 0.05 Hz lies in the fact that the lowest vibrational mode of the system is found to be at 0.1 Hz. Hence, to attenuate resonance of the system the cut-off frequency must be selected lower than the lowest vibrational mode. The shaped doublet input is then injected in the main rotor (*u1*) of the TRMS and the *pitch* (*y1*) and *yaw* (*y2*) responses are measured. The low-pass Butterworth filtered doublet is shown in Figure 4.8 and the corresponding *pitch* and *yaw* responses in Figure 4.9 and 4.10. It is noted that the attenuation in the level of vibration at the first and second resonance modes of the *u1* → *y1* channel are 10.45 dB and 20.91 dB respectively, as shown in Figure 4.9, with the shaped input in comparison to the unshaped doublet. An attenuation of 24.22 dB is achieved for the *u1* → *y2* channel, see Figure 4.10.

For the *u2* → *y2* channel, a spectral attenuation of 10.63 dB is obtained using the shaped input as is shown in Figure 4.11. Notice that the cut-off frequency of 0.05 Hz, which is very close to the rigid-body motion dynamics, results in substantial attenuation of the input to the rigid-body mode. This is reflected in the low magnitude responses as compared to the unshaped responses.

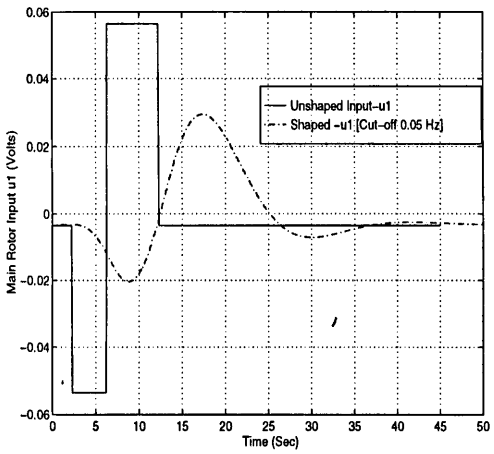

(a) Time domain.

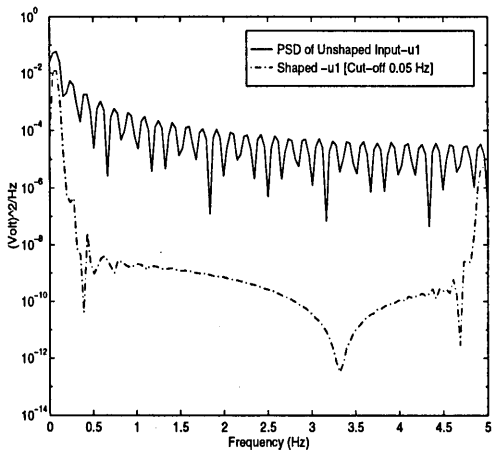

(b) Power spectral density.

Figure 4.8. Doublet input using a low-pass filter.

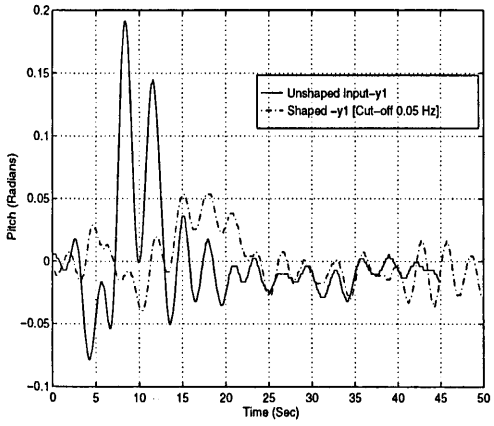

(a) Time domain.

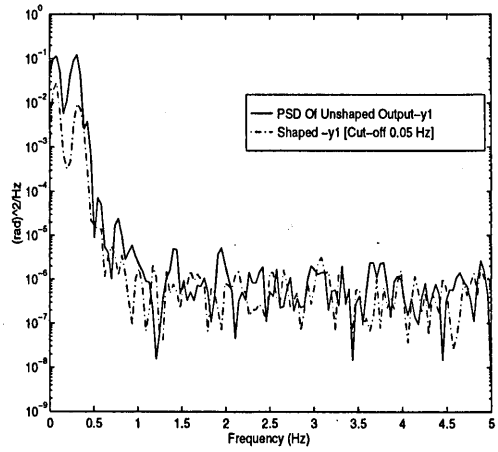

(b) Power spectral density.

Figure 4.9. Pitch response to a low-pass doublet input, *u1* → *y1*.

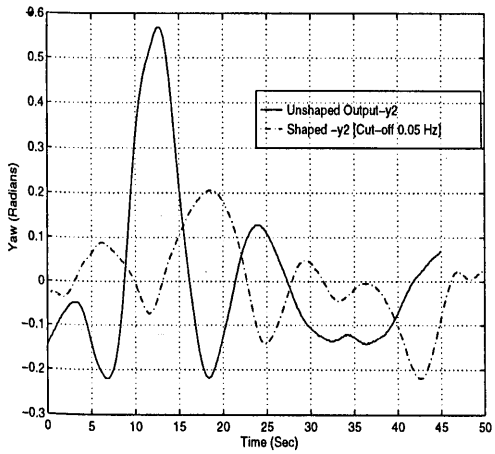

(a) Time domain.

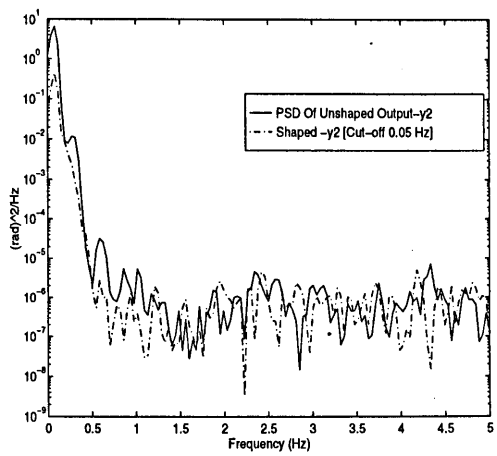

(b) Power spectral density.

Figure 4.10. Yaw response with a low-pass doublet input, *u1* → *y2*.

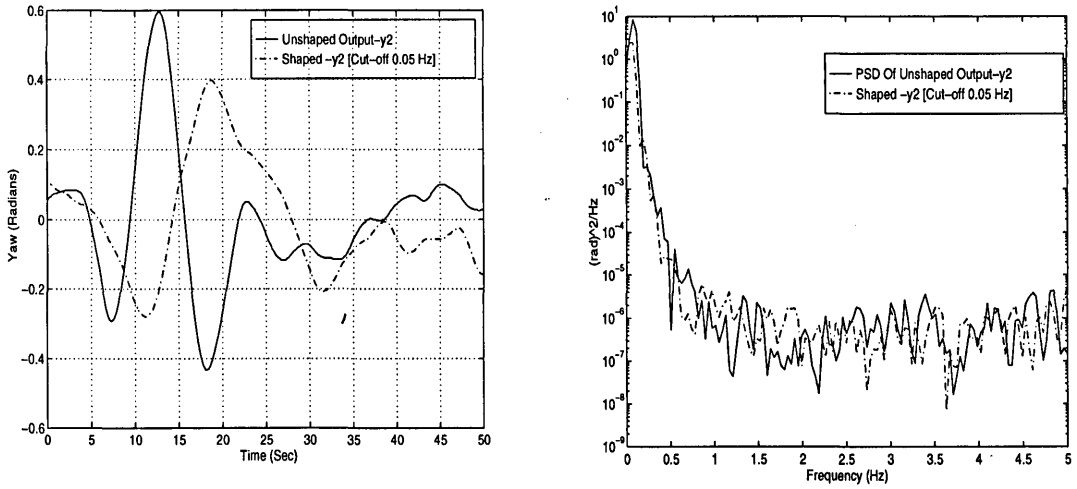

(a) Time domain. (b) Power spectral density.

Figure 4.11. Yaw response to a low-pass doublet input, *u2* → *y2*.

4.7 Band-stop shaped input

As before, a second order digital elliptic filter was used to study the TRMS performance with a band-stop shaped input. For effective suppression of the vibrations of the system, the centre frequency of the band-stop filter has to be exactly at the same frequency or as close as possible to the resonance frequency. From Table 4.1, it is observed that the main resonant mode lies at 0.1 Hz and 0.34 Hz for the *u1*→ *y1* axis and at 0.1 Hz for the *u1* → *y2* and u2 → *y2* channels. Thus, three filters with different band-stop frequency range were investigated i) 0.25-0.4 Hz ii) 0.05-0.15 Hz and 0.25-0.4 Hz iii) 0.05-0.15 Hz. A band-stop shaped doublet input, shown in Figure 4.12 by dotted and dashed lines, was used and the responses were measured.

It is observed from Figure 4.13, that the dominating 0.34 Hz vibration mode has been reduced by almost 14 dB with the use of Filter 1. The time-history reveals reasonable damping and residual vibration disappearing quickly. Obviously this filter has no bearing on the *u1* → *y2* axis. The shaped input has not lost much of its profile, hence the response *y1* is fairly smooth. The intent in using this filter i.e. just suppressing 0.34 Hz mode, was to gauge the system performance and compare it with the performance of Filter 2.

Filter 2 is designed to suppresses prominent resonant modes appearing in both the channels. Some observations are noted for this Filter

- shaped input is badly distorted, hence good tracking of the command is unlikely
- time-history of Figures 4.13, 4.14, and 4.15 display good damping (i.e. no overshoot) and minimal residual vibrations
- the response *y1* is not smooth, indicating inconsistent and attenuated kinetic energy supply to the system.
- like in low-pass case, a band-stop frequency very close to the rigid-body mode, results in significant deterioration of the output magnitude and shape.
- it is noted that the spectral attenuation in the level of system vibration at the first (0.1 Hz) and second (0.34 Hz) mode are 20 dB and 13.98 dB respectively for the *u1* → *y1* channel and 36.25 dB for *u1* → *y2* axis.

Filter 3, was employed for the *u2* → *y2* axis, and recorded vibration reduction of 18.59 dB. The results of the MIMO open-loop experiments are summarized in Table 4.3.

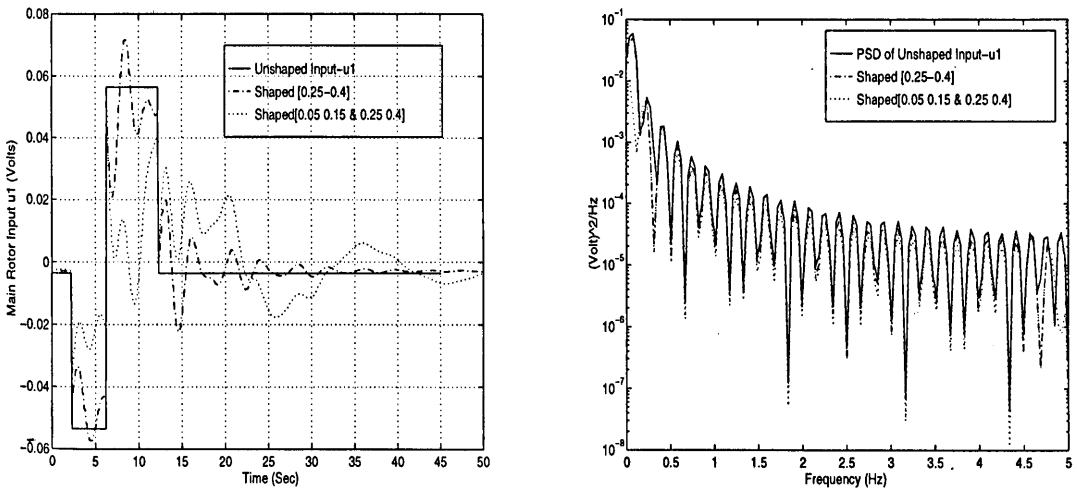

(a) Time domain. (b) Power spectral density.

Figure 4.12. Doublet input using bandstop filter.

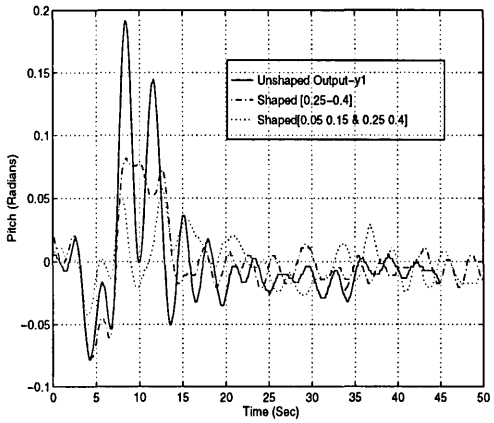

(a) Time domain.

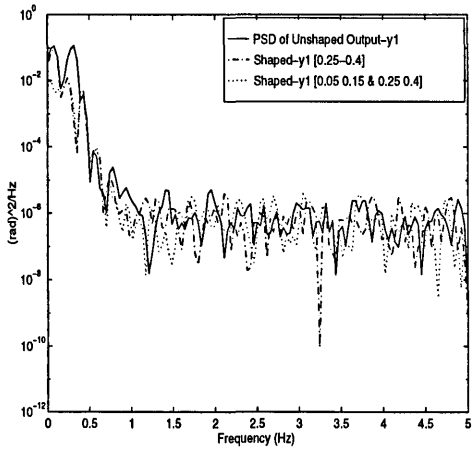

(b) Power spectral density.

Figure 4.13. Pitch response with bandstop filtered doublet input, *u1* → *y1*.

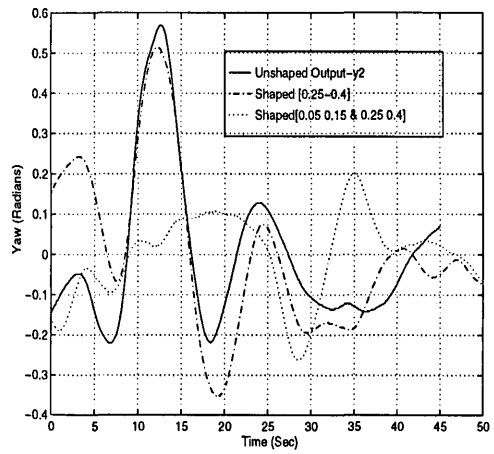

(a) Time domain.

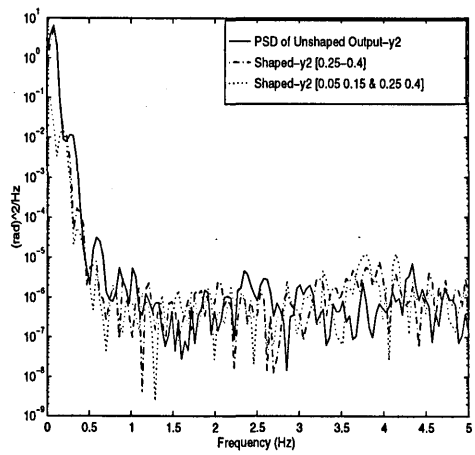

(b) Power spectral density.

Figure 4.14. Yaw response with bandstop filtered doublet input, *u1* → *y2*.

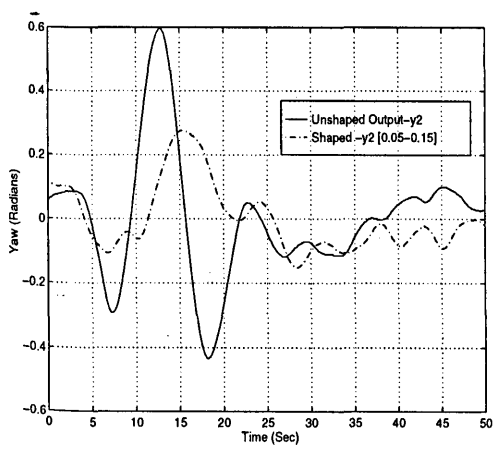

(a) Time domain.

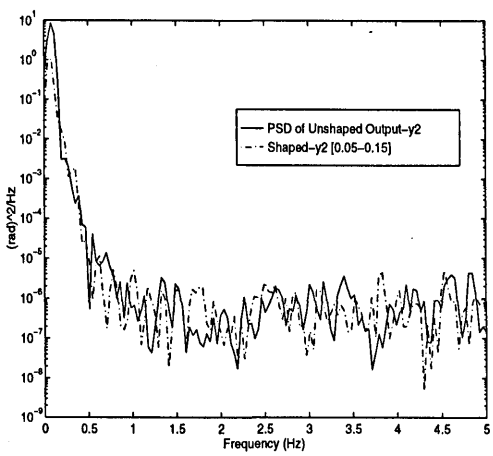

(b) Power spectral density.

Figure 4.15. Yaw response with bandstop filtered doublet input, *u2* → *y2*.

Channel	Modes-Hz	Band-stop Filter Attenuation			Low-Pass Filter
		Filter-1 [0.25-0.4] Hz	Filter-2 [0.01-0.15; 0.25-0.4] Hz	Filter-3 [0.05-0.15] Hz	Cut-off [0.05] Hz
u1→ y1	0.1		20 dB		10.45 dB
	0.34	13.98 dB	13.98 dB		20.91 dB
u1→ y2	0.1		36.25 dB		24.22 dB
u2→ y2	0.1			18.59 dB	10.63 dB

Table 4.2. MIMO open-loop control: mode attenuation.

4.8 Concluding remarks

This Chapter investigated a feedforward control technique which is related to a number of approaches known as "input shaping control". In these methodologies, a feedforward input signal is shaped so that it does not contain spectral components at system's resonant eigenfrequencies. Initially, a 1 DOF TRMS rig configuration was considered for open-loop control design and analysis. After gaining sufficient insight into the system performance, the concept was extended to a 2 DOF TRMS set-up. The study revealed that a better performance in attenuation of system vibration at the resonant modes is achieved with low pass filtered input, as compared to the band-stop filter. This is due to indiscriminate spectral attenuation of frequencies above the cut-off level in the low-pass filtered input. However, this is at the expense of slightly higher response time as compared to band-stop filter.

Open-loop control offers several advantages in this application, a) it reduces the settling time of the commanded manoeuvre, hence subsequent command signals can be processed quickly, thereby making the system faster, b) vibrational modes are suppressed, therefore improving the stability characteristics of the system, and c) feedback controllers for the MIMO systems are generally designed for each channel and are decoupled from the other channels. If modal couplings exist, they cannot eliminate vibration caused by the motion in the other channels. However, this type of vibration can be effectively suppressed by the shaped reference inputs.

Open-loop control using digital filters forms an important preliminary part of closed loop control design. In particular, for flexible systems such as flexible aircraft/TRMS.

To acheive good tracking and disturbance rejection characteristics open-loop is not sufficient. Hence, for overcoming the limitations of this approach, feedback control techniques are investigated in Chapter 6.

Chapter 5

Nonlinear modelling of a 1 DOF TRMS using radial basis function networks

High fidelity nonlinear system models are often employed for accurate representation of the plant in the simulation environment. This Chapter utilises a nonlinear system identification method to model the 1 DOF TRMS.. Extensive time and frequency-domain model-validation tests are employed to instil confidence in the estimated model. The estimated model has a good predictive capability and can be utilised for nonlinear simulation studies.

5.1 Introduction

Recent advances in aircraft technology has led to the development of many new concepts in aircraft design, which are strikingly different from their predecessors. The differences are in both aircraft configuration and control paradigms. This trend can be attributed to the increasing emphasis on the aircraft to be agile (i.e. high Angle Of Attack), low-observable (stealth), multi-purpose etc. for varied civilian and military operations. These new generation air vehicles have presented a variety of unprecedented challenges and opportunities to aerodynamicists and control engineers. The expectations of the new generation air vehicles to be highly agile and multi-functional demands that they perform over a large flight envelope. Enhanced agility in control terms implies a large excursion from the trim condition. In such a situation the linearized models can no longer describe the aircraft dynamics well enough. Hence, there is a need for high fidelity nonlinear dynamic models. Such models are essential for the design of control systems, validation and for piloted simulation.

This Chapter presents a suitable modelling technique for such air vehicles. In this work, a nonlinear system identification technique based on Radial basis function (RBF) is utilised to model the TRMS. While the Newtonian mechanics or the Lagrange equations

of motion can be used to find the nonlinear differential equations in a *generic* form, the unknown parameters must still be identified. Such model based identification is commonly employed with practical systems. There are numerous examples that demonstrate the applicability, feasibility and versatility of the model based concepts. For instance, neural networks have been employed for estimating the aerodynamic coefficients of unmanned air vehicles (UAV's) [33]. More recently, RBF networks were used by Kim and Calise [53] to capture variations in aircraft mach number. Here the neural network (NN) is used to perform the dual roles of i) identifying the input-output model parameters (off-line learning) using the mathematical model of an aircraft and, ii) an adaptive network that compensates for imperfect inversion and in-flight changes in the actual aircraft dynamics. An innovative time-domain nonlinear mapping-based identification method is presented by Lyshevski [54] for identification of unsteady flight dynamics. Lately, B-splines have been investigated in modelling and identification of aircraft's nonlinear aerodynamic functions [55]. In all these cases the model structure is *known*. However, in the present study, no model structure was assumed *a priori* i.e. black-box modelling. Such an approach yields input-output models with neither *a priori* defined model structure nor specific parameter settings reflecting any physical aspects.

In this study RBF networks are used to demonstrate these concepts by successfully modelling the dynamical behaviour of the TRMS. Such a high fidelity nonlinear model is often required for the nonlinear flight simulation studies. Since, there is no reliance on the mathematical model, the estimated RBF model has to be thoroughly verified using rigorous time and frequency domain tests. If the model structure and the estimated parameters are correct then the residuals (difference between model and system output) should be unpredictable from all linear and nonlinear combinations of past inputs and outputs. This is ensured by carrying out higher order cross-correlation tests, proposed by Billings and Voon [56].

This Chapter first describes the nonlinear modelling approach adopted in Section 5.2, which is followed by a discussion of RBF networks in Section 5.3. The type of excitation signal and data pre-processing needed to identify the nonlinear model is outlined in Section 5.4. Implementation and results are presented in Section 5.5. In Section 5.6 the nonlinear model and the linear model from Chapter 3 are compared. Finally, the main findings of this Chapter are summarised in Section 5.7.

5.2. Nonlinear modelling

There are a number of different types of nonlinear models that are potentially suited to this problem. Some examples are the output-affine model, the polynomial model and the rational model. In this investigation, a nonlinear autoregressive model with exogenous inputs (NARX) [57], which provides a concise representation for a wide class of nonlinear systems, is employed. The model is of the form:

$$y(t) = f(y(t-1),...y(t-n_y),u(t-1),...u(t-n_u)) + e(t) \qquad (5.1)$$

where, y(t), is the output, u(t) is the input and e(t) accounts for uncertainties, possible noise, unmodelled dynamics, etc. n_y, n_u are the maximum lags in the output and the input; { e(t)} is assumed to be a zero mean white noise sequence; and f(.) is some vector valued nonlinear function of y(t) and u(t) respectively. The NARX model is also referred in the literature by various other names such as one-step ahead predictor or as series-parallel model. Because the system noise e(t) is generally unobserved, it can only be replaced by the prediction error or residual ε (t), and equation (5.1), can be re-written as:

$$y(t) = f((y(t-1),...y(t-n_y),u(t-1),...u(t-n_u)) + \varepsilon(t) \qquad (5.2)$$

Where the residual is defined as:

$$\varepsilon(t) = y(t) - \hat{y}(t) \qquad (5.3)$$

where $\hat{y}(t)$ is the model predicted output.

Two considerations are of practical importance for the application of the NARX approach. The nonlinear functional form f(.) should be capable of describing nonlinear input-output space. Secondly, an efficient identification procedure for selecting a parsimonious model structure is required. The present study employs an RBF network to model the input-output relationship. This is depicted in Figure 5.1. The nonlinearity within the RBF can be selected from a small set of typical nonlinear functions, such as the thin-plate-spline function, the Guassian function, the multiquadratic and the inverse multiquadratic functions. A generally held opinion is that the choice of the nonlinearity is not crucial for performance [58].The nonlinear functional form, f(.) in the RBF expansion, used in this study is the Guassian function. Orthogonal least square (OLS)

[58], provides an elegant method for determination of model parameters. If the OLS is employed with the polynomial NARX model then it selects a parsimonious model structure as well as estimates the selected model parameters. However, if the NARX-RBF model structure is adopted then the OLS routine yields optimal model parameters i.e. weights and centres.

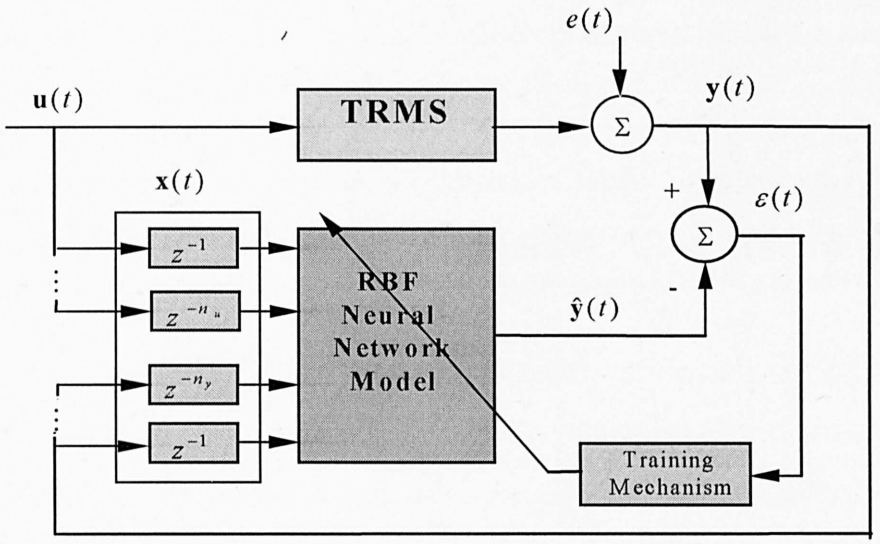

Figure 5.1. NARX model identification with RBF networks.

5.3 Radial basis function

An RBF network can be regarded as a special two layer network which is linear in the parameters provided all the RBF centres are prefixed. Given fixed centres i.e. no adjustable parameters the first layer or the hidden layer performs a fixed nonlinear transformation, which maps the input space onto a new space. The output layer then implements a linear combiner on this new space and the only adjustable parameters are the weights of this linear combiner. These parameters can therefore be determined using the linear least square method, which is an important advantage of this approach.

A schematic of the RBF network with n inputs and a scalar output is shown in Figure 5.2. Such a network could be represented as:

$$\hat{y}(t) = w_0 + \sum_{i=1}^{n_r} w_i f_r\left(\left\|\mathbf{x}(t) - c_i\right\|\right) \tag{5.3}$$

where $\hat{y}(t)$ is the network predicted output, **x**(t) is the network's input vector containing all regressors of equation (5.1), that is,

$$\mathbf{x}(t) = [(y(t-1),...y(t-n_y), u(t-1),...u(t-n_u)]^{\mathrm{T}} \tag{5.4}$$

w_i, are the weights or parameters, w_0 is the bias or the d.c level term at the output, c_i *are* known as RBF centres and n_r is the number of centres or the hidden neurons. Once the functional form $f(.)$ and the centres c_i are fixed, and the set of input **x**(t) and the corresponding desired output vector (y(t) in this study) provided, the weights w_i can be determined using the linear least squares method. Clearly, $\hat{y}(t)$ is the nonlinear model predicted output determined by the past values of the system output vector y(t), and the input vector u(t), with maximum lags n_y, and n_u respectively.

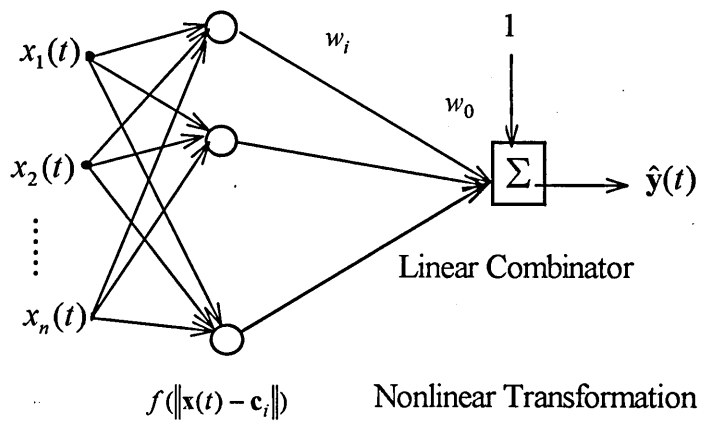

Figure 5.2. Radial basis function network.

The Guassian form for the RBF $f_i(\mathrm{x})$ is

$$f_i(\mathrm{x}_1(\mathrm{t}),\ \mathrm{x}_2(\mathrm{t}),\ ....\mathrm{x}_n(\mathrm{t})) = e^{-\left[(\mathrm{x}_1(\mathrm{t})-c_{1i})^2 + (\mathrm{x}_2(\mathrm{t})-c_{2i})^2 + ...+(\mathrm{x}_n(\mathrm{t})-c_{ni})^2\right] / \sigma_{i2}} \tag{5.5}$$

where $c_i = (c_{1i}, c_{2i} ....., c_{ni})$ is a vector which defines the centre of the RBF f_i in neuron i, and σ_{i2} is the "shape" of the function or the spread constant. Input patterns **x** activate the nodes according to their distance $\|\mathrm{x}-c_i\|$ from the node centres c_i. Thus,

each hidden neuron responds only to inputs which are in a region (*receptive field*) around its centres c_i. Other functions can also be used as the activation functions of radial basis nodes, without significantly affecting the performance of the RBF network. The scalar output $\hat{y}(t)$ is the sum of the linear combination of the RBF outputs, $f_i(\mathrm{x})$, with the weights w_i, of the connections from the hidden to the output nodes:

$$\hat{y}(t) = \sum_{i=1}^{n_r} w_i f_i(\mathrm{x}_1(\mathrm{t}),\ \mathrm{x}_2(\mathrm{t}),\ \ldots.\mathrm{x}_n(\mathrm{t}))$$

or,

$$\hat{y}(t) = \sum_{i=1}^{n_r} w_i f_i(\mathrm{x}(\mathrm{t})) \tag{5.6}$$

The above discussion could be best understood by assuming the RBF network in equation (5.3) as a special case of the linear regression model

$$y(\mathrm{t}) = \sum_{\mathrm{i}=1}^{\mathrm{M}} p_i(\mathrm{t})\theta_{\mathrm{i}} + \varepsilon(\mathrm{t}) \tag{5.7}$$

where, $y(t)$ is the desired output, p_i are known regressors, which are some nonlinear functions of lagged outputs and inputs. That is

$$p_i(t) = p_i(\mathbf{x}(t))$$

with $\mathbf{x}(t)$ defined in (5.4). A constant term (w_0 *in* Figure 5.2) can be included in equation (5.7) by setting the corresponding term $p_i(\mathrm{t}) = 1$. The residual $\varepsilon(t)$ is assumed to be uncorrelated with the regressors $p_i(t)$. It is clear that a given centre c_i with a given nonlinear function $f(\,.\,)$ corresponds to $p_i(\mathrm{t})$ in equation (5.7).

Equation (5.7) for $t = 1,...N$, data length, can be written in the matrix form

$$\mathbf{y} = \mathbf{P}\,\Theta + \mathbf{E} \tag{5.8}$$

the solution to find the parameter vector Θ, is given by the well known least squares (LS) method, provided the centres are fixed.

5.3.1 RBF-NN learning algorithms

The task of a learning algorithm, or an optimisation routine, in an RBF network is to select the centres and to find a set of weights that makes the network perform the desired mapping. In essence, the objective is to minimise the variance or the sum squared of the residual.

$$\hat{\sigma}'_{\varepsilon^2} = \sum_{t=1}^{N} \varepsilon^2(t) \tag{5.9}$$

A number of algorithms are frequently utilised for this purpose [59], for instance,

- random centre selection and a least square algorithm.
- clustering and a least square algorithm.
- nonlinear optimisation of all the parameters i.e. centres, output weights and other free parameters.
- the orthogonal least square algorithm (OLS).

Among these the OLS is widely used. The orthogonal least squares (OLS) method proposed by Chen *et al* [58], yields both number of centres c_i, i.e. significant regressors, as well as the corresponding parameter vector Θ in equation (5.6). The underlying idea of the algorithm is to transfer the regression equation into an equivalent orthogonal form. Then the RBF centres can be selected and weights optimised in a simple procedure according to a criterion referred as the "error-reduction-ratio" (ERR) due to the orthogonality property. Details of the OLS can be found in Chen *et al* [58].

5.4 Excitation signal and data pre-processing

In this Section the characteristic of the excitation signal for nonlinear identification is delineated followed by some guidelines for input-output data pre-processing before applying it to the neural networks.

5.4.1 Excitation signal

In nonlinear system identification, the type of input signal to be used plays a crucial role and has a direct bearing on the fidelity of the resulting identified model. The excitation signal should have two important characteristics:

- it should be able to excite all the dynamic modes of interest, that is the spectral content of the input signal should be rich in frequency corresponding to system bandwidth. Such a signal is referred to as *persistently exciting*.
- it should be rich in amplitude level, that is have different levels of input amplitudes over the whole range of operation.

These two conditions can generally be fulfilled by selecting an input such as sine wave, Guassian signal, independent uniformly distributed process and ternary pseudorandom sequence [56]. In order to excite the system modes of interest i.e. up to 1 Hz two different signals; (i) independent uniformly distributed signal (noise) and, (ii) pseudo random binary sequence (PRBS), of 2 Hz and 5 Hz band limit respectively, are employed in this study. Figure 5.3, shows these two signals along with their amplitude distribution.

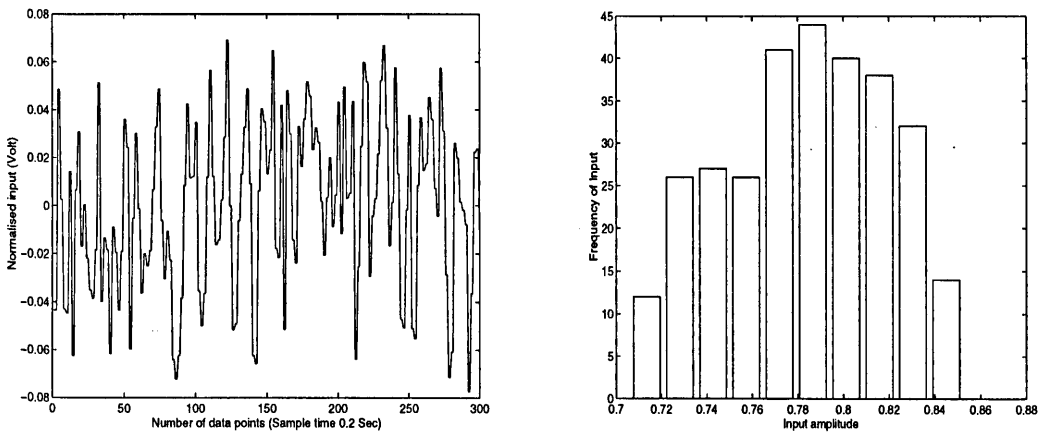

(a)

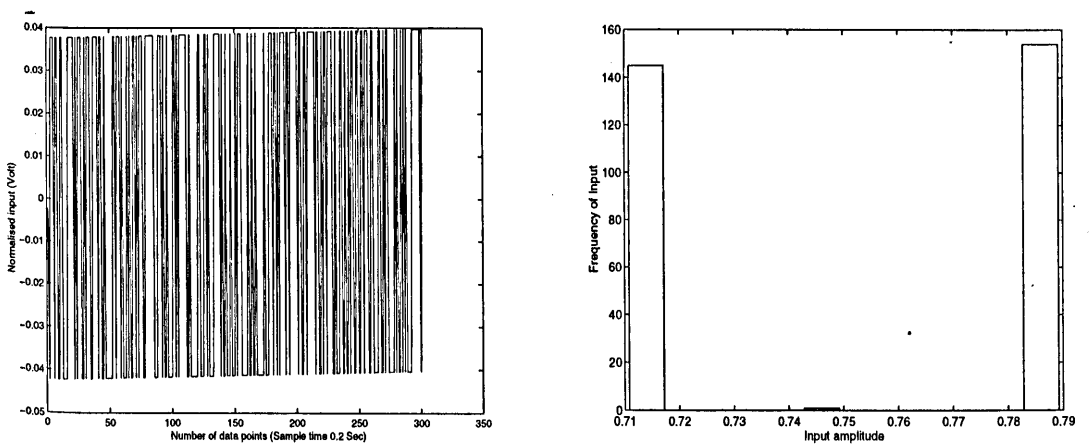

(b)

Figure 5.3. Excitation signal (a) Noise, (b) PRBS.

5.4.2. Data pre-processing

Processing of the raw input-output data obtained from the experiments is recommended for system identification. Pre-processing could involve removal of outliers, stray data points and normalisation. In the case of identifying a system model using NN, it is advantageous to apply pre-processing transformations to the input data before presenting it to the network. Reducing the difference of magnitude of input variables used to train network leads to faster convergence. One of the common method of pre-processing is the linear rescaling of the input variables. The normalised data is obtained by carrying out the following data manipulation:

$$\tilde{x}_i^n = \frac{x_i^n - \bar{x}_i}{\sigma_i} \tag{5.10}$$

where $\bar{x}_i$ is the mean and σ_i^2 is the variance of each variable of the training set and defined as:

$$\bar{x}_i = \frac{1}{N}\sum_{n=1}^{N} x_i^n \tag{5.11}$$

$$\sigma_i^2 = \frac{1}{N-1}\sum_{n=1}^{N}(x_i^n - \bar{x}_i)^2 \tag{5.12}$$

Where $n = 1,\cdots,N$ are the number of data points or the data length. The re-scaled variables defined by $\tilde{x}_i^n$ have zero mean and unit standard deviation. The target values are also subjected to similar linear rescaling.

5.5 Implementation and results

In this Section results of modelling the TRMS with neural networks is described. The modelling with NN was carried out with the TRMS pitch response to a uniformly distributed noise signal as described in the previous section. The rationale of using the noise signal is that the two level PRBS signal may not be good enough to capture nonlinearities, if present, in the system. For the sake of comparison the two-level PRBS input shown in Figure 5.3 is also utilised for modelling the 1 DOF TRMS. Results obtained with the main rotor input and the pitch output are described below.

Similar to linear modelling, *identification* (ID) of the model structure, *estimation* of parameters and *verification* are the fundamental issues in nonlinear system identification too. Since, the RBF is chosen as the model structure, the remaining two issues of estimation and verification are addressed in this section.

5.5.1. Mode determination

In order to detect the dominant system modes, spectral plots of the TRMS output and nonlinear model output are analysed. The solid line curve in Figure 5.4 shows the power spectral density (PSD) plot of the actual pitch response of the TRMS to the independent uniformly distributed input signal of 2 Hz bandwidth.

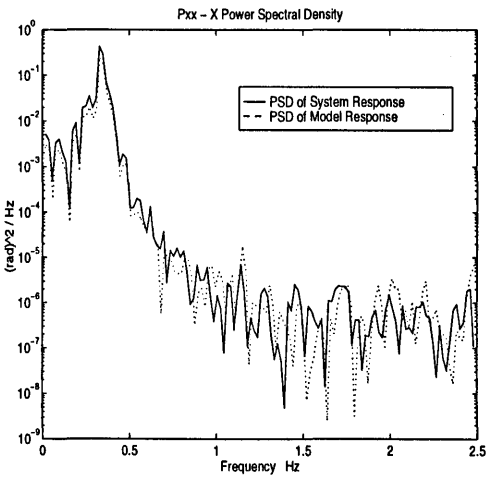

Figure 5.4. Power spectral density of output.

As noted, this shows closely spaced modes between 0-1 Hz as expected, with a main resonant mode at 0.34 Hz, which can be attributed to the main body dynamics. A model order of 2, 4 or 6 corresponding to prominent normal modes at 0.25, 0.34, and 0.46 Hz is thus anticipated.

The next step is to capture or model the plant dynamics using an RBF network. The Matlab neural-network toolbox [60], is utilised to carry out the *parameter estimation,* which uses an OLS learning algorithm. An iterative procedure can be devised to identify the NARX models using the RBF expansion by linking the OLS routine and the model validity tests. The nonlinearity function in the RBF expansion is the Gaussian function. The main steps in the identification can be summarised as follows.

(i) Choose n_y, and n_u. Initially the set of candidates centres are all the

$$\mathbf{x}(t) = [(y(t-1),...y(t-n_y),u(t-1),...u(t-n_u)]^{\mathrm{T}}$$

(ii) Select the Guassian spread constant σ_i and define the error goal.

(iii) An iterative loop is then entered to update the model based on the "error-reduction-ratio" (ERR) criteria [58].

(iv) Different time and frequency domain validity tests are performed to assess the model. If the model is good enough the procedure is terminated. Otherwise go to step (i).

The OLS learning method selects a suitable set of centres c_i (regressors) from a large set of candidates as well as estimates the linear parameters w_i, or the weights. The iterative procedure described above is used to identify the RBF model. The RBF model was trained with 300 data points and different combinations of input-output lags were tried. Using a generate-and-test method, an 8th order NARX model was found to give a better representation of the system dynamics in the frequency domain (see Figure 5.4) than the 6th order model as envisaged. This model reached a sum-squared error level of 0.002 after 13 training passes. The identified model included a constant term and 13 centres or neurons. The PSD obtained from the RBF model and the experimental data are superimposed in Figure 5.4. It is observed that the dominant modes of the model and the plant coincide quite well, implying good model predicting capability of the important system dynamics. Thus, it is assumed that the identified model is fairly accurate and suitable for system analyses.

5.5.2. Correlation tests

In the previous section frequency domain test was employed to detect the system modes. In order to ensure further confidence in the identified model time domain correlation tests are employed next.

A more convincing method of model validation is to use correlation tests. If a model of a system is adequate then the residuals or prediction errors $\varepsilon(t)$ should be unpredictable from (uncorrelated with) all linear and nonlinear combinations of past inputs and outputs. This can be tested by means of the following correlation functions [56]:

$$\phi_{\varepsilon\varepsilon}(\tau) = E[\varepsilon(t-\tau)\varepsilon(t)] = \delta(\tau)$$

$$\phi_{u\varepsilon}(\tau) = E[u(t-\tau)\varepsilon(t)] = 0 \qquad \forall\tau$$

$$\phi_{u^2\varepsilon}(\tau) = E[(u^2(t-\tau) - \overline{u}^2(t))\varepsilon(t)] = 0 \qquad \forall\tau \qquad (5.13)$$

$$\phi_{u^2\varepsilon^2}(\tau) = E[(u^2(t-\tau) - \overline{u}^2(t))\varepsilon^2(t)] = 0 \qquad \forall\tau$$

$$\phi_{\varepsilon(\varepsilon u)}(\tau) = E[\varepsilon(t)\varepsilon(t-1-\tau)u(t-1-\tau)] = 0 \qquad \tau \geq 0$$

where $\phi_{u\varepsilon}(\tau)$ indicates the cross-correlation function between $u(t)$ and $\varepsilon(t)$, $\varepsilon u(t) = \varepsilon(t+1)u(t+1)$, and $\delta(\tau)$ is an impulse function.

In the case of linear modelling, discussed in Chapter 3, the first two tests alone were adequate to test the model validity. The first two linear correlation tests in equation (5.13) alone are not sufficient to validate nonlinear models. Hence, higher-order correlation tests are also included in this study. All five tests defined by equation (5.13) should be satisfied if the $u(.)$'s and $y(.)$'s are used as network input nodes. In practice normalised, correlation's are computed. In general, if the correlation functions in equation (5.13) are within the 95% confidence intervals, $\pm 1.96/\sqrt{N}$, where, N is the total number of data points, the model is regarded as satisfactory.

Figure 5.5, shows the correlation tests described by equation (5.13). It is important to note that only the first few lags are significant. The lags in the *x-axis* of Figure 5.5 are equivalent to sampling period, that is, each lag (τ) is equivalent to 0.2 seconds. The *y-axis* of each plot in Figure 5.5 is given by the corresponding correlation function of equation (5.13).

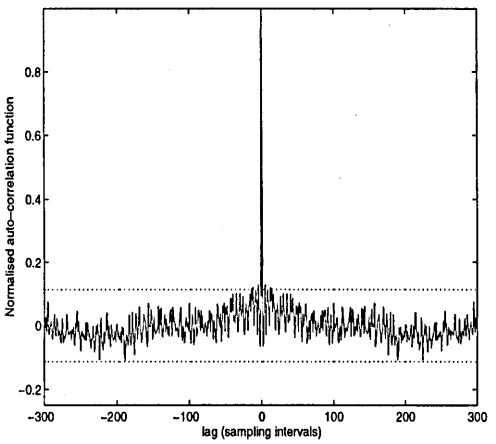

(a)

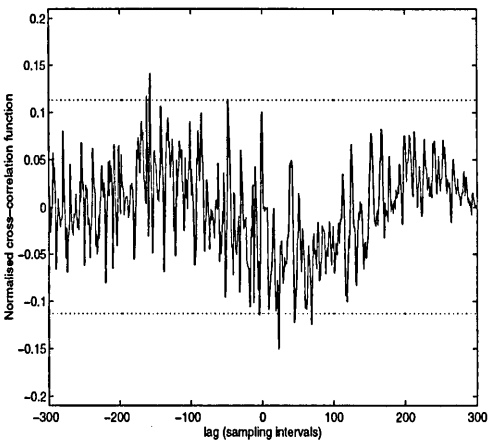

(b)

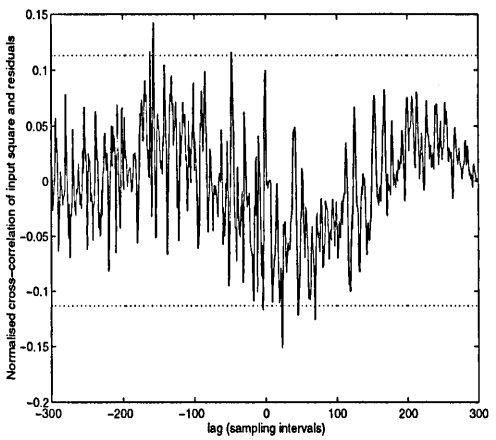

(c)

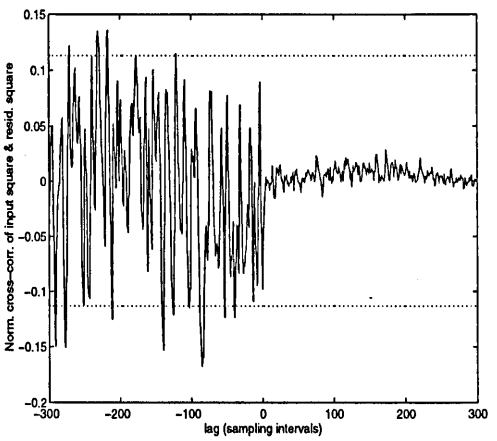

(d)

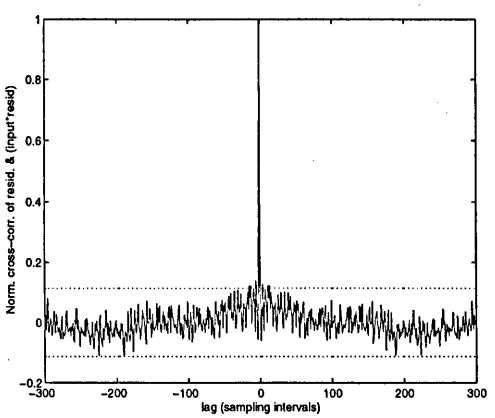

(e)

Figure 5.5. Correlation tests. (a) $\phi_{\varepsilon\varepsilon}(\tau)$, (b) $\phi_{u\varepsilon}(\tau)$, (c) $\phi_{u^2\varepsilon}(\tau)$, (d) $\phi_{u^2\varepsilon^2}(\tau)$, (e) $\phi_{\varepsilon(\varepsilon u)}(\tau)$. Dashed line: 95% confidence interval.

All the results of the correlation tests, as shown in Figure 5.5, are within the 95% confidence interval indicating a high-level of approximation of the actual data set. The model validity tests thus, corroborate that the estimated model is adequate. Having accomplished the first two tasks of *structure* determination and parameter *estimation*, the final important step is model *verification*.

5.5.3. Verification

Verification in the time domain is a key final step. In this research process, the predictive quality of the identified model is assessed with data that was not used for modelling. The uniformly distributed noise signal was used for excitation and multi-step (3211) and doublet input, were used for validation. Note that the signals for cross-validation are the same that were used in SISO linear modelling (Section 3.3.3) and are shown in Figures 5.6 and 5.7 respectively. In nonlinear system identification using neural networks, generally, one-step ahead (OSA) prediction and model predicted output (MPO) are employed for cross-validating the estimated model. Here, the results of MPO are presented which is a more robust test and often difficult to achieve than the OSA prediction. This is expressed as:

$$\hat{y}_d(t) = f(u(t), u(t-1), \ldots, u(t-n_u), \hat{y}_d(t-1), \ldots, \hat{y}_d(t-n_y)) \qquad (5.14)$$

In Figure 5.8 and 5.9 the simulated nonlinear model predicted output (MPO) and the experimental outputs are compared for the 3211 and the doublet excitation respectively. It is observed that the model and the system response match closely. Overall, the predictive capability of the model is quite good, especially considering the very sensitive nature of the TRMS to ambient disturbances. This has been a major problem in consistently reproducing the same response to an input.

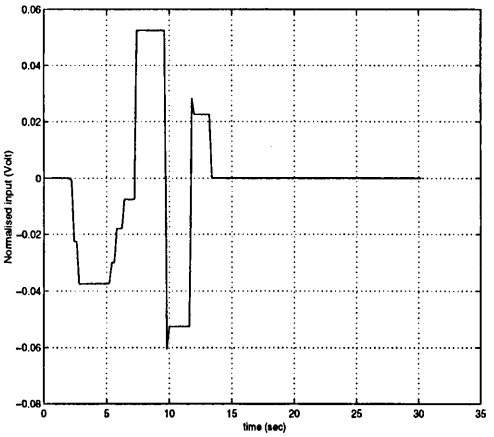

(a) Multi-step input (3211).

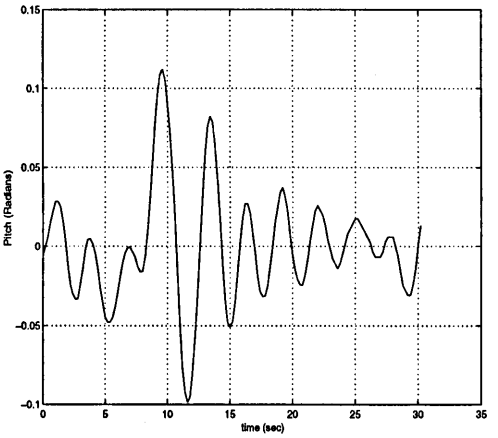

(b) System response to a multi-step input.

Figure 5.6. Input and output signals used for model cross validation.

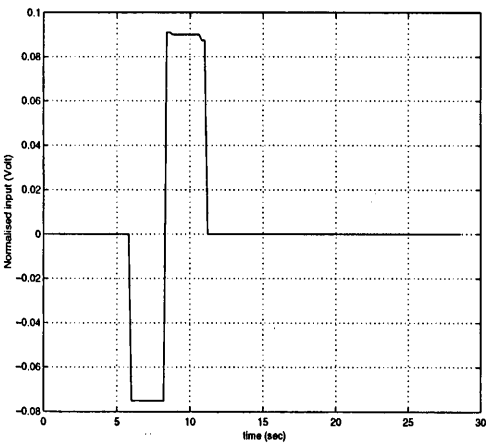

(a) Doublet input.

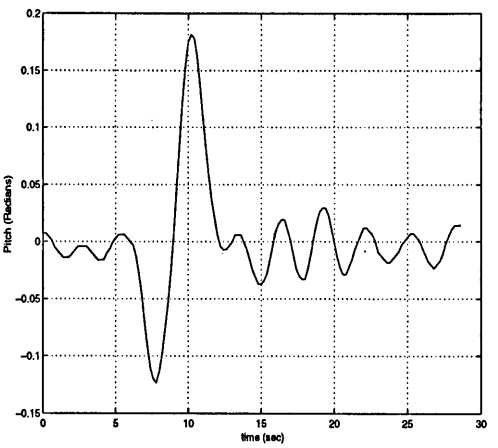

(b) System response to a doublet.

Figure 5.7. Input and output signals used for model cross validation.

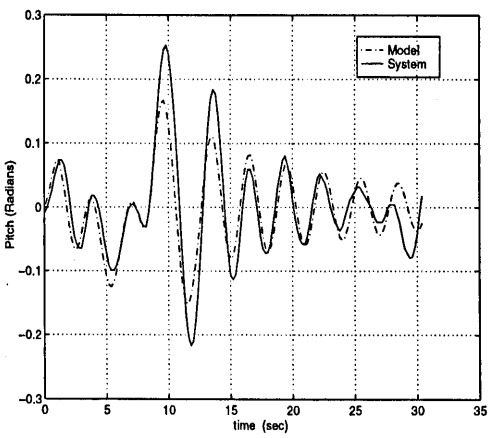

(a) with a 3211.

Figure 5.8. The system and the nonlinear model response: noise signal used for ID.

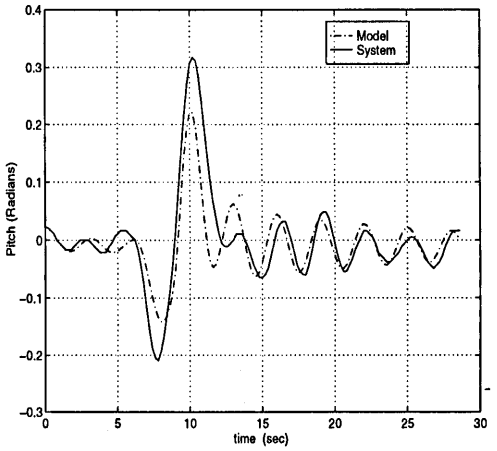

(a) with a doublet.

Figure 5.9. The system and the nonlinear model response: noise signal used for ID.

An analogous procedure is repeated with the PRBS signal and result reported in Figures 5.10.

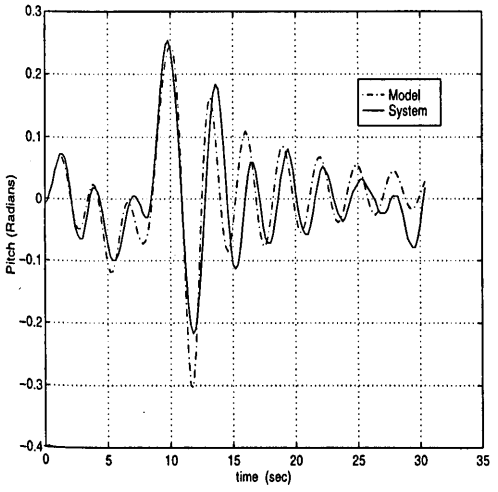

(a) with a 3211.

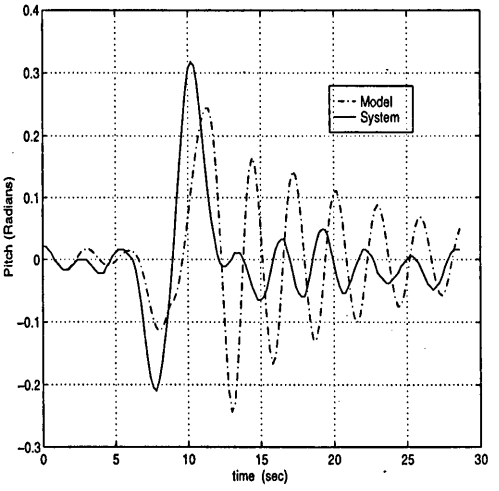

(b) with a doublet.

Figure 5.10. The system and the nonlinear model response: PRBS used for ID.

Comparing the MPO due to noise and PRBS inputs, it is clearly noted that, the model obtained by the noise signal has captured the dynamics better than the PRBS. This is primarily due to the excitation of dynamics across the input range, unlike the PRBS where only two levels of amplitude is all that is present in the input. Thereby, unable to excite the nonlinear dynamics associated with the other input amplitudes. Therefore, only results with a uniformly distributed noise signal will be used for comparison with the linear model in the next Section.

5.6 Comparison between linear and nonlinear modelling

The aim of this Section is to compare the predictive capabilities of the nonlinear modelling of this Chapter and the linear one presented in Chapter 3. The time and the frequency domain plots for the linear and nonlinear system identification are placed adjacent to each other in Figures 5.11, 5.12 and 5.13 respectively. The linear time domain plots and PSDs are those identified in Chapter 3, Section 3.3.3 for the 1 DOF TRMS modelling. The plots are reproduced here for ease of comparison. From the time domain plots, it is observed that the nonlinear model gives slightly better prediction of the system response. In particular it is noticed, that that the nonlinear model is superior in predicting the slower system dynamics, this is discernible from Figure 5.12, where the nonlinear model closely follows the slow oscillatory TRMS motion. The spectral plots for linear and nonlinear are shown in Figure 5.13. Here again, the PSD of the nonlinear model predicted ouput shows better quality of overlapping of the plant modes as compared to the linear model. This signifies accurate modelling of not so prominent system dynamics. As a consequence, this is reflected in a fairly accurate time domain nonlinear model prediction.

Finally, the variances of residual $\varepsilon(t)$ of these two different approaches are computed and presented in Table 5.1. Although the nonlinear model has a smaller variance the difference between the two variances is negligible.

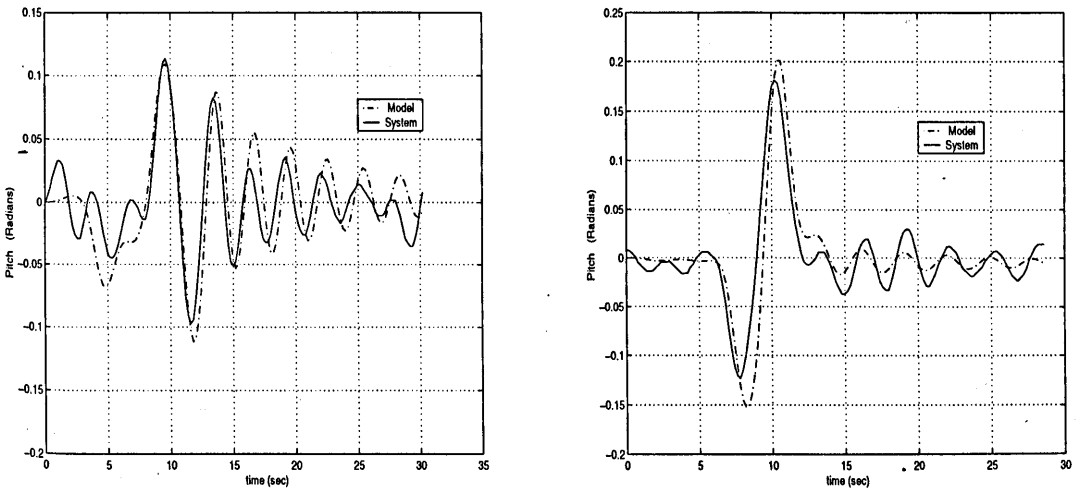

(a) with a 3211 input. (b) with a doublet input.

Figure 5.11. The system and the linear (ARMAX) model response.

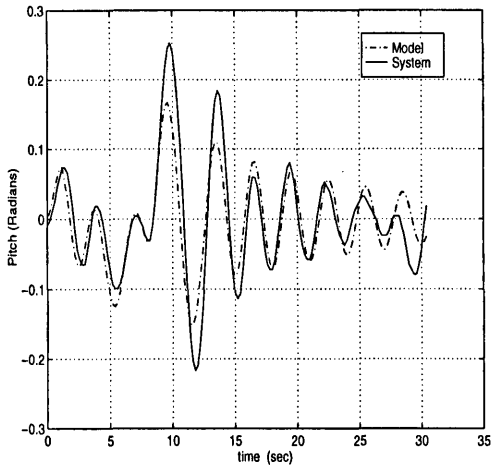

(a) with a 3211 input.

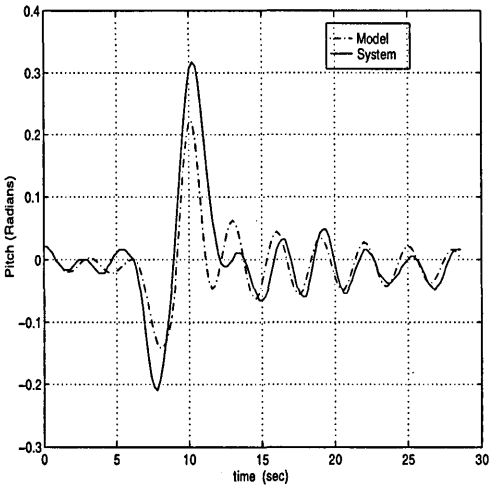

(b) with a doublet.

Figure 5.12. The system and the nonlinear (NARX) model response.

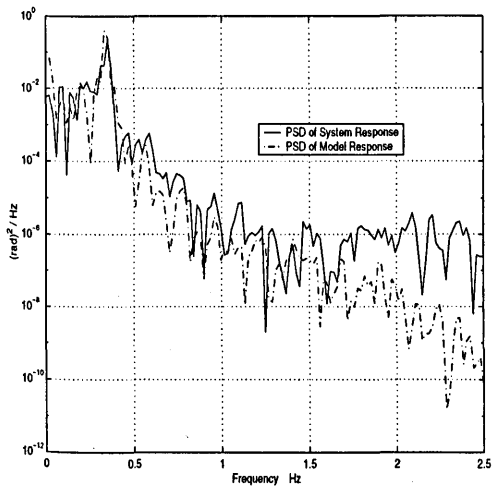

(a) linear ARMAX model

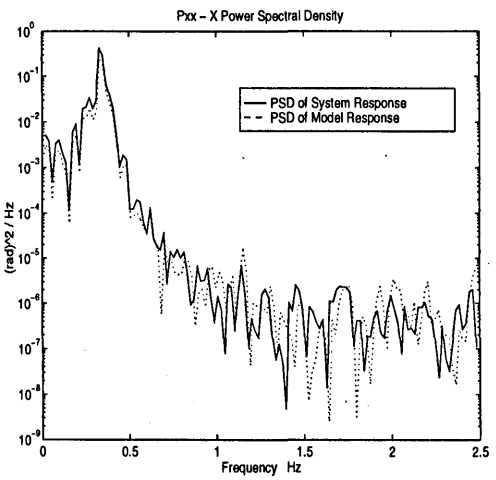

(b) nonlinear NARX model.

Figure 5.13. Power spectral densities of linear and nonlinear model predicted output: shown by dotted lines.

Modelling method for a 1 DOF TRMS	Variance of residuals $\varepsilon(t)$
Linear (ARMAX)	8.93e-06
Nonlinear (NARX-RBF)	6.42e-06

Table 5.1. Linear and nonlinear model variance comparison.

5.7. Concluding remarks

Friction, which is a nonlinear phenomenon, is the primary cause of inducing nonlinearities in a mechanical system. Thus, it can be argued that, most of the electro-mechanical systems, like the TRMS, in general are nonlinear. Hence, nonlinear modelling technique is an obvious choice to characterise such systems. Radial basis function networks are shown to be suitable for modelling complex engineering systems, where the dynamics are not well understood or simple to establish from first principles, such as the next generation UAVs.

Careful selection of the excitation signal(s) is an important part of nonlinear system identification. Without due consideration to this issue, the obtained model would not be able to capture the system dynamics, resulting in a poor model. Since no mathematical model is available, extensive model validation is imperative. This has been ensured by carrying out higher order cross-correlation tests and MPO analysis. The extracted model has predicted the system behaviour well. Such a high fidelity nonlinear model is often required for gauging the performance of control design and system analysis. The time and frequency domain analysis indicate superior prediction of the nonlinear model as compared to the linear model of Chapter 3. Moreover, a comparison of variances of the linear and the nonlinear model reveals a very minor difference between them. In many engineering applications (such as the TRMS), the trade-off between model accuracy and simplicity tends to favour simplicity. Therefore, in the present study, the nonlinear model will not be used in the control design study of the next Chapter, although this was the original intention. However, the nonlinear modelling technique would be of immense use where significant nonlinearities exist, such as a high angle of attack aircraft manoeuvre or if the system is excited beyond its linear operating range. In case of the TRMS, the $u1 \rightarrow y2$ channel (Section 3.5) exhibits a slight nonlinear behaviour, therefore, the RBF model would be of benefit while simulating the controller performance for this channel.

The underlying theme of this Chapter was to demonstrate the nonlinear modelling technique, which has various other applications apart from its utility as a "true" representation of the plant in the simulation environment for the controller evaluation. For instance nonlinear models are essential for the design of nonlinear control laws, such as the back-stepping method. Dynamic inversion of the plant model using RBF to cancel out the system resonances are increasingly employed in aerospace [53] and robotics [50] applications.

Chapter 6

Control law development for a 1 DOF TRMS

The goal of this Chapter is to develop methods to reduce motion and uneven mass induced vibrations in the TRMS during operation. This Chapter employs an optimal control strategy for the 1 DOF TRMS model obtained in Chapter 3. Two different control structures are investigated, Stability Augmentation System and Command and Stability Augmentation System. Simulations are presented which demonstrate a good tracking capability for both controllers. It is also shown that, Command and Stability Augmentation System is able to effectively deal with problems of vibrations and actuator constraints.

6.1 Introduction

In the preceding Chapter, a nonlinear model was developed using an artificial neural networks, primarily to incorporate the nonlinear model into the controller design environment. The rational was that a nonlinear model would capture the system dynamics better than the linear model. Hence, a more accurate compensator behaviour could be predicted. Such nonlinear models are often employed in aerospace application for-evaluating the controller(s) performance. However, as demonstrated in the last chapter, the linear model matches the nonlinear model for small perturbations about the nominal TRMS operating condition. Since there is a negligible difference between the linear and nonlinear model, it is deemed fit to utilise the linear model for controller performance analysis.

It is evident from the rig that structural vibrations occur due to the presence of rotor load at the end of the cantilever beam and motor torque, inducing bending movement, while in operation. These vibrations appears in the system response as oscillations with long settling times. Several different approaches have been proposed to reduce residual vibration in flexible systems. The open-loop method for attenuating oscillations was

examined in Chapter 4. However, in order to achieve a good tracking capability of command inputs and disturbance rejection properties, this method on its own is inadequate. Therefore, closed-loop strategies employing constant feedback gains have also been designed for robust tracking and attenuation of residual vibration of elastic systems. Both classical and modern feedback methods have been proposed to manoeuvre flexible systems.

Doughtery *et al* [61] and Franklin *et al* [62] applied classical controllers to space structures, to control the vibration and attitude (orientation). The control design adopted basically treats the flexible modes as separable subsystems. Therefore, the gains originally chosen for the rigid body alone need to be decreased for lower bandwidth to assure stability when flexible modes are present. Azad [63] demonstrated control of a single link flexible manipulator utilising a collocated PD feedback incorporating hub angle and hub velocity feedback variables. This is then extended, additionally, to incorporate non-collocated end-point acceleration feedback through a PID controller, achieving a hybrid collocated and non-collocated feedback control mechanism. The Naval Research Laboratory's (NRL) foldable remotely piloted UAV, adopted classical techniques for controlling different flight phases, such as boost, transition to the cruise phase and the cruise phase. [64]. Take off to a particular height, land and cruise mode control of Georgia Tech [65] robot helicopter is accomplished using the classical PID controller structure.

Modern control paradigms have been studied for a variety of complex systems, some of which are discussed here. Recently, Teague *et al* [66] developed, a novel method for active control of the attitude and vibration of a flexible space structure using the Global Positioning System (GPS) as a sensor. Linear Quadratic Regulator (LQR) feedback was employed in this study. Franklin *et al* [62], in addition to PD control, used modern optimal control methods to achieve command tracking and vibration suppression of a space satellite. LQR based control design for commercial aircraft control applications was investigated by Blight *et al* [67] to redesign an autopilot control law in order to improve stability and reduce sensitivity to plant parameter variations. An improved control law wasdesigned compared to classical approaches, flight tested and implemented in the autopilot of the Boeing 767 commercial transport airplane. Their experience in implementing the LQR paradigm is documented in [67].

In the autonomous flight control study of an UAV Aerial, LQR is used as a baseline line inner loop controller [68]. It is expected to track commands generated by the 6 DOF manoeuvre algorithm. The controller is employed to gauge the adverse effects of uncertainty in the UAV aerodynamic and control derivatives (i.e. parameters) on the stability and performance of the closed-loop system. LQR has also been adopted for an autopilot design for a high-altitude, supersonic air-to-air bank-to-turn (BTT) missile [69]. One of the design requirements for such systems is a high level of robustness to parameter variations, which is difficult to meet with classical method.

LQR well-known counterpart LQG with an in-built observer design has also been successfully employed for plants with elastic modes. Henrichfriese *et al* [70] developed a controller with an observer to estimate the vibrating states based on a detailed system model. Kosut *et al* [71] studied the robustness properties of several linear LQG based designs. Design of control algorithms for a supersonic air-to-air missile presents a very a challenging problem for the control engineer. Severe coupling between the guidance law and autopilot is the main cause of design complexity. Added complexity occurs when steering the missile in the terminal phase. The digital LQG compensator for such systems is considered by Langehough and Simons [72] and found to be better than the classical and eigenstructure methods. Control law development for a HAVE DASH II missile autopilot is investigated by Lin [73] who employed LQR and LQG topologies. Pitch, roll-yaw and combined pitch and roll-yaw designs are developed and shown to be robust against plant parameter and operating range variations.

The LQG-Loop Transfer Recovery (LTR) approach has been investigated in areas such as control of large space structures [73], weapon control [74], missile autopilot design [73,75] and Integrated Flight Propulsion and Control [73]. More recently, LQG-LTR and H-∞ based attitude control system have been designed for a large flexible space structure with subassemblies [19]. Such large structures with flexible appendages are the subject of considerable interest at present. Here, vibrations are not controlled directly, the effect of flexibility is incorporated as modelling error. The controller design is thus made robust against unmodelled flexible dynamics ensuring that instability in the closed-loop system will not arise.

Modelling and H-∞ control of a single link manipulator is reported in [76]. The H-∞ controller is compared experimentally with a PI controller and shown to give improved

vibration control in the vertical plane. One of the seminal works on H-∞ flight control, is that of Hyde [77]. Here, H-∞ is applied to a Generic Vertical Short Take-Off and Landing (VSTOL) Aircraft Model (GVAM) developed by the Royal Aerospace Establishment. A systematic procedure for the H-∞ loop-shaping and the results of flight tests are given in [77]. The H-∞ control theory was used to design the controller for a VTOL UAV and described in [78]. The control strategy was tested using real-time hardware-in-the-loop simulation.

Robust control design can also be achieved via the eigenstructure assignment method. This method has found to be particularly suitable for the aerospace applications. Livet *et al* [16,17] has extensively studied the utility of this approach for a highly flexible aircraft.

A dynamic inversion method has been investigated for flexible manipulators [50], BTT air-to-air missile [79] and high angle of attack combat aircarft [80]. This approach has a low design complexity and has several practical advantages.

6.1.1 Laboratory platforms

There is a small but growing body of literature on laboratory platforms to simulate complex aircraft manoeuvres and problems, and to investigate different control paradigms. A multimodel approach to robust controller design is illustrated for a 2 DOF laboratory aircraft model, developed to model the behaviour of a vertical-take-off aircraft by Werner and Meister [32]. In this work, the Linear Matrix Inequality (LMI) formulation in conjunction with convex programming for robust command tracking and disturbance rejection in normal operation as well as in failure mode is employed. This platform is quite similar to the TRMS. It has roll and yaw movement where as the TRMS has pitch and yaw motion.

A radio controlled (RC) model helicopter is adopted as a platform by Morris *et al* [30] to study various modern identification and robust control synthesis techniques. The helicopter is mounted on a 3 DOF wrist which in turn is connected to a 3 DOF stand. This experimental set up is perceived as the hover mode. Stabilising LQG and H-∞, controllers with setpoint tracking are designed and compared for the RC helicopter. The Caltech ducted fan flight control experiment is designed to represent the dynamics of

either a Harrier in hover mode or a thrust vectored aircraft such as the USAF F18-HARV or X-31 in forward flight [29]. A comparison of several different linear and nonlinear controllers was performed by Kantner *et al* [81] on the same same rig. The Georgia Tech model helicopter and NRL's foldable UAV, mentioned early in this section, and VTOL UAV referred earlier [78], fall under the small experimental platform category. These platforms are thus, ideal test-bench for modelling, design and control research.

6.1.2 Evaluation of different control methods

From the earlier discussion it is clear that, there are many theoretical techniques that are available for complex modern control system design. The classical single input single output (SISO) control design methods utilising design criteria such as the phase and gain margin, bandwidth, maximum overshoot and damping ratio, lead to systems that would satisfy the desired performance criteria but are not optimised. Modern optimal control theory relies on design techniques that maximise or minimise a performance index, yielding a designed system that is optimal in some prescribed sense. For an LQR controlled system, i.e. assuming all the states are available and no stochastic inputs, it is well known that the open-loop regulator transfer function has a phase margin greater than sixty degrees and an infinite gain margin. Therefore, this control method not only ensures stability, but also provides the system with a good robustness properties. However, LQR necessitates measurement of all states, which may not be possible or could be expensive or unreliable to measure. On the other hand, for an LQG controlled system with a combined Kalman filter and LQR control law, unmeasured states can be estimated. This approach however, lacks the robustness characteristics of the LQR full state feedback design.

Doyle and Stein [82] proposed LQG-LTR method, to address the issue of deterioration of the robustness caused by the introduction of the estimator. The LQG-LTR formulation requires the plant to be minimum phase, which is a fundamental drawback of this paradigm. A further disadvantage is that, the design process introduces high gain which may cause problems with unmodelled dynamics [83]. Robustness characteristic for a SISO controller design are accomplish by ensuring satisfactory gain and phase margins. For multivariable systems, gain and phase margin are unreliable because they cannot cater for simultaneous perturbation in different loops. The H-∞ method addresses this issue by explicitly addressing the issue of robustness in its design

formulation. Because of this property, it has attracted lot of attention in academia, but has not yet been fully accepted in industry. The intuitive reasons are that, H-∞ is mathematically involved and complex, and that, the weights selection procedure is tedious. For aerospace applications, other factors are also critical such as flight certification. Although the computations involved in eigenstructure design are straight forward, there are concerns about its ability to deal with robust stability and robust performance. Dynamic inversion methods have a low design complexity and have several practical advantages. A practical limitation of dynamic inversion is that it implicitly assumes full state feedback. Also as the plant zeros becomes controller poles, this would render system unstable, hence dynamic inversion method is not directly applicable to non-minimum phase systems.

6.1.3 Control paradigm selection

In this Section, a number of potential design methodologies are examined to asses their suitability for the TRMS application. The TRMS has the following important features:

- multi input multi output system,
- non-minimum phase system model (Chapter 3),
- full state feedback is not available,
- flexible dynamics,
- cross-coupling between pitch and yaw plane, and
- is dynamically similar to a helicopter,

While designing controllers for multivariable systems, such as the TRMS, the designer is motivated to look for techniques that are inherently multivariable and also addresses the optimality issue in some sense. Classical robustness pointers such as gain and phase margins are unreliable when applied to multivariable systems because they cannot cater for simultaneous perturbation in different loops [83]. Further, modern controller design techniques exploit the full multi-variable nature of the plant. This aspect is particularly useful in dealing with cross-coupling terms since all the feedback loops are available to the controller which can then utilise any combination of inputs.

The TRMS's MIMO structure, with cross-coupling between different channels, renders it unsuitable for classical design methods and hence, a modern MIMO control approach is an obvious choice. From the previous discussion on the TRMS, LQG appears to be an attractive starting point. Primarily because the LQG has:

- an in-built estimator for constructing the unavailable states,
- no non-minimum phase restrictions, and
- its suitability for aerospace systems.

Thus, use of modern optimal LQG design technique is a prudent and pragmatic choice.

The goal of this Chapter is to develop methods to reduce motion and uneven mass induced vibrations in the TRMS during operation. The assumption is that the motion and the rotor load are the main source of system vibration as highlighted in Chapter 3. A practical way of controlling a system with resonant modes is to use a combination of feedback and feedforward. The feedforward option was demonstrated in Chapter 4. In this Chapter, a Linear Quadratic Guassian (LQG) compensator is used as a state feedback inner loop controller and digital filters as a feedforward compensator. The inner feedback controller is referred as the *Stability Augmentation System* (SAS). The background theory on optimal control is given in Section 6.2 to Section 6.5. The TRMS control problem is defined in Section 6.6, and the integral LQG design is formulated in Section 6.7. The SAS results with LQG as the feedback mechanism are given in Section 6.8. The combined feedforward and feedback control technique, referred as *Command and Stability Augmentation System* (CSAS) is presented in Section 6.9. This combined approach has been widely employed in aircraft control design [67]. The approach requires that the natural resonant frequencies of the system be determined through suitable identification and modelling techniques. Some important observations are given in Section 6.10.

6.2 Concept of optimal control

Optimal control is based on state variable models of the system. The *pole-placement* design approach using state feedback is appropriate for SISO systems. In this approach, if the system is completely state controllable, then poles of the closed-loop system may be placed at any desired locations by means of state feedback via a suitable state feedback gain matrix [84]. *Optimal control* methods provide an alternate way of placing the closed loop poles of a system in order to achieve some desired behaviour. In this case, the designer does not know the exact closed-loop pole locations. Instead, the eigenvalues are placed by the controller, in locations which seek to make the resulting closed loop performance the best possible hence, *optimal,* in some sense that the designer can specify in advance. Thus, optimal control methods are one more way of

selecting the contents of the feedback gain matrix. However, unlike *pole-placement*, which is not amenable for MIMO systems, an *optimal* approach is quite appropriate. In the design of SISO schemes by *pole-placement,* there is a unique feedback gain matrix which would place the closed-loop poles in the desired position. In order to see the limitations of the *pole-placement* approach, consider a multivariable case, having n states and m inputs, the dimensions of the feedback gain matrix are $m \times n$, so that it contains $m \times n$ feedback gains. However, only n of these are needed to position the closed-loop poles which are n in number. Optimal control is one way of constructively using up the extra degrees of freedom in satisfying complicated design objectives.

To refine the meaning of "optimal control" it is necessary to define a rule for determining the control action, subject to certain constraints, so as to minimise some measure of the deviation from ideal behaviour. That measure is usually provided by the chosen *Performance Index* (PI), which is a function whose value is considered to be an indication of how well the actual performance of the system matches the desired performance. In most cases, the behaviour of the system is optimised by choosing the control vector **u**(k) in such a way that the PI is minimised [84]. A good introduction on optimal control can be found in [84,85].

6.2.1 Formulation of optimisation problems

The problem of optimisation of a control system may be formulated if the following information is given:

- system equations
- class of allowable control vectors
- constraints on the problems
- performance index
- system parameters

The solution of an optimal control problem is to determine the optimal control vector **u**(k) within the class of allowable control vectors. This vector **u**(k) depends on:

- the nature of the performance index
- the nature of the constraints
- the initial state or initial output

- the desired state or desired output

An important characteristic of the optimal control law based on a quadratic PI is that it is a linear function of the state vector **x**(k). The state feedback control paradigm requires that all state variables be available for feedback. It is imperative, therefore, to represent the system in terms of measurable state variables. If all the state variables cannot be measured, one needs to estimate or observe the unmeasurable state variables. The measured and estimated state variables are then used to generate optimal control signals.

Such systems are commonly encountered and can be addressed by employing, the *separation theorem* which decouples the full stochastic control problem (i.e. system with noise) into two separate parts:

- the control part of the decoupled problem calculates the optimum deterministic controller with a quadratic PI, assuming that complete and precise information of all the state variables of the system is available. This design mechanism is referred to as the optimal linear-quadratic-regulator or LQR. The deterministic system model implies that, i) there are no disturbances acting on the plant (e.g. TRMS), and, ii) plant and output variables can be measured exactly, and controller dynamics are known accurately.

- the second part of the problem is that of a stochastic estimator which uses the noisy and incomplete measurements of the states of the system to provide the least-square-error estimates of the system states. This is essentially a Kalman filter design step. These estimates are then used as if they were known exactly by the optimum controller (LQR).

The *separation theorem* assures that the composite system of controller (LQR) and estimator (Kalman filter) will be together optimum stochastic controller, termed as linear-quadratic-gaussian regulator or compensator (LQG). These two distinct mechanism are illustrated in Figure 6.1.

Next, the equations necessary to find the optimal feedback gain matrix **K**, using the LQR concept and the estimator gain matrix **L**, employing the Kalman filter will be

given. Subsequently, they will be combined to yield a combined LQG compensator expression.

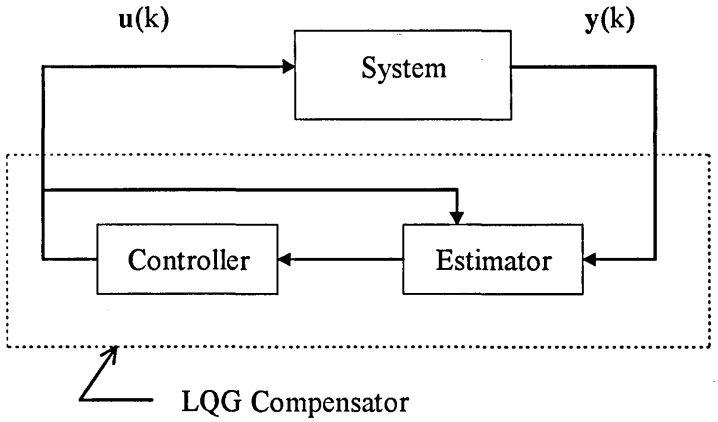

Figure 6.1. Illustration of the separation principle.

6.3 Linear quadratic regulator (LQR) - optimal state feedback

In the preceding sections, the LQR problem was briefly discussed. In the this section, the linear-quadratic state regulator will be discussed in particular, to develop the optimal feedback control law **u**(k), in a framework which would be conveniently applicable to the TRMS.

Consider the discrete-time linear deterministic system characterised by

$$\mathbf{x}(k+1) = \mathbf{A}\mathbf{x}(k) + \mathbf{B}\mathbf{u}(k) \qquad (6.1)$$

where,

x(k) = n-dimensional state vector
u(k) = r-dimensional plant control input vector
A = $n \times n$ matrix
B = $n \times r$ matrix

It is desired in the quadratic optimal control problem to determine a law for the control vector **u**(k) = - **K**x(k), such that a given quadratic performance index is minimised.

An example of quadratic performance index is;

$$\mathbf{J} = \frac{1}{2}\sum_{k=0}^{N}\left[\mathbf{x}^{T}(k)\mathbf{Q}\,\mathbf{x}(k) + \mathbf{u}^{T}(k)\mathbf{R}\,\mathbf{u}(k)\right] \qquad (6.2)$$

subject to the constraint equation:

$\mathbf{x}(k+1) = \mathbf{A}\mathbf{x}(k) + \mathbf{B}\mathbf{u}(k)$

where, the superscript denotes matrix transposition;
$\mathbf{Q}$ = is a $n \times n$ positive definite or semi-definite matrix.
$\mathbf{R}$ = is a symmetric $n \times n$ positive definite-definite matrix.

The weighting matrices $\mathbf{Q}$ and $\mathbf{R}$ are selected by the control-system designer to place bounds on the trajectory and control respectively. From a design point of view, the control system designer may design the system so that the term $\mathbf{x}^{T}(k)\mathbf{Q}\mathbf{x}(k)$ is chosen to penalise deviations of the regulated state $\mathbf{x}(k)$.

The control law that minimises $\mathbf{J}$ can be given by

$$\mathbf{u}(k) = -\mathbf{K}\mathbf{x}(k) \qquad (6.3)$$

with

$$\mathbf{K} = [\mathbf{R} + \mathbf{B}^{T}\mathbf{P}\mathbf{B}]^{-1}\mathbf{B}^{T}\mathbf{P}\mathbf{A} \qquad (6.4)$$

Where $\mathbf{P} = \mathbf{P}^{T} \geq 0$, is the unique positive definite solution, found by solving the discrete matrix *Riccati* equation:

$$\mathbf{P} = (\mathbf{Q} + \mathbf{A}^{T}\mathbf{P}\mathbf{A} - \mathbf{A}^{T}\mathbf{P}\mathbf{B}(\mathbf{R} + \mathbf{B}^{T}\mathbf{P}\mathbf{B})^{-1}\mathbf{B}\mathbf{P}\mathbf{A} \qquad (6.5)$$

Limitations

Generally, assumptions necessary for a unique positive definite solution $\mathbf{P} = \mathbf{P}^{T} \geq 0$, to the discrete LQR problem to exist are [85],

- Matrix $\mathbf{Q}$ must be symmetric and positive semi-definite.
- Matrix $\mathbf{R}$ must be symmetric and positive definite.
- The pair $[\mathbf{A},\mathbf{B}]$ must be controllable.
- The matrix $\mathbf{A}$ must be non-singular.

The optimal control given by equation (6.3) is a feedback form of control and is referred to as the *Linear-quadratic regulator* or *LQR*, shown below.

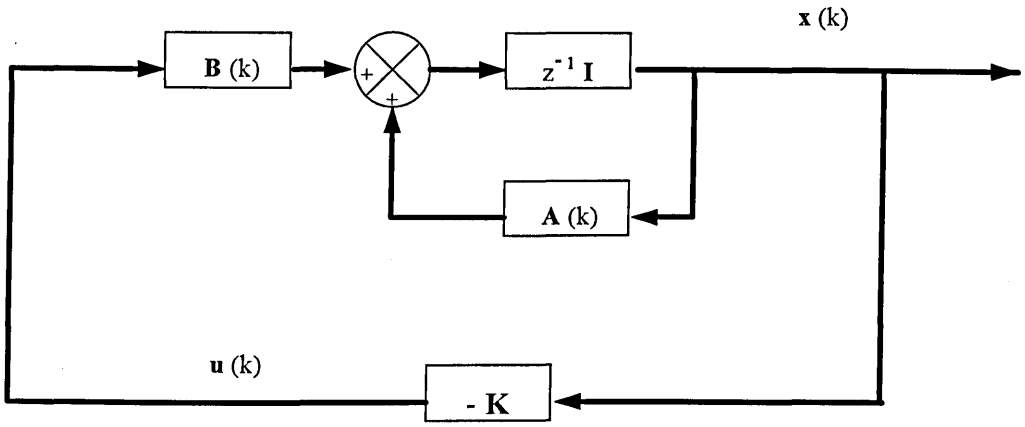

Figure 6.2. The optimal state regulator (LQR).

Stability of LQR

Incorporating the control law, $\mathbf{u(k) = - Kx(k)}$ in the state equations gives

$$\mathbf{x}(k+1) = (\mathbf{A} - \mathbf{BK})\mathbf{x}(k)) \qquad (6.6)$$

Where, $(\mathbf{A} - \mathbf{BK})$ are the closed loop eigenvalues and $\mathbf{x}(k)$ is the optimal state generating the above optimal system. equation (6.6) is asymptotically stable, that is, all of the eigenvalues are within the unit circle. This is the main advantage of employing the LQR scheme.

6.4 Optimal linear-quadratic-quassian (LQG) regulator

In order to implement the deterministic LQR discussed in the previous section, it is necessary to measure exactly all the states. Formulation of equations for estimating the unavailable states is the subject matter of this section.

Properties of the LQG regulator

Consider the discrete stochastic linear system model governed by the known linear state and measurement equations:

$$\mathbf{x}(k+1) = \mathbf{A}\mathbf{x}(k) + \mathbf{B}\mathbf{u}(k) + \mathbf{B}_1\mathbf{w}(k) \tag{6.7}$$

$$\mathbf{y}(k) = \mathbf{C}\mathbf{x}(k) + \mathbf{D}\mathbf{u}(k) + \mathbf{v}(k) \tag{6.8}$$

where,

$\mathbf{y}(k)$ = is the m -dimensional output vector.
$\mathbf{C}$ = is $m \times n$ matrix.
$\mathbf{D}$ = is a $n \times r$ direct feedthrough matrix.
$\mathbf{w}(k)$ = process noise.
$\mathbf{v}(k)$ = measurement noise.

and process and measurement noise covariances:

$\mathbf{E}[\mathbf{w}\mathbf{w}^T] = \mathbf{Q}_e$
$\mathbf{E}[\mathbf{v}\mathbf{v}^T] = \mathbf{R}_e$
$\mathbf{E}[\mathbf{w}\mathbf{v}^T] = 0$
$\mathbf{E}[\mathbf{w}] = \mathbf{E}[\mathbf{v}] = 0$

Where,

$\mathbf{E}$ is the expectation operator and,
$\mathbf{Q}_e$ is a symmetric and positive semi-definite i.e., $\mathbf{Q}_e = \mathbf{Q}_e{}^T \geq 0$.
$\mathbf{R}_e$ is a symmetric positive definite i.e., $\mathbf{R}_e = \mathbf{R}_e{}^T \rangle 0$.

Now, it is desired to produce an estimate $\hat{\mathbf{x}}(k)$, of the state $\mathbf{x}(k)$, using only the noisy input and output measurement data. This can be achieved by forming the state error vector, given by,

$$\mathbf{e}(k) = \mathbf{x}(k) - \hat{\mathbf{x}}(k) \tag{6.9}$$

and minimising the mean square error, i.e. the covariance of the estimate error, $\mathbf{P}_e$, defined to be

$$\mathbf{P}_e = \mathbf{E}\left[\left\|\mathbf{x}(k) - \hat{\mathbf{x}}(k)\right\|^2\right] \tag{6.10}$$

$$= \mathbf{E}\left[\, \mathbf{e}^T(k)\mathbf{e}(k) \,\right] \tag{6.11}$$

this is further elaborated in Section 6.4.2.

6.4.1 Observer formulation

It is assumed that the estimator takes the form of an observer, given by [85]

$$\hat{\mathbf{x}}(k) = \bar{\mathbf{x}}(k) + \mathbf{L}_c[\mathbf{y}(k) - \mathbf{C}\bar{\mathbf{x}}(k) - \mathbf{D}\mathbf{u}(k)] \tag{6.12}$$

where $\bar{\mathbf{x}}(k)$ is the predicted estimate based on a model prediction from the previous time estimate, that is

$$\bar{\mathbf{x}}(k) = \mathbf{A}\hat{\mathbf{x}}(k-1) + \mathbf{B}\mathbf{u}(k-1) \tag{6.13}$$

These equations are referred as the Measurement update and the Time update respectively.

Upon substitution of the Time update in the Measurement update yields,

$$\hat{\mathbf{x}}(k) = \mathbf{A}\hat{\mathbf{x}}(k-1) + \mathbf{B}\mathbf{u}(k-1) + \mathbf{L}_c[\mathbf{y}(k) - \mathbf{C}\mathbf{A}\hat{\mathbf{x}}(k-1) - \mathbf{C}\mathbf{B}\mathbf{u}(k-1) - \mathbf{D}\mathbf{u}(k)] \tag{6.14}$$

The above equation is referred as the *current estimator* by Franklin *et al* [85] and shown in Figure 6.3.

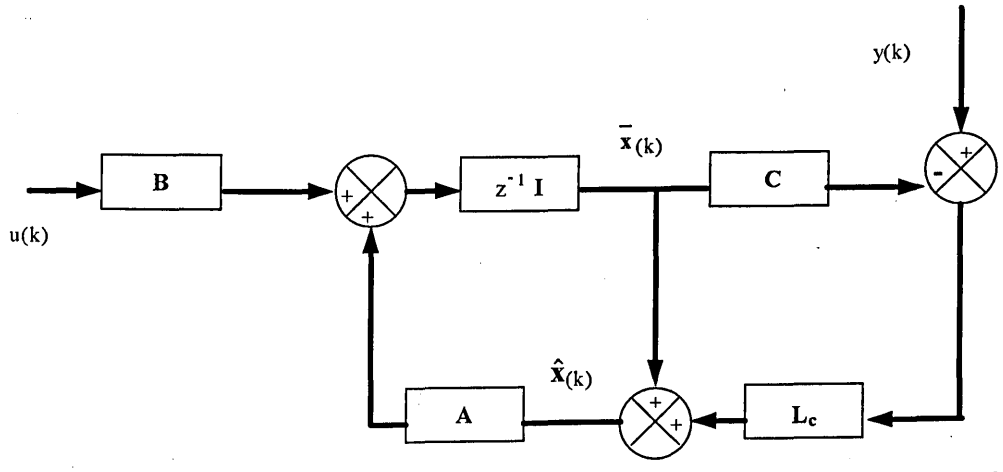

Figure 6.3. Block diagram of the estimator.

6.4.2 Error dynamics

Clearly, the observer provides the estimate $\hat{\mathbf{x}}(k)$ based on the input-output measurements and given matrix $\mathbf{L}_c$.

The estimation error as defined earlier

$$\mathbf{e}(k) = \mathbf{x}(k) - \hat{\mathbf{x}}(k) \tag{6.15}$$

is a measure that determines the performance of the estimator. Utilising the foregoing formulations, it can be shown that for the stochastic system describe by equation (6.7) and (6.8).

$$\mathbf{e}(k+1) = \mathbf{x}(k+1) - \hat{\mathbf{x}}(k+1)$$

which can be written as

$$\mathbf{e}(k+1) = \mathbf{x}(k+1) - \bar{\mathbf{x}}(k+1) - \mathbf{L}_C[\mathbf{y}(k+1) - \mathbf{C}\bar{\mathbf{x}}(k+1) - \mathbf{D}\mathbf{u}(k+1)] \tag{6.16}$$

after some algebraic manipulation results in:

$$\mathbf{e}(k+1) = [\mathbf{L}_C\mathbf{C} - \mathbf{I}][\bar{\mathbf{x}}(k+1) - \mathbf{x}(k+1)] - \mathbf{L}_C\mathbf{v}(k+1) \tag{6.17}$$

employing the error term $\mathbf{e}(k)$, thus, gives:

$$\mathbf{e}(k+1) = [\mathbf{A} - \mathbf{A}\mathbf{L}_C\mathbf{C}]\mathbf{e}(k) + [\mathbf{I} - \mathbf{L}_C\mathbf{C}]\mathbf{B}_1\mathbf{w}(k) - \mathbf{L}_C\mathbf{v}(k+1) \tag{6.18}$$

Equation 6.18 represents the dynamics of the estimation error **e**, where **w** and **v** are the forcing functions and the eigenvalues of $[\mathbf{A} - \mathbf{A}\mathbf{L}_C\mathbf{C}]$ determine the nature of the convergence process of the state estimate given the initial condition $\mathbf{e}(0) = \mathbf{e}_0$.

6.4.3 The optimum observer estimator

The main issue in the preceding section is the estimator gain matrix $\mathbf{L}_C$, which minimises the expectation of $\mathbf{e}^2$, that is, equation 6.10, namely, the covariance of **e**, which is denoted by $\mathbf{P}_e$. As per the assumptions (not necessarily realistic) that **v** and **w** are white noise processes. Therefore, the weighted sum of the **v** and **w** is also a white noise process:

$$\eta = [\mathbf{I} - \mathbf{L}_C\mathbf{C}]\mathbf{B}_1\mathbf{w}(k) - \mathbf{L}_C\mathbf{v}(k+1) \tag{6.19}$$

Thus,

$$\mathbf{e}(k+1) = [\mathbf{A} - \mathbf{A}\mathbf{L}_C\mathbf{C}]\mathbf{e}(k) + \eta \tag{6.20}$$

is a linear system excited by white noise, therefore, the poles of $[\mathbf{A} - \mathbf{AL_C C}]$ are the poles of the estimator. Naturally, these poles should be stable, or the estimator will fail to estimate the states, i.e. the error must become small and not large. In the absence of noise, i.e. $\eta = 0$, $\mathbf{e}$ will converge from some initial value $\mathbf{e}_0$ to zero.

6.4.4 Kalman gain $\mathbf{L_C}$

The optimal choice of $\mathbf{L_C}$, i.e. the Kalman gain matrix, which minimises equation 6.10 is given by [85]

$$\mathbf{L_C} = (\mathbf{R_e} + \mathbf{CP_eC^T}]^{-1}\mathbf{P_eC^T} \quad ; \tag{6.20}$$

Here, $\mathbf{P_e} = \mathbf{P_e}^T \geq 0$ is the covariance of the estimate error (which under assumptions is constant , since $\mathbf{e}(k)$ is also stationary) and is found by solving the discrete filter Riccati equation [84],

$$\mathbf{P_e} = (\mathbf{B_1 Q_e B_1} + \mathbf{AP_eA^T} - \mathbf{AP_eC^T}(\mathbf{R_e} + \mathbf{CPC^T})^{-1}\mathbf{CP_eA^T} \tag{6.22}$$

The solution $\mathbf{P_e} = \mathbf{P_e}^T \geq 0$, is the unique positive definite, and a sufficient condition for $\mathbf{P_e}$ to exist is that the pair [**A**, **C**] is completely observable. This condition may be relaxed to detectability, in which case it is necessary and sufficient, and $\mathbf{P_e}$ may be positive semidefinite. The constraints required for a unique positive definite solution to the discrete LQE problem to exist can be summarised as [85]:

- Matrix $\mathbf{Q_e}$ must be symmetric and positive semi-definite i.e., $\mathbf{Q_e} = \mathbf{Q_e}^T \geq 0$.
- Matrix $\mathbf{R_e}$ must be symmetric positive definite i.e., $\mathbf{R_e} = \mathbf{R_e}^T \rangle 0$.
- The pair [**A**,**C**] must be observable.
- The matrix **A** must be non-singular.

Since, the Kalman gain matrix $\mathbf{L_C}$ can be determined *a priori* and remains constant, this kind of filter is referred as the *stationary* or *constant-gain Kalman filter*. It is important to note that it is an estimator whose gain matrix has been optimised on the basis of statistical models of the process and measurement noises. Obviously, if the actual noise statistics vary with time, the optimality of the filter is not retained.

6.5 LQG compensator: Combined control law and estimator

Having defined the expressions for the regulator and the estimator independently, now it is desired to get an equation for the LQG compensator. That is the dynamic output feedback compensator made up of the regulator and observer equations:

Equation for the current estimator is given by equation (6.14),

$$\hat{\mathbf{x}}(k) = \mathbf{A}\hat{\mathbf{x}}(k-1)+\mathbf{B}\mathbf{u}(k-1)+\mathbf{L}_c[\mathbf{y}(k)-\mathbf{C}\mathbf{A}\hat{\mathbf{x}}(k-1)-\mathbf{C}\mathbf{B}\mathbf{u}(k-1)-\mathbf{D}\mathbf{u}(k)] \quad (6.23)$$

and the control law is given by,

$$\mathbf{u}(k) = -\mathbf{K}\hat{\mathbf{x}}(k) \quad (6.24)$$

In block diagram form, the compensator and plant are illustrated in Figure 6.4.

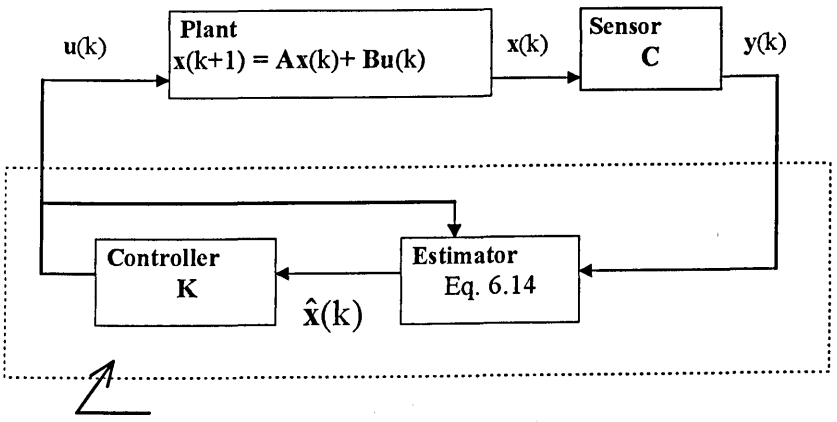

Figure 6.4. Schematic of combined estimator and controller.

The poles of the compensator when no direct feed through exist are given by [85] as:

$$|z\mathbf{I}-\mathbf{A}+\mathbf{B}\mathbf{K}+\mathbf{L}_c\mathbf{C}\mathbf{A}-\mathbf{L}_c\mathbf{C}\mathbf{B}\mathbf{K}| = 0 \quad (6.25)$$

and are *neither* the control law poles, equation. 6.6, nor the estimator poles, equation 6.18, These poles are not always stable. However, it can be shown that the closed loop system is indeed guaranteed to be stable, which is crucial.

6.5.1 Closed-loop system stability: *The separation principle*

A closed loop system's stability can be determined by examining at the eigenvalues of the system.

Consider the state equation:

$$\mathbf{x}(k+1) = \mathbf{A}\mathbf{x}(k) + \mathbf{B}\mathbf{u}(k)$$

with control; $\mathbf{u}(k) = -\mathbf{K}\hat{\mathbf{x}}(k)$

therefore, will give

$$\mathbf{x}(k+1) = \mathbf{A}\mathbf{x}(k) - \mathbf{B}\mathbf{K}\hat{\mathbf{x}}(k) \tag{6.26}$$

using, $\mathbf{e}(k) = \mathbf{x}(k) - \hat{\mathbf{x}}(k)$, i.e.

$$\hat{\mathbf{x}}(k) = \mathbf{x}(k) - \mathbf{e}(k)$$

$$\begin{aligned}\mathbf{x}(k+1) &= \mathbf{A}\mathbf{x}(k) - \mathbf{B}\mathbf{K}(\mathbf{x}(k) - \mathbf{e}(k)) \\ &= (\mathbf{A} - \mathbf{B}\mathbf{K})\mathbf{x}(k) + \mathbf{B}\mathbf{K}\mathbf{e}(k)\end{aligned} \tag{6.27}$$

Recall that, $\mathbf{e}(k+1) = [\mathbf{A} - \mathbf{A}\mathbf{L}_c\mathbf{C}]\mathbf{e}(k)$

thus combining state and error dynamics equations gives

$$\begin{bmatrix}\mathbf{e}(k+1) \\ \mathbf{x}(k+1)\end{bmatrix} = \begin{bmatrix}\mathbf{A} - \mathbf{A}\mathbf{L}_c\mathbf{C} & \mathbf{O} \\ \mathbf{B}\mathbf{K} & \mathbf{A} - \mathbf{B}\mathbf{K}\end{bmatrix}\begin{bmatrix}\mathbf{e}(k) \\ \mathbf{x}(k)\end{bmatrix} \tag{6.29}$$

The characteristic equation or the closed loop poles of the LQG system is given by

$$\begin{vmatrix}\mathbf{z}\mathbf{I} - \mathbf{A} + \mathbf{A}\mathbf{L}_c\mathbf{C} & \mathbf{O} \\ \mathbf{B}\mathbf{K} & \mathbf{z}\mathbf{I} - \mathbf{A} + \mathbf{B}\mathbf{K}\end{vmatrix} = 0 \tag{6.30}$$

which because of the zero matrix in the upper right can be written as

$$\left|\mathbf{z}\mathbf{I} - \mathbf{A} + \mathbf{A}\mathbf{L}_c\mathbf{C}\right| \left|\mathbf{z}\mathbf{I} - \mathbf{A} + \mathbf{B}\mathbf{K}\right| = 0 \tag{6.31}$$

Therefore, the closed-loop poles of the overall LQG system are simply the poles of the regulator and the poles of the estimator, which as shown are guaranteed to be stable. The combined controller-estimator system has the same eigenvalues as those of the

control alone and the estimator alone and yet they can be used together. This is called as the *Separation principle.* The optimal controller employing the Kalman filter can be used even if there is no noise or disturbances present in the system [84].

6.6 Problem definition

The presence of the main resonance mode at 0.34 Hz, evident from Section 3.2.2, is the primary cause of residual vibration in the TRMS. The residual motion (vibration) is induced in flexible structures primarily as a result of faster motion commands. The occurrence of any vibration after the commanded position has reached will require additional settling time before the new manoeuvre can be initiated. Therefore, in order to achieve a fast system response to commanded input signals, it is imperative to reduce this vibration. This feature is desirable in any fast manoeuvring systems, such as fighter aircraft. Various approaches have been proposed to reduce vibration in flexible systems. They can be broadly categorised as feedforward, feedback or a combination of feedforward and feedback methods. The latter structure is considered in this work.

6.6.1 The 1 DOF TRMS model

Having successfully obtained a linear model for a 1 and 2 DOF TRMS in Chapter 3, the second important issue is to design a suitable controller which is robust to modelling errors. Heres a, 1 DOF, the pitch (vertical) plane SISO model will be considered for controller design and implementation purpose. A discrete-time SISO transfer function model, obtained via the system identification of Chapter 3, is :

$$\frac{y1}{u1} = \frac{(z-9805+1.3281i)(z-9805-1.3281i)(z+1.0743)}{(z-0.8926-0.4095i)(z-0.8926+0.4095i)(z-0.7541)(z-0.4685)} \qquad (6.32)$$

where, $y1$ = pitch angle, radians ; and
$u1$ = main rotor input, volts.

Note, that the system is nonminimum phase with zeros outside the unit circle. The detrimental affect of this on the swiftness of response will be evident in the later section. The equivalent pitch plane state-space representation for the 1 DOF pitch plane model is then:

$$\mathbf{A}=\begin{bmatrix} 3.007 & 1.0 & 0 & 0 \\ -3.5 & 0 & 1.0 & 0 \\ 1.8096 & 0 & 0 & 1.0 \\ -0.341 & 0 & 0 & 0 \end{bmatrix} \quad \mathbf{B}=\begin{bmatrix} 0.0205 \\ -0.0278 \\ 0.0458 \\ -0.0033 \end{bmatrix} \tag{6.33}$$

$$\mathbf{C}=[1.0 \quad 0 \quad 0 \quad 0] \qquad \mathbf{D}=[0.0097]$$

6.6.2 Performance requirements

This controller is expected to satisfy a desired performance specification consisting of:

- robust tracking of commanded *pitch* angle with low overshoot and quick settling time of residual oscillations i.e. control of rigid as well as flexible dynamics.
- closed-loop stability, vibration attenuation and good disturbance rejection capability.
- high response bandwidth (i.e. short rise time) consistent with the dynamic capabilities of the TRMS airframe and available control energy.
- insensitivity to modelling errors and unmodelled dynamics.

The TRMS operational condition is a flat horizontal boom, representing a hover mode.

6.7 LQG regulator

The LQG control synthesis procedure discussed, is adopted here for the TRMS model. The objective of the LQG controller is to minimise the average energy over all frequencies captured by the closed-loop transfer function from exogenous inputs to the error signal. The plant output error is augmented with an integrator to achieve zero steady-state tracking error. The goal of LQR controller is therefore, to find the control sequence u(t) which minimises a quadratic cost on the states and inputs:

$$\mathbf{J} = \frac{1}{2}\sum_{k=0}^{N} \left[\mathbf{x}^{T}(k)\,\mathbf{Q}\,\mathbf{x}(k) + \mathbf{u}^{T}(k)\,\mathbf{R}\,\mathbf{u}(k)\right] \tag{6.34}$$

where $\mathbf{x}$ is the augmented state vector including the state of the integrator, $\mathbf{R}$ is a positive scalar and yields a matrix of optimal gains $\mathbf{K}$ for state feedback and $\mathbf{Q}$ is the weighting matrix on the states. The Riccati equation is:

$$\mathbf{P} = \mathbf{Q}+\mathbf{A}_a{}^{T}\mathbf{P}\mathbf{A}_a - \mathbf{A}_a{}^{T}\mathbf{P}\mathbf{B}_a(\mathbf{R}+\mathbf{B}_a{}^{T}\mathbf{P}\mathbf{B}_a)^{-1}\mathbf{B}_a\mathbf{P}\mathbf{A}_a \tag{6.35}$$

The plant matrix $\mathbf{A_a}$ in the Riccati equation is an augmented matrix including the additional error state vector. This is equivalent to including integral action on the tracking error of the system as described earlier, and $\mathbf{B_a}$ is a suitably augmented control matrix. Furthermore, the plant model has four states, with only one state, however, being measurable, necessitating the inclusion of an observer. The optimal observer design is the *dual* of the optimal regulator, hence, the observer gain matrix $\mathbf{L_C}$ is computed in a similar manner as that of regulator, except that the observer gains are computed only for the plant states, i.e., integral error state is not included. It was ensured that the estimator roots are faster than the closed-loop control roots, so that the total system response is dominated by the control roots. This was achieved by choosing suitable standard covariances matrices, $\mathbf{Q_e}$ and $\mathbf{R_e}$. The LQG compensator is obtained by combining the state feedback with the estimator, as shown in Figure 6.4.

6.7.1 Selection of weighting matrices Q and R.

The dynamic characteristics of the closed-loop system depend on the matrices $\mathbf{A_a}$ and $\mathbf{B_a}$ as well as the weighting matrices **Q** and **R**, and are quite complex [86]. A pragmatic approach is therefore, to choose a range of **Q** and **R** matrices, generate corresponding regulator gain matrices **K** and subsequently simulate the closed-loop response. The gain matrix that satisfies the performance criteria is a satisfactory one. Another rule is to define **Q** and **R** as

$\mathbf{Q}$ = diag ($q_1, q_2, \ldots\ldots q_n$,) and $\mathbf{R}$ = diag ($r_1, r_2, \ldots\ldots r_n$,) > 0.

and to use an initial guess of q_i, and r_i, [87] as

$$q_i = \left[\frac{1}{(z_i)_{max}}\right]^2 \quad \text{and} \quad r_i = \left[\frac{1}{(u_i)_{max}}\right]^2 \tag{6.36}$$

where z_i, u_i, are the values of the *i* th elements of the corresponding vectors, and the subscript *"max"* defines the maximum acceptable value. This approach implicitly trades between tracking and control-energy performance.

6.7.2 Selection of covariance matrices $\mathbf{Q}_e$ and $\mathbf{R}_e$.

The covariance matrices $\mathbf{Q}_e$ and $\mathbf{R}_e$ can regarded as design parameters in tuning the bandwidth and characteristics of the Kalman filter. Given an actual design problem, one can assign a meaningful value to $\mathbf{R}_e$ based on the sensor accuracy. The same cannot be said of $\mathbf{Q}_e$. The assumption of white process noise is often a mathematical artifice that is used because of the ease of solving the resulting optimisation problem. Physically, $\mathbf{Q}_e$ is crudely accounting for unknown disturbances, whether they be steps, white noise or somewhere in between, and for the imperfection in model. The disturbance noise model should be selected to approximate that of the actual known disturbances when practical, but the designer often settles on acceptable values based on the quality of the estimation that results from subsequent simulations including all known disturbances, white or otherwise [85].

In the present study, various combinations of Q and R were employed. Two cases are reported here.

Case I: $\mathbf{Q} = \mathbf{I}$, $\mathbf{R} = 75$, and
Case II: $\mathbf{Q} = \mathbf{I}$, $\mathbf{R} = 1$.

This choice implies that the states are equally weighted and the actuator signal a) is heavily penalised to ensure an overdamped response, and b) control is "cheap", respectively. The equivalent covariance matrices for the observer are selected by trial and error to get faster estimator poles and are maintained the same in both the cases. The **Q** and **R** matrices are to be adjusted to obtain good disturbance rejection, high damping and a bandwidth that provides fast response without saturating the control.

6.8 LQG simulation results

In order to test the controller, different simulations of the linear model of the TRMS were carried out with a square wave input. The controller performance, thus developed, was tested within the Simulink simulation environment. The structure of the controller is shown in Figure 6.5, with $H(s)$ representing the LQG controller with integral action. The inner loop control is referred to, as the *Stability Augmentation System* (SAS), whose primary role is to maintain static and dynamic stability.

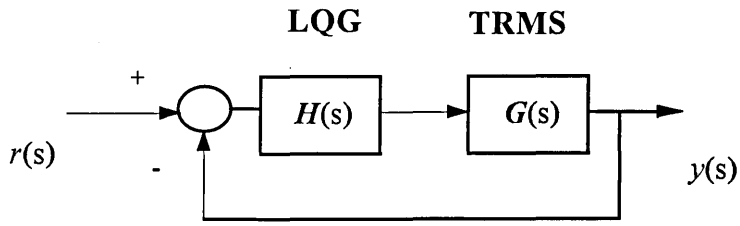

Figure 6.5. Stability Augmentation System (SAS).

Case I: The tracking capability in following a square wave *pitch* angle command is shown in Figure 6.6 along with the control effort. The performance of the LQG compensator for the nominal TRMS model is characterised by an overdamped response, considerable rise time (3 sec.), little overshoot, and a slow settling time (12 sec.). The control effort is found to be high and saturates the actuator limit, denoted by dashed lines.

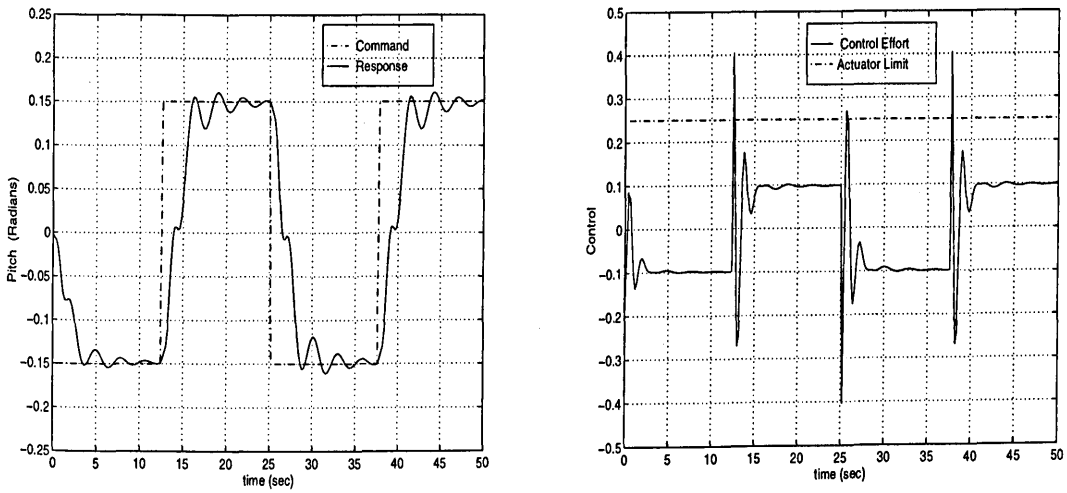

Figure 6.6. SAS response to square wave input, **Q** = **I**, **R** = 75.

Case II: Simulation results with this state feedback design, are depicted in Figure 6.7. The plots shows short rise time (1 sec.), high overshoot and a fast settling time of residual vibrations (5-6 sec.). In this case too, the control effort is too high and much beyond the actuator limit.

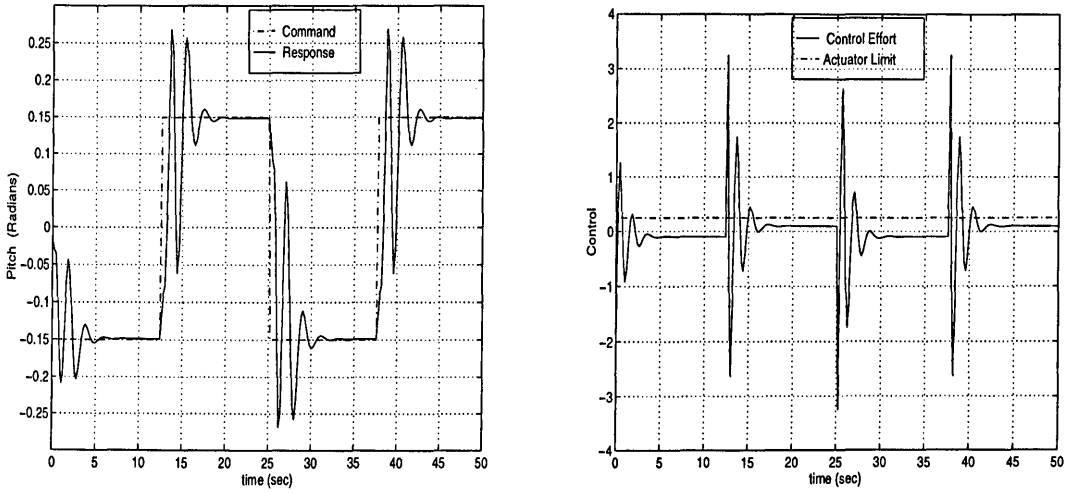

Figure 6.7. SAS response to square wave input, **Q = I, R = 1**.

It can be inferred from the above results that, although SAS provides dynamic stability it has inadequate direct control over *response shaping.*

6.9 Command path prefilter

It is apparent, that performance criteria, such as, speed of response or manoeuvrability, flying and handling qualities, imposed on an aircraft/TRSMS are difficult to achieve entirely by *aerodynamic* means alone (i.e. using control surfaces in aircraft or rotors for the TRMS) which at the same time maintaining the dynamic stability of the airframe. This is particularly valid for highly agile *new generation* air vehicles, which are designed to operate over extended flight envelopes and in aerodynamically difficult flight regimes. The TRMS performance can be further enhanced by employing *artificial non aerodynamic* means. This, in essence, implies appending a command path prefilter or feedforward precompensator to the SAS. The new control structure shown in Figure 6.8, is known as *Command and Stability Augmentation System* (CSAS).

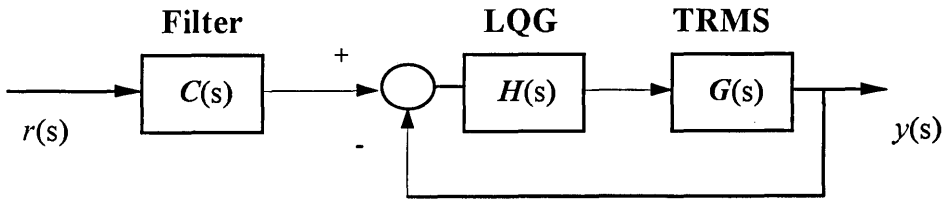

Figure 6.8. Command and Stability Augmentation System (CSAS).

The command signal r(s), is conditioned by a command control law which determines the control and response characteristics y(s) of the augmented system. The consequence of this is a *shaped response* and reduced control effort, which translates into reduced pilot workload and improved passenger comfort in the case of an aircraft.

Referring to Figure 6.8, the overall closed-loop transfer function can be written as:

$$\frac{y(s)}{r(s)} = C(s)\left(\frac{H(s)G(s)}{1+H(s)G(s)}\right) \tag{6.37}$$

It is important to note that the prefilter has no bearing on the system stability since it is outside the closed loop and does not appear in the characteristic equation of the augmented plant.

The transfer function of equation (6.37) is that of the augmented TRMS and replaces that of the unaugmented TRMS $G(s)$. Clearly, by judicious choice of $C(s)$ and $H(s)$ the control engineer has considerable scope for achieving the desired stability, control and handling characteristics of the augmented system. The command prefilter $C(s)$ in this study comprise digital filters used to pre-process the input to the TRMS so that no energy is put into the system near its resonance. Thus, command input profiles which do not contain energy at the system natural frequencies do not excite structural vibrational modes and hence require no additional settling time.

6.9.1 Prefilter results

To study the augmented system performance, a square wave is used and the corresponding system response is measured. The main objective of this section is to

further improve the augmented system performance by *non-aerodynamics* means. This is achieved by suppressing system vibrations at the first few dominant resonance modes. Two strategies, namely low-pass filtered and band-stop filtered input shaping are used.

6.9.2 Low-pass shaped input

A low-pass Butterworth filter (LPF) of order two with a cut-off frequency at 0.2 Hz was designed and employed for processing the command input. The motive behind selecting the cut-off frequency at 0.2 Hz lies in the fact that the lowest vibrational mode of the system is found to be at 0.25 Hz. Hence, to attenuate resonance of the system the cut-off frequency must be selected lower than the lowest vibrational mode. For **Case I** the system response to low-pass filtered command square wave is shown in Figure 6.9 along with the corresponding control effort. Compared to Figure 6.6, it is noted that the attenuation in the level of vibration is significant with quicker settling time (7-8 sec.). However, this is at the cost of increased rise time (4.5 sec.).

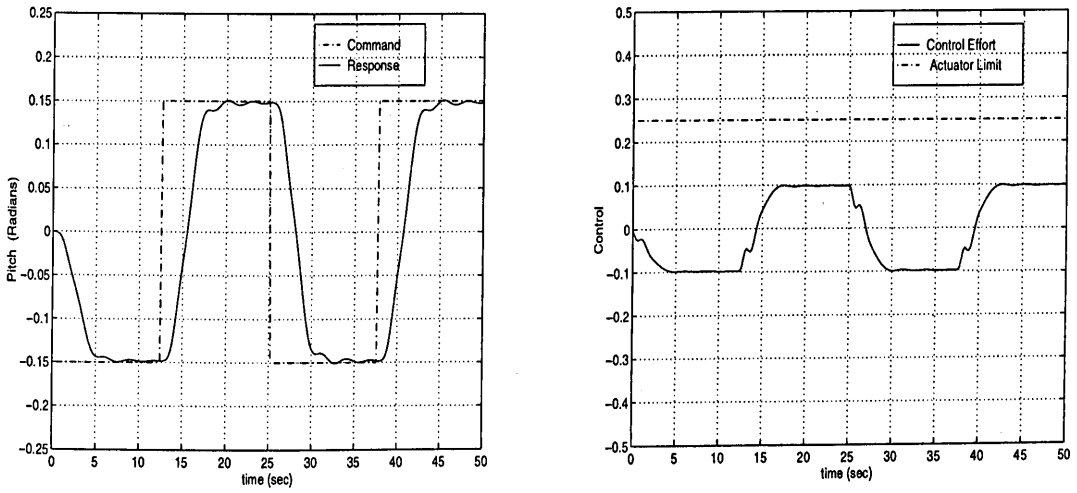

Figure 6.9. CSAS response using LPF (0.2 Hz cut-off), **Q** = **I**, **R** = 75.

The closed loop system rise time characteristics can be further accentuated by allowing more "energy" into the system. Therefore, the command prefilter with a cut-off frequency of 0.3 Hz is next investigated. The anticipated improvement in the rise time (3 sec.) is evident from Figure 6.10, but, this has led to degradation of settling time (10 sec.).

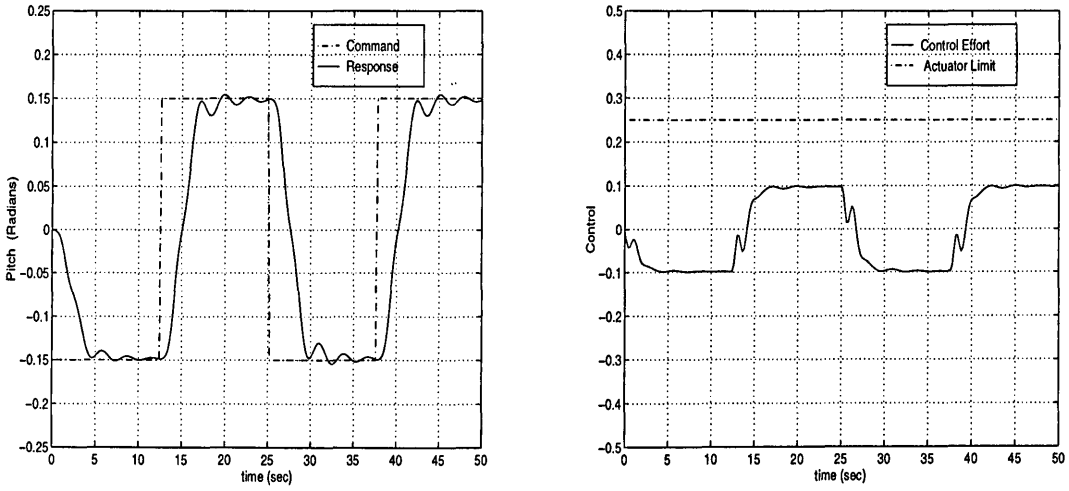

Figure 6.10. CSAS response using LPF (0.3 Hz cut-off), **Q** = **I**, **R** = **75**.

An important observation is that, after adding a command prefilter, the control is within the actuator limit and displays improved behaviour. This is a significant improvement over the feedback controller alone.

Similarly, this procedure was repeated for **Case II**, with cut-off frequencies as before, and the responses are shown in Figures 6.11 and 6.12 respectively. It can be noticed that the filter with 0.2 Hz cut-off, satisfies the control constraint as well as has acceptable level of performance. The response with 0.3 Hz cut-off is better than 0.2 Hz LPF, but saturates the control.

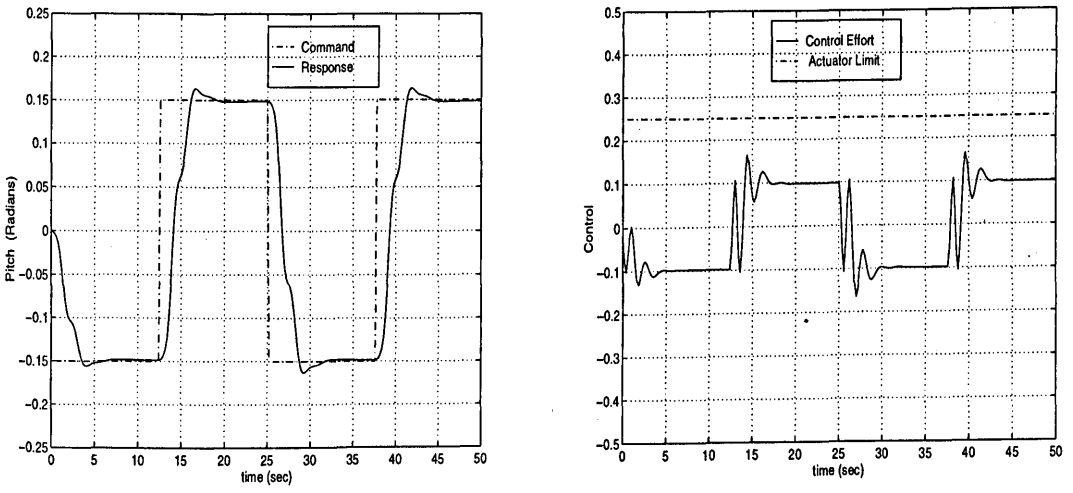

Figure 6.11. CSAS response using LPF (0.2 Hz cut-off), **Q** = **I**, **R** = 1.

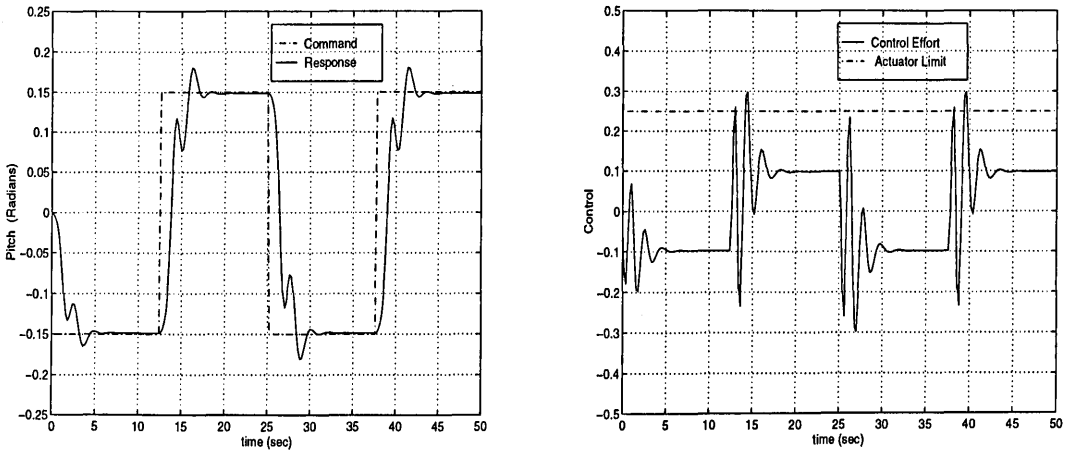

Figure 6.12. CSAS response using LPF (0.3 Hz cut-off) **Q** = **I**, **R** = 1.

6.9.3 Band-stop shaped input

As before, a second-order digital Butterworth filter is used to study the CSAS performance with a band-stop shaped input. For effective suppression of vibrations, the centre frequency of the band-stop filter (BSF) has to be exactly at the same frequency or as close as possible to the resonant modes. For the 1 DOF modelling experiments of Section 3.2.2, it is observed that the main resonant modes lies at 0.25 and 0.34 Hz, with additional clustered modes in a close proximity to the main modes. Thus, a band-stop filter with centre frequency (CF) of 0.25 and 0.34 Hz with a bandwidth of 0.2 Hz was selected. A band-stop shaped square wave input was accordingly used and the pitch response was measured, Figure 6.14 and 6.15, for the two cases. In both cases, the control energy requirement is high, and, response settling time is unacceptably large.

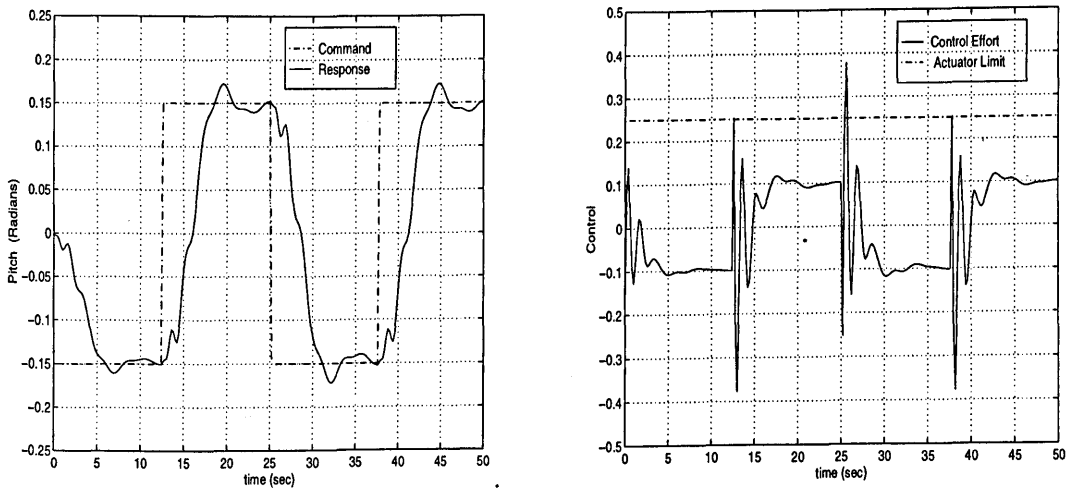

Figure 6.13. CSAS response using BSF (CF 0.25 & 0.34 Hz), **Q** = **I**, **R** = 75.

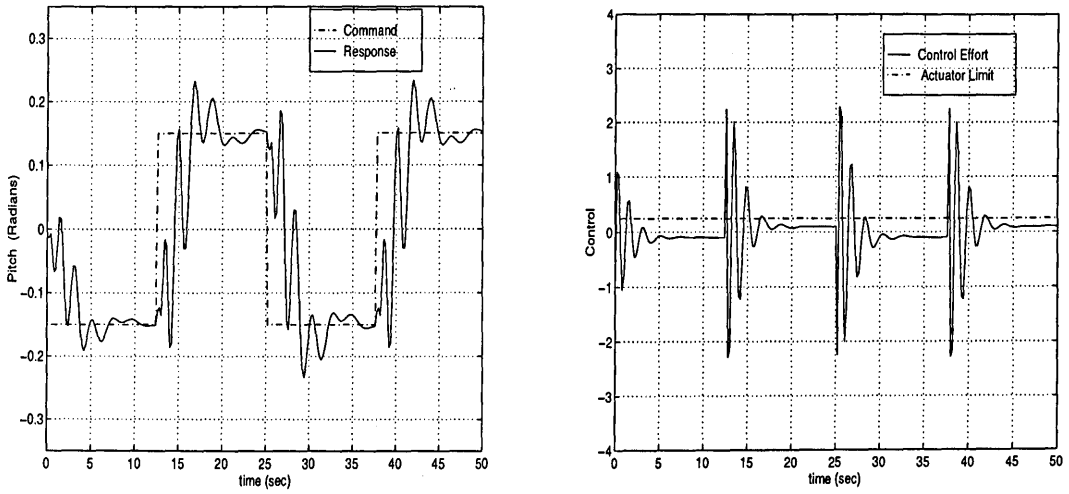

Figure 6.14. CSAS response using BSF (CF 0.25 & 0.34 Hz), $\mathbf{Q} = \mathbf{I}$, $\mathbf{R} = 1$.

From the foregoing analysis, it is deduced that, the *command path* prefilter, serves as a principal means for *response shaping*. Good response shaping characteristics are highly desirable in fast manoeuvring systems with rapidly changing command input.

6.10 Observations

The overall results of feedback and combined feedback and feedforward control structure are logged in Table 6.1. It is evident that the CSAS design with a low-pass filter yields a satisfactory system performance. The particulars of the system response with this design is illustrated by the shaded portion of Table 6.1.

Equation (6.33) revealed the nonminimum phase nature of the TRMS. The speed of response to the input command for a nonminimum phase plant is limited by the existence of the nonminimum phase transmission zeros. Such a system has a slow speed of response and this detrimental effect is discernible in all the simulation results, except Figure 6.7, where unrealistically high control effort is needed to achieve fast response.

Since minimum phase airframes exhibit minimal response time, highly agile aircraft are augmented by including additional control surfaces called canard or "flaperons" to the airframe [75]. A similar strategy could be adopted here or any other platforms, where such feature is desirable.

Control Structure	FB: LQG (SAS)	LPF (CSAS)		BSF (CSAS) CF = 0.25 & 0.34 Hz
		Cutoff 0.2 Hz	Cutoff 0.3 Hz	
Q=I, R=75:				
TR (sec)	3	4.5	3	4
TS (sec)	12	7-8	10	13
Control	high	ok	ok	high
Q=I, R=1:				
TR (sec)	1	2.5	3	2.5
TS (sec)	5-6	6-7	5.5	12
Control	high	ok	high	high

Table 6.1. Shaded region represents optimal result, TR: Rise-time. TS: Settling time.

6.11 Concluding remarks

This chapter has investigated the design of an optimal control scheme which stabilizes the TRMS and results in a good command tracking capability using the *aerodynamic* means (i.e. using main rotor). However, this was achieved at the cost of "expensive" control. The performance of the feedback control was improved by using an additional *artificial non-aerodynamic* means, i.e. by employing a command prefilter.

The feedforward filter conditioned the tracking command or setpoint so that system's residual vibrations (oscillations) are reduced. Quick elimination of residual vibrations is important for fast manoeuvring platforms, where the command signal changes rapidly. The advantage of this method is that, it is not necessary to change the feedback control law in order to attenuate system's vibration.

The study revealed that better performance in attenuation of the system vibration is achieved with a low-pass filtered command input, as compared to band-stop filter. This is due to indiscriminate spectral attenuation of frequencies above the cut-off level in the low-pass filtered input. However, this is at the expense of slightly higher response time as compared to band-stop filter.

With a command pre-filter, the control effort is found to be within the actuator limits. Several different combinations of weighting matrices and command prefilter are essential to achieve optimal performance. Thus, an appropriately designed feedforward and feedback controller is a practical approach to satisfy the design specification.

Chapter 7

Experimental investigation of optimal control paradigm

The Stability Augmentation System (SAS) and the Command and Stability Augmentation System (CSAS) developed in the last Chapter will be executed in this Chapter. The control law is implemented in real-time, on the TRMS platform.

7.1 Introduction

In the last Chapter various control schemes for controlling the TRMS were developed and tested within a simulation environment. The crucial test for any control paradigm is when implemented on the real system in presence of real world uncertainties and disturbances. The aim of this Chapter is to apply these schemes to the TRMS. The TRMS hardware and software configuration was described in Chapter 2 and the control strategies are those developed in the previous Chapter. It will be shown however, in Section 7.3, that the two cases investigated in the simulation environment are inadequate to get the desired closed-loop system performance. Hence, more cases are investigated. The experimental results of SAS are first presented in Section 7.3.1, followed by those of CSAS in Section 7.3.2. Finally, optimal control scheme robustness to disturbances is demonstrated in Section.7.4. The findings of experiments are encapsulated in Section 7.5.

7.2 The general control problem revisited

The various stages involved in establishing a control system for a physical plant were described in Chapter 1. So far, the first four stages have been addressed, this Chapter will cover the crucial final step of control law implementation. The five steps can be re-cast in a general control problem (GCP) framework. A schematic of the general control problem is illustrated in Figure 7.1. [88]. This figure shows two worlds, a real world

and a mathematical world. In the real world, plants are ill-defined and often difficult to describe, hence the rugged boundaries. In contrast, the mathematical world is generally well defined, hence the smooth circular boundary. The five steps are re-visited in the light of Figure 7.1.

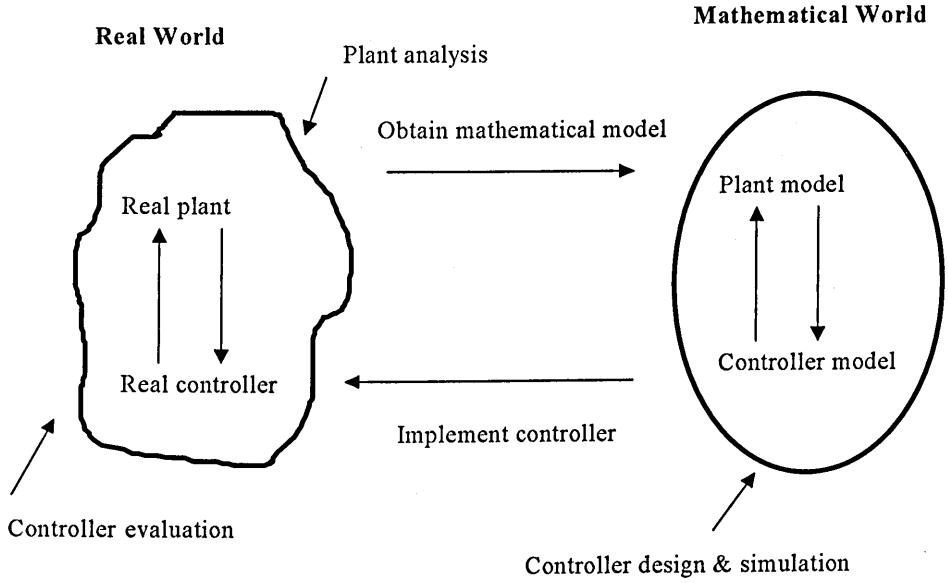

Figure 7.1. The general control problem.

System design and requirement: It is expected from the application specific designer to design a sophisticated system but not too complex to achieve the desired control system requirements. Therefore, interaction and involvement of control specialist at an early stage is essential.

Modelling of the given system: This step entails migration from the real world to the mathematical world in the GCP framework. Both modelling and system identification can be used depending upon whether the system exists or is still being designed and whether the plant dynamics are well understood. The modelling step is the most demanding and crucial stage in the whole control design process.

Control design and control system analysis: These tasks occur in the mathematical world. A controller is designed using the plant model in order to satisfy the system specifications determined in the system design phase. While designing the controller it is vital to understand the relationship between a model and the real plant. Other concepts like the equilibrium point, different operating regimes, actuator saturation limits, and so on, need to be well understood and translated in the control design exercise. The control system analysis examines the controlled system behaviour and determines if the controller is good enough to be transferred to the plant.

Control implementation: There is a strong focus on simplicity at the controller implementation stage. Simplicity means reduced hardware, which in turn means a cheaper control system which weighs less and takes up less space. Simplicity also results in greater integrity of the control system which is vital for safety critical systems such as for aerospace applications. For instance the A320 Airbus triplicates all hardware for the control law, plus there is a fourth independently designed back-up control law [89].

Once the designer is convinced that the controller performs well in the mathematical world, and that it has a good chance of meeting the required specifications in the real world, the controller can be implemented. The implemented controller then need to be evaluated functionally. This is rarely a one step procedure and, as will be shown later in this Chapter, requires several set of control laws are needed to meet or achieve acceptable functional requirements. It is tedious trial and error procedure from the simulation (mathematical world) steps 3 and 4, to implementation (real world) step 5. The remainder of this Chapter will focus on the last step.

7.3 Controller implementation results

The controllers designed in the last Chapter are linked to the TRMS in real-time through the MATLAB-Simulink interface described in Chapter 2. Both control schemes, the Stability Augmentation System (SAS) and the Command and Stability Augmentation System (CSAS) will be executed. Essentially, the task of the LQG controller is to achieve robust tracking of commanded *pitch* angle by manipulating the input to the main rotor. The controlled output (*pitch* angle) is expected to have low overshoot, quick settling time of residual oscillation and reasonably fast speed of

response without control saturation. Note that the operating point for this experiment is the flat horizontal main body, representing hover mode.

7.3.1 SAS implementation results

The details regarding the real-time experiments are given in Chapter 2. Recall from Chapter 3, Section 3.2.4, that the sampling time for modelling and control should be the same. Hence, the sampling period is 5 Hz and is set before the experiments using the MATLAB command ***hl_call*** **(*'Setsampletime'*, sampletime)**. The steady state condition is allowed to reached before injecting the square wave command input. The primary role of SAS is to ensure the stability of the system in the prescribed operating region.

Case 1: Q = I, R = 75.

The controllers ability to track the commanded square wave input and the control energy expended are shown in Figure 7.2. Although the controller tracks the reference signal, the response is characterised by significant overshoot and erratic settling time. Poor control behaviour is also observed on the negative phase of the command cycle, which was absent in the simulations. The negative command essentially represents the downward motion of the main body. A sharp drop from the positive pitch angle, aided by gravity, exacerbate the inherent oscillatory nature of the TRMS. Without sufficient damping, control in these region is therefore poor. Similar to the simulation trials, the control saturates, but the system remains stable.

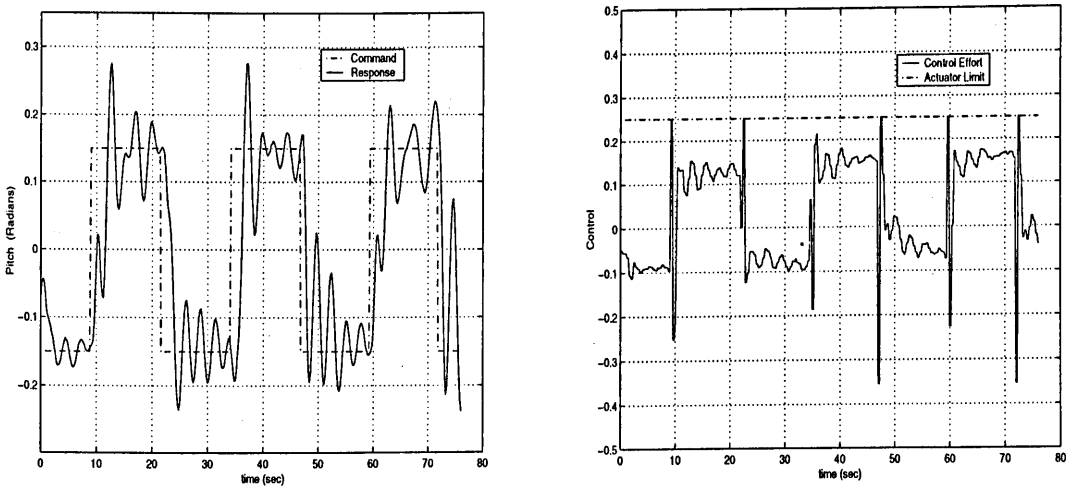

Figure 7.2. SAS response to square wave input. **Q = I, R = 1.**

Case II : Q = I, R = 1.

This is the second of the two cases studied in the simulation environment. This controller failed to perform in real-time, which was marked by unstable behaviour. The likely causes appear to be slow observer poles in comparison to the regulator poles. In-spite of functioning well in the mathematical domain, it fails in the real world, clearly indicating a gap that exist between theory and practice.

Since **Case 1** SAS results are unsatisfactory and the failure of **Case II**, the trial and error procedure becomes apparent. Hence, it was necessary to go back to the mathematical world i.e., steps 2 and 3 carry out few more controller designs and return once again to the real world. The following additional cases are investigated:

Case III : Q = I, R = 100; and
Case IV : Q = I, R = 125.

The rational for choosing these weights is to achieve further damped response, which is possible by penalising the input.

Case III : Q = I, R = 100.

Figure 7.3 represents SAS performance. Here, the response is better than **Case I,** with relatively less overshoot and reasonable output settling time. However, analogous to **Case I,** the closed-loop plant is unable to maintain a tight control on the negative pitch command, indicating a need for further damping. On the control effort side, performance is acceptable with slight saturation. The overall system remains stable.

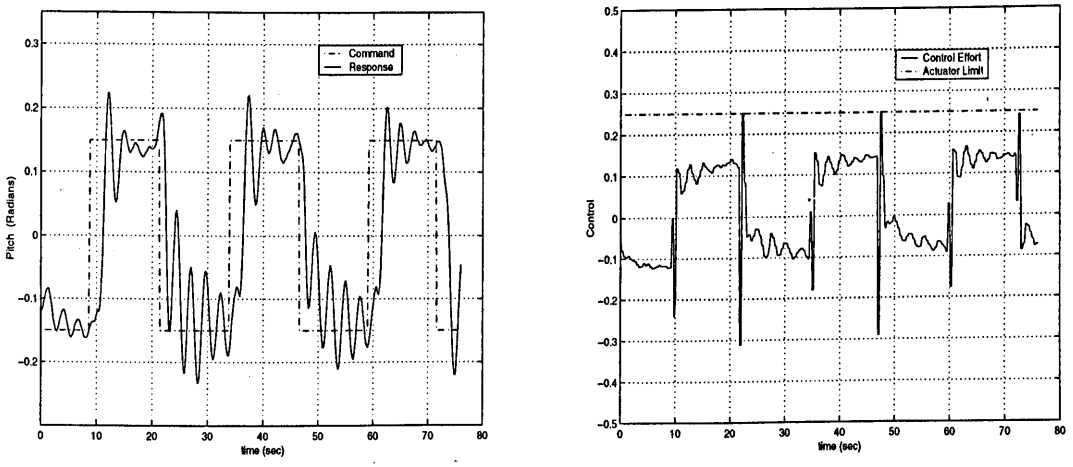

Figure 7.3. SAS response to square wave input. **Q = I, R = 100.**

Case IV : Q = I, R = 125.

The TRMS response to the square wave reference signal is illustrated in Figure 7.4. Much improved tracking is obtained on positive and negative cycles of the reference signal, implying good damping and hence, tighter control. There is hardly any overshoot with smooth and acceptable settling time. Note that minor oscillations are due to inherent characteristic of the TRMS, which exhibits a minor oscillatory tendency even in steady state condition Thus, good settling behaviour is assumed. The control signal is also within the saturation boundaries, but operates very close to it.

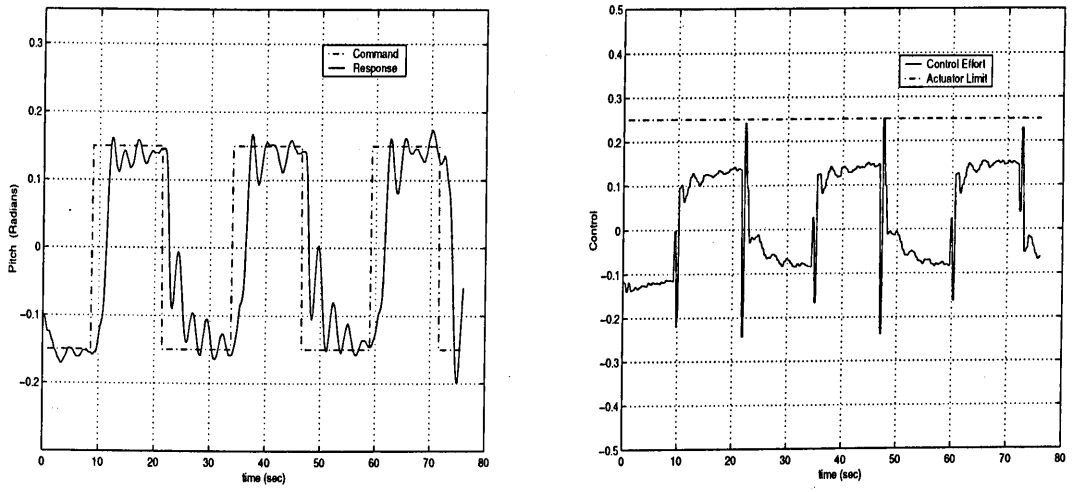

Figure 7.4. SAS response to square wave input. **Q = I, R** = 125.

In all the cases discussed above, the control demands are sharp, i.e. require a sudden burst of energy when the step command is applied. Such behaviour is undesirable, as it is detrimental for the plant operational life span. The jerky actuator movement will induce fatigue and thereby cause mechanical wear and tear of the TRMS.

7.3.2 CSAS implementation results

As explained in the simulation studies of Chapter 6, improvement in the response characteristics of the augmented plant is sought using the command path pre-filter. In line with simulations study, low-pass and band-stop filter are employed for input shaping.

7.3.2.1 Low-pass shaped input

Three low-pass Butterworth filter (LPF) of order two with a cut-off frequency at 0.1 Hz, 0.2 Hz and 0.3 Hz were designed and utilised for filtering the reference square wave input. LPF of 0.1 Hz is included in the experimental investigation in order to observe the rigid body behaviour, with all the major resonant modes suppressed.

Case 1: Q = I, R = 75.

Figure 7.5. shows the TRMS pitch response to the 0.1 Hz filtered command signal. The input square wave is followed reasonably well with acceptable overshoot, also displaying a good settling time characteristic. Control energy requirements are also minimal. However, it is found to have a slow rise time.

With 0.2 Hz LPF, the TRMS pitch response is better than that achieved with 0.1 Hz filter as seen in Figure 7.6. The response rise time, settling time, overshoot and control energy expenditure are all satisfactory.

Finally, a 0.3 Hz LPF is employed, which allows more input energy into the TRMS. The results are illustrated in Figure 7.7. As anticipated, improved rise time behaviour is evident, but at the expense of greater overshoot and longer settling time. No saturation of actuator is noticed.

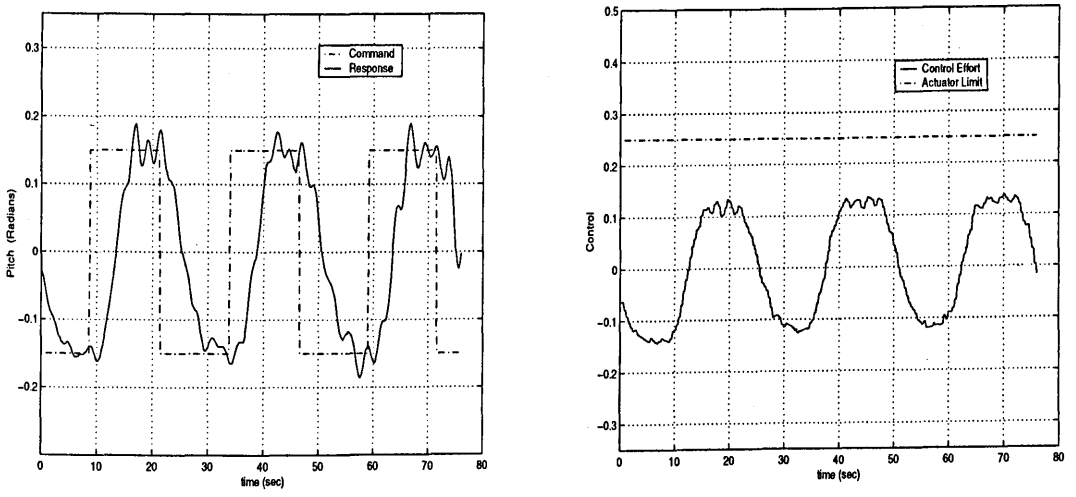

Figure 7.5. CSAS response using LPF (0.1 Hz cut-off) **Q = I, R = 75.**

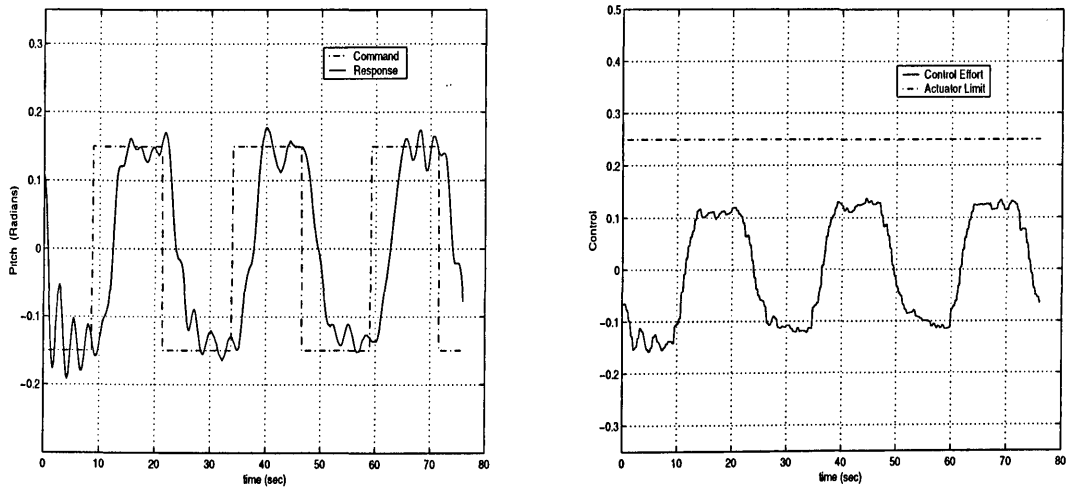

Figure 7.6. CSAS response using LPF (0.2 Hz cut-off) **Q** = **I**, **R** = 75.

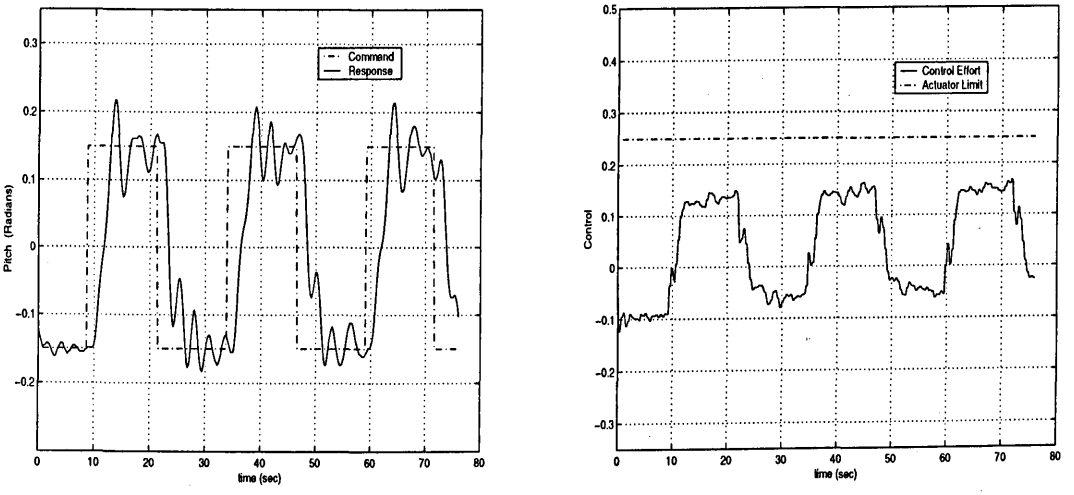

Figure 7.7. CSAS response using LPF (0.3 Hz cut-off) **Q** = **I**, **R** = 75.

Case III : Q = **I**, **R** = 100 ; and
Case IV : Q = **I**, **R** = 125.

The system responses for the remaining two cases are illustrated in Figures 7.8, 7.9, 7.10, and Figures 7.11, 7.12, 7.13. A closer observation reveals a very similar pitch response to the reference signal and control pattern to that of **Case I,** with a marginal differences. Like **Case I, Case III** and **Case IV** exhibit fairly good performances with low pass filters of 0.1 and 0.2 Hz cut-off frequencies. However, analogous to **Case I,** system performance deteriorates for **Case III** and **Case IV** with a command path pre-filter of 0.3 Hz cut-off. The degradation in performance is due to the excitation of

flexible modes in the 0 -0.3 Hz bandwidth. This in turn induces oscillatory motion as can be seen from Figures 7.10 and 7.13 respectively. In **Case III** and **Case IV** too, the actuator limits are not violated. A discernible feature of CSAS design with a low pass filter, is smooth actuator movements unlike SAS scheme which causes sharp undesirable control movement.

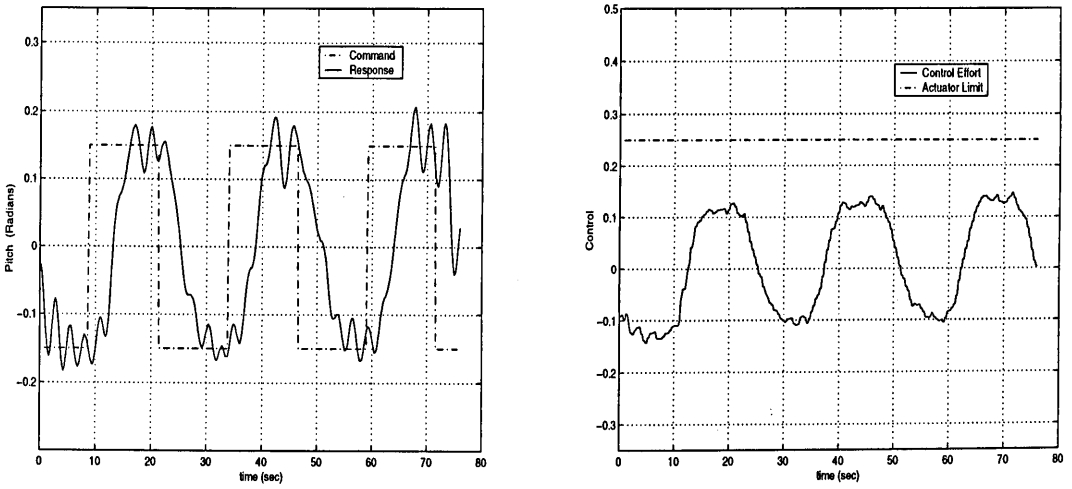

Figure 7.8. CSAS response using LPF (0.1 Hz cut-off) **Q** = **I**, **R** = 100.

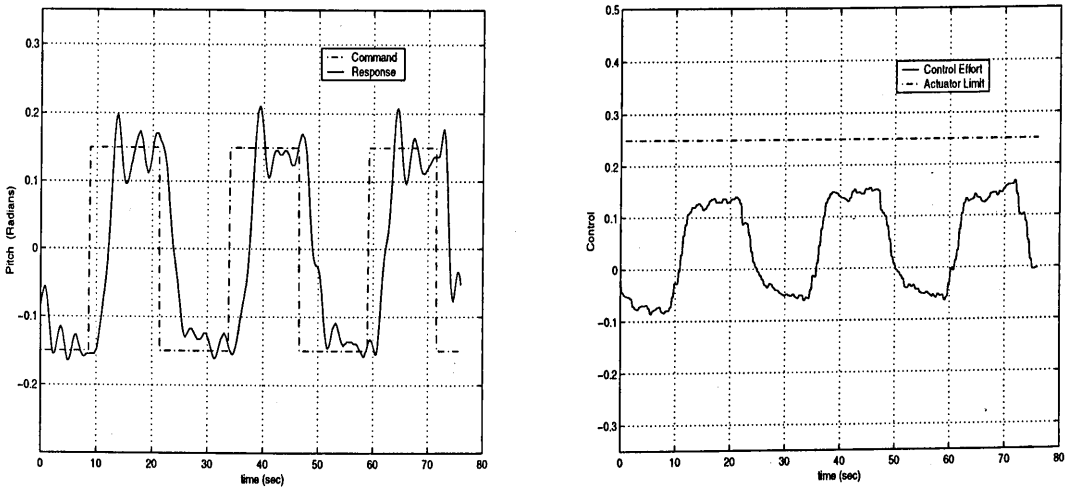

Figure 7.9. CSAS response using LPF (0.2 Hz cut-off) **Q** = **I**, **R** = 100.

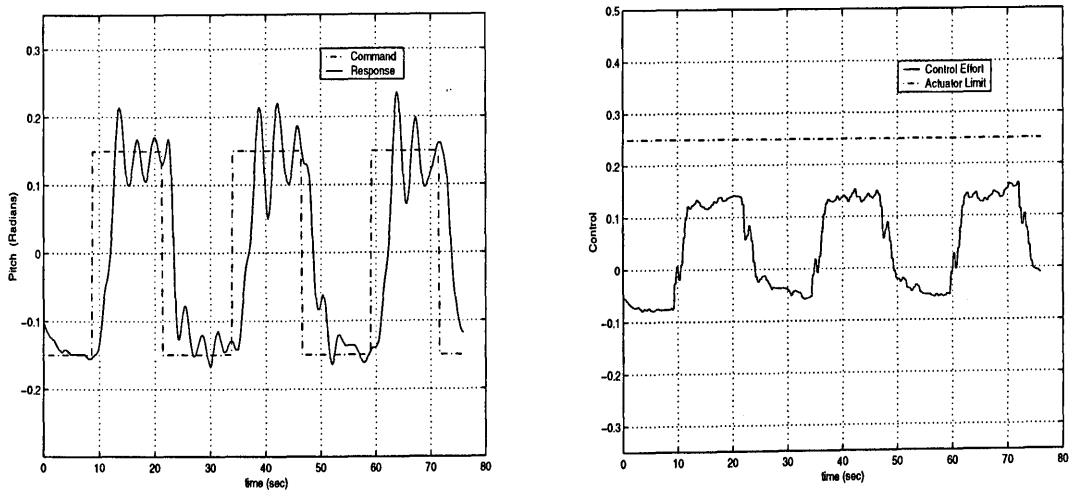

Figure 7.10. CSAS response using LPF (0.3 Hz cut-off) **Q** = **I**, **R** = 100.

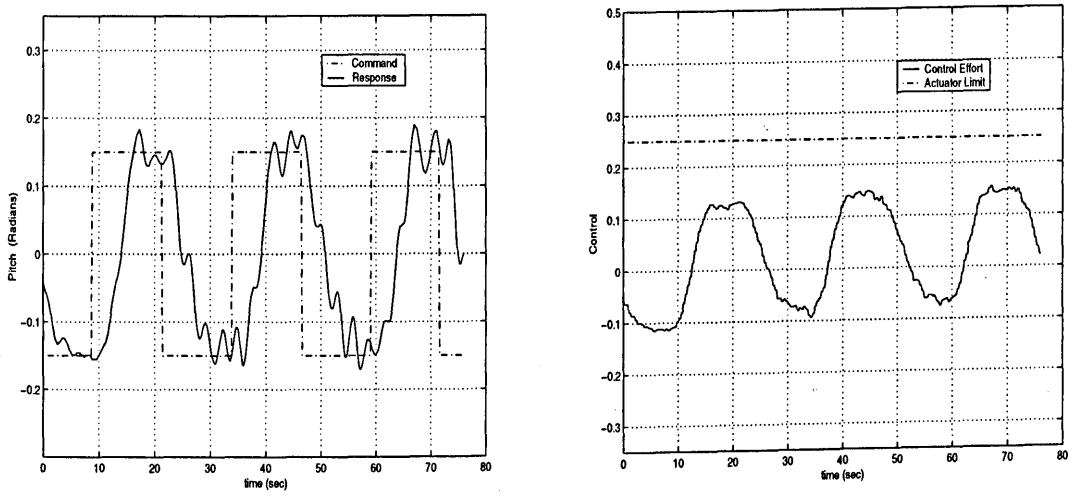

Figure 7.11. CSAS response using LPF (0.1 Hz cut-off) **Q** = **I**, **R** = 125.

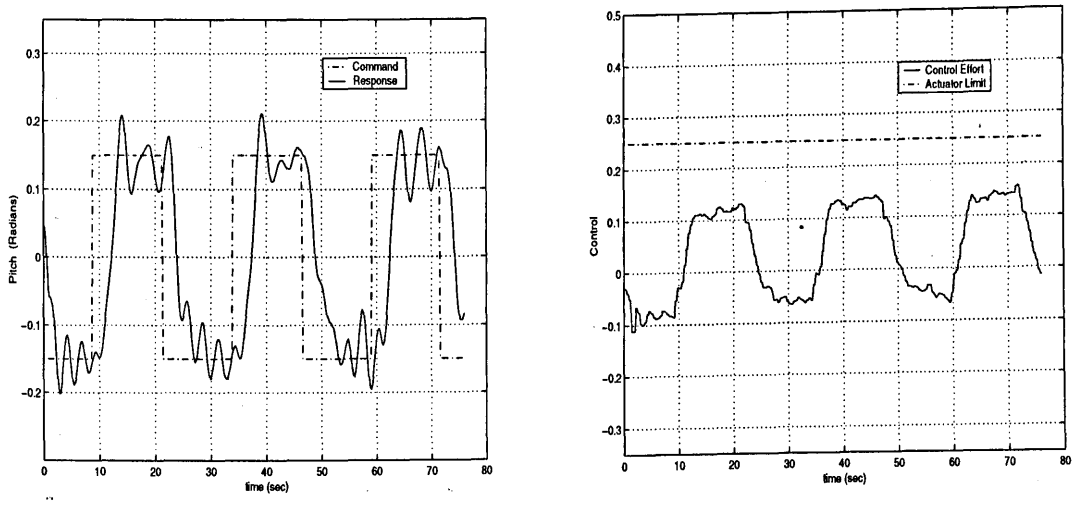

Figure 7.12. CSAS response using LPF (0.2 Hz cut-off) **Q** = **I**, **R** = 125.

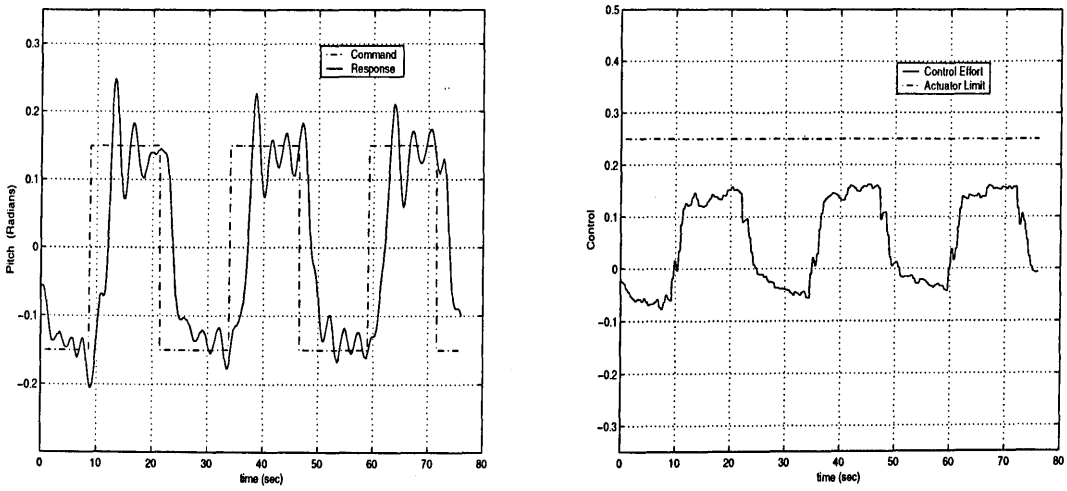

Figure 7.13. CSAS response using LPF (0.3 Hz cut-off) **Q** = **I**, **R** = 125.

7.3.2.2 Band-stop shapped input

From the simulations it is clear that, the Band-stop filter (BSF) does not yield acceptable results. Nevertheless, for completness its capability is examined. Analogous to LPF design, a second order digital Butterworth filter is utilised to investigate the CSAS behaviour with a band-stop filtered square wave command input.

In this section a BSF with a centre frequency (CF) of 0.34 Hz with a bandwidth of 0.2 Hz is selected. Recall that the 0.34 Hz corresponds to the main resonant mode of the TRMS. The response for the three cases using this filter is depicted in Figures 7.14, 7.15 and 7.16 respectively. The TRMS tracking capability for **Case I** and **Case III,** is poor with high overshoot, long settling duration's and inadequate control on the negative side of the reference trajectory. For **Case IV,** response is slightly better. In all the three cases however, control energy requirement is high. Sharp control movement is also noted in all the cases, which again is unacceptable.

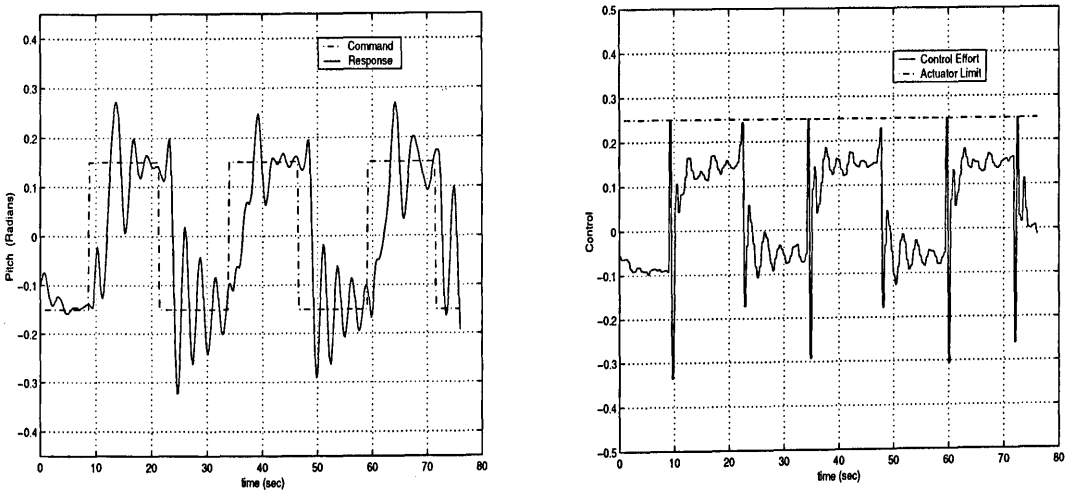

Figure 7.14. CSAS response using BSF (CF 0.34 Hz) **Q** = **I**, **R** = 75.

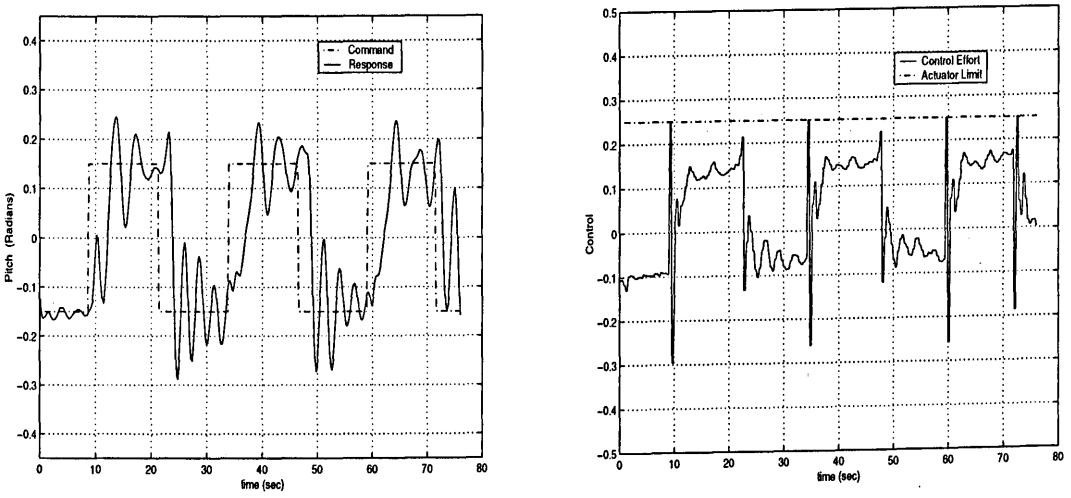

Figure 7.15. CSAS response using BSF (CF 0.34 Hz) **Q** = **I**, **R** = 100.

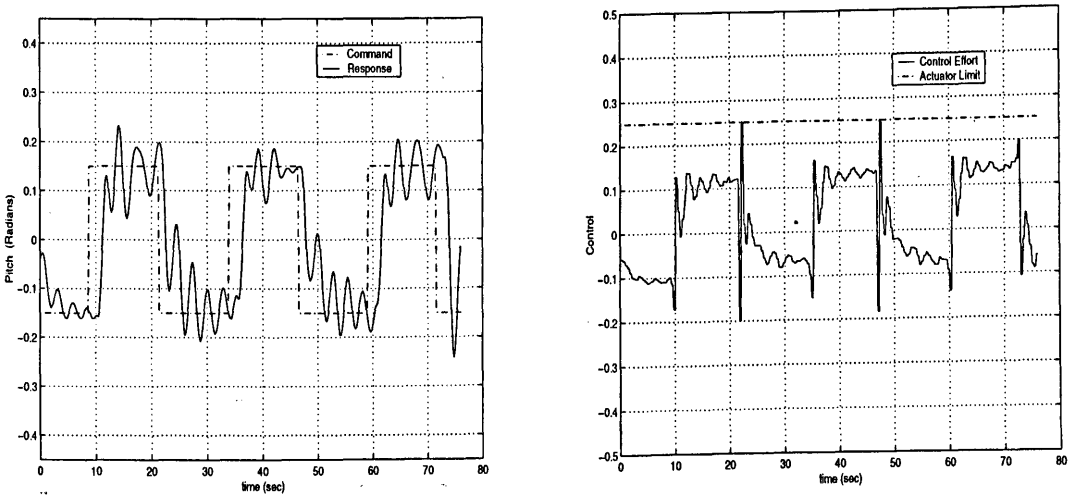

Figure 7.16. CSAS response using BSF (CF 0.34 Hz) **Q** = **I**, **R** = 125.

7.4 Robustness to disturbance

Robustness to external disturbance, such as wind gust, is also highly desirable for the TRMS application. The disturbance rejection capability of the controller is tested by applying a disturbance to the main body. The results are presented in Figures 7.17 to 7.19. for the three different controllers. The disturbance was applied at around 18-20 seconds interval, which is discernible by a sharp TRMS response from an early steady state condition. The moment disturbing force is applied, the controller activity is increased as can be seen from the control profiles of these plots. The controller rejects the applied disturbance and reverts back to its original equilibrium state. Notice, the oscillatory TRMS behaviour in all figures even in steady state before the disturbance is applied.

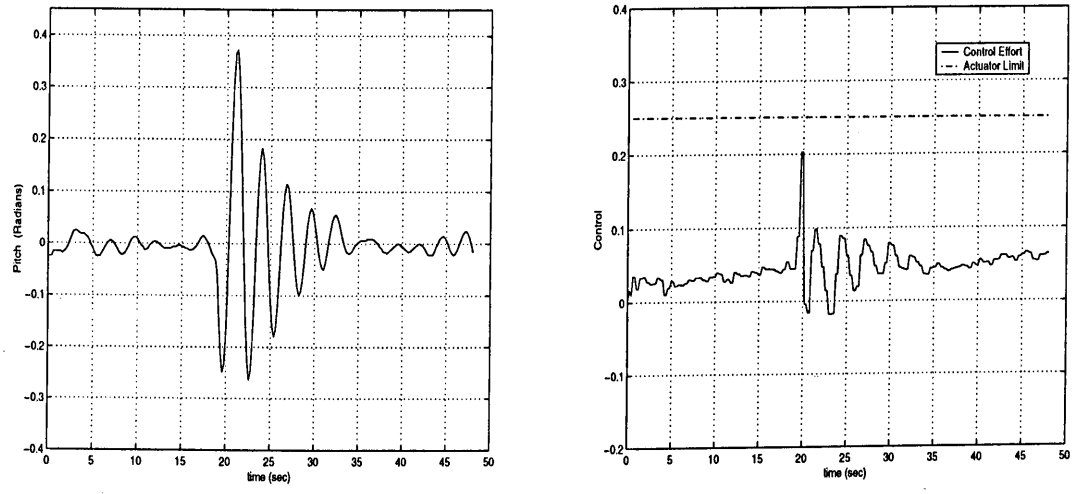

Figure 7.17. Disturbance rejection for **Q** = **I**, **R** = 75.

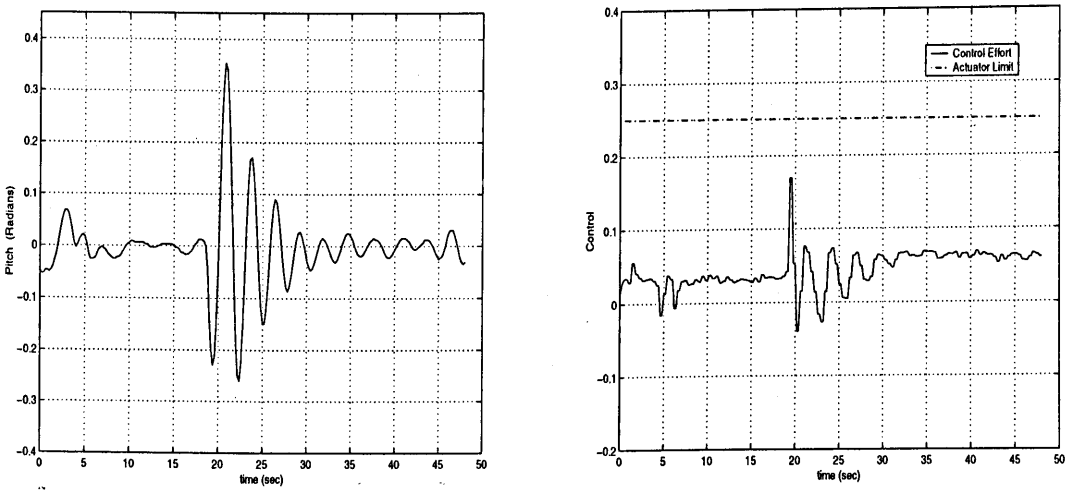

Figure 7.18. Disturbance rejection for **Q** = **I**, **R** = 100.

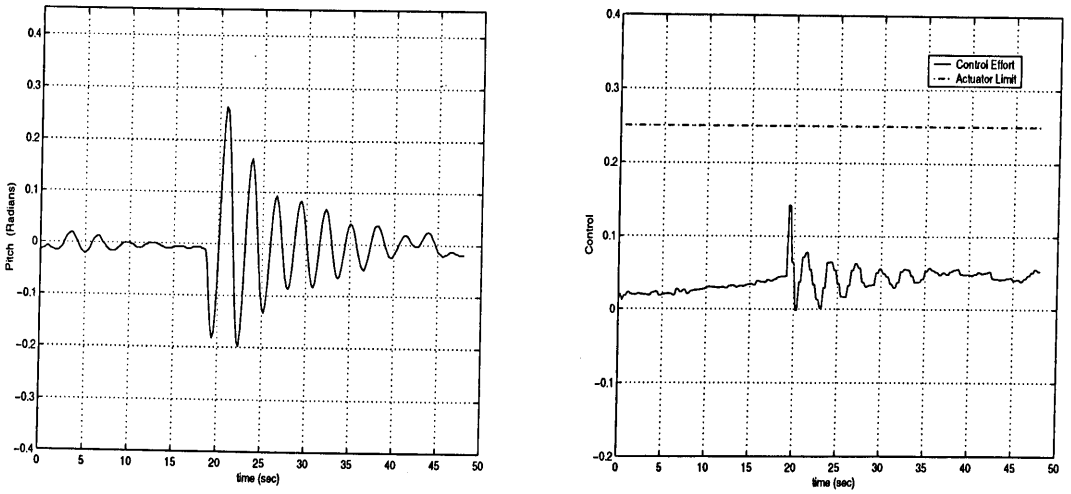

Figure 7.19. Disturbance rejection for **Q** = **I**, **R** = 125.

7.5 Concluding remarks

The SAS and CSAS control schemes developed in the previous chapter and tested in the simulation environment have been implemented. SAS results for **Case I** were found to be below par as compared to the simulation study. **Case II**, could not be implemented due suspected slower estimator poles. Two additional cases were designed in search of better performance than those obtained by **Case I**. The SAS scheme for **Case I** and **Case III** appears to be almost identical, where as **Case IV**, yields best result. An objectionable feature of SAS structure is the sharp control requirement which is detrimental to the system operational life. Therefore, even though **Case IV** of SAS scheme gives good time domain performance, a close scrutiny of the actuator profile reveals sharp control movements. As pointed out, this feature is undesirable.

Very identical and acceptable results are noticed for CSAS with 0.2 Hz cut-off LPF in all cases, without saturating the actuator limits. As was the case in the simulation study, BSF performance was found to be unacceptable for all cases. Finally, all cases demonstrated reasonable disturbance rejection characteristic/property when subjected to an external force. It is important to notice that, due to very sensitive and oscillatory nature of the TRMS even in steady state mode, response profiles are found to have occasional sharp peaks and mild oscillations. Note that, the successful implementation of the controller also validates the accuracy of the model obtained in Chapter 3.

Sampling period selection is an important design criteria for modelling as well as for control application. Therefore, successful execution of controller further corroborates the rationale of sampling period choice.

Chapter 8

Conclusions and future work

8.1 Conclusion

Research interest in innovative air vehicles or new generation, such as unmanned air vehicles (UAV's), oblique wing aircraft configurations, tilt rotor, tilt wing, delta-wing, canard, X-wing and tilt body is rapidly growing. There is also a small but growing literature on laboratory platforms simulating complex aircraft manoeuvres and problems. The interest stems from the fact that such air vehicles are highly agile, stealthy, multi-purpose and capable of executing different tasks such as surveillance, aerial mapping and inspection, which is beyond the domain of their conventional counterparts. These new generation air vehicles have presented a variety of unprecedented challenges and opportunities to aerodynamicists and control engineers.

In this research a laboratory platform which has 2 degrees of freedom, the Twin Rotor MIMO System has been investigated. Although, the TRMS does not fly, it has a striking similarity with a helicopter, such as system nonlinearities and cross-coupled modes. The TRMS therefore, can be viewed as an unconventional and complex "air vehicle" and possesses formidable challenges in modelling, control design and analysis and implementation. These issues have been addressed in this work.

Reasonable linear system models are essential for controller design and nonlinear models for subsequent controller evaluation. In this research, a black-box system modelling was adopted to achieve a fairly good system representation. Linear models have been obtained for both, 1 and 2 DOF TRMS with no *a priori* knowledge of plant model order or parameters providing any insight into plants physical characteristics. Initially, a 1 DOF SISO plant model was obtained, then the concept was extended to a 2 DOF MIMO plant. The modelling of a MIMO system is a non-trivial task and in this research a systematic methodology has been developed to model the 2 DOF TRMS.

The difficulty in the modelling procedure for the two input two output system is compounded due to the presence of cross-coupling between the planes of motion. The coupled nature is also a typical characteristic of helicopters. The identified models have been exhaustively validated using time and frequency domain tests in order to instil confidence in the models for their subsequent use in the controller design. For the MIMO plant, coherence analysis has also been used to detect system nonlinearities and the degree of coupling between the various channels. The coherence metric is often employed in helicopter modelling procedure [22]. The modelling procedure adopted is suitable for a class of new generation air vehicles whose dynamics are not well understood or difficult to model from first principles. The approach presented here is an important contribution of this thesis. The identified models include the rigid as well as the flexible plant dynamics.

Vibrations due to random excitation of structures are common phenomena experienced by large space structures with flexible appendages, ships, flexible aircraft and missiles. Although flexible structures are desirable, the vibrations are not. These vibrations may cause discomfort to passengers and degrade system performance. Vibration suppression can be accomplished via active, passive or hybrid active and passive means. Passive treatment is essential but is limited in rendering the desired accuracy. Hence, active control is needed. The modelling exercise for the TRMS revealed the presence of resonant system modes which are responsible for inducing unwanted vibrations during, and at the end of, system manoeuvres. In this research, open-loop, closed-loop and combined open and closed-loop strategies have been investigated to address this problem. Open-loop control methods have been developed based on the identification of the resonant modes of the TRMS. These have been detected through the analysis of the plant spectral responses and the modelling process. Low pass and band-stop filters have been developed to shape the command signals. This method ensures that the system does not experience the undesirable resonant eigen-frequencies, thereby preventing the excitation of vibrational modes. The effectiveness of this concept has been demonstrated on the TRMS rig for 1 and 2 DOF motion, with significant reduction in vibration. This is evident from smooth time domain responses as well as from the attenuated resonant modes in the frequency domain. The band-stop filter is found to be effective in the selective removal of energy from the input signal corresponding to significant dynamic modes, thereby retaining the maximum amount of energy in the input signal. On the contrary, if the number of closely spaced vibration modes contribute to the system vibration, low pass filtered inputs are recommended.

Once the controller has been designed using the linear system model, its performance is often gauged in a simulation environment using a nonlinear plant model. This is a common practise in the aerospace industry. To study the performance of next generation air vehicles researchers are increasingly relying on nonlinear modelling and control techniques. Therefore, a nonlinear plant model is essential for predicting the system behaviour accurately in order to evaluate the controlled system performance, as well as for controlling a highly nonlinear plant by the dynamic inversion control method. In this research, neural networks were utilised to obtain the nonlinear system model. Unlike linear system identification, nonlinear techniques for modelling require special excitation signals, rich both in frequency and amplitude as well as higher order correlation tests for model validation. An RBF based NN model was identified for the 1 DOF plant. The nonlinear modelling method adopted in this work is appropriate for modelling complex new generation highly agile air platforms with significant nonlinearities. The main aim of NN based modelling has been to achieve a highly accurate model. It has been noted, however, that the nonlinear model is only slightly better than the linear 1 DOF model. For this reason, the nonlinear model is not incorporated in the controller evaluation, rather the linear model is used for simplicity. However, the utility of the nonlinear model cannot be precluded in 2 DOF controller analysis, in particular for the $u1 \rightarrow y2$ channel that exhibits nonlinear behaviour. Hence, the RBF model will be of benefit while analysing the controller performance for this channel.

In addition to vibration attenuation, it is also desirable to achieve other performance criteria such as command tracking, disturbance rejection, fast rise time and robustness to modelling errors. These objectives cannot be achieved by open-loop mechanisms alone, thus closed-loop strategies have also been investigated. An inner feedback LQG compensator was initially designed and analysed in the simulation environment for the 1 DOF TRMS, using the identified system model. This feedback mechanism referred to as *Stability Augmentation System (SAS)* demonstrates good tracking capabilities but requires high control effort and has inadequate authority over residual system vibrations. These problems were resolved by further augmenting the system with a command path prefilter. The combined feedforward and feedback compensator is known as the *Command and Stability Augmentation System (CSAS)* and satisfies the performance objectives and obeys the actuator constraint.

Finally, the crucial test for any control design is the implementation. The *SAS* and *CSAS* control schemes developed in this work here, have been evaluated on the TRMS test rig. One of the controllers faired poorly as compared to the simulation runs for the SAS scheme. While the other failed due to the slow estimator poles, hence could not be evaluated. Therefore, two additional controller were designed with a larger penalty on the control in search of better performance. Implementation of the new controllers showed much improved results. An important drawback of the SAS scheme is the sharp or abrubt control requirement which eventually could lead to mechanical wear and tear of the plant. On the other hand quite similar and acceptable results are observed for the CSAS scheme with 0.1 and 0.2 Hz cut-off low-pass filter in all cases, without saturating the actuator limits. A desirable feature of this scheme being the smooth control movement. With the CSAS, performance objectives are realised in a fewer control design iterations as opposed to SAS scheme. This is another advantage of the CSAS strategy. Analogous to the simulation study, band stop filter performance was unacceptable, however, this was investigated for completeness. Robustness to external disturbance such as wind gust has also been demonstrated with an acceptable disturbance rejection capability.

This research has presented a black-box approach to model the TRMS. The method is generic and provides a novel alternative to model a class of unconventional air vehicles [90-92]. A similar scheme is proposed to derive nonlinear models for highly manoeuvrable air platforms [93]. Further, this work also presented approaches to effectively deal with undesirable flexible dynamics in modern systems [94,95]. The presence or inclusion of flexible dynamics leads to higher order system models, which renders the control design difficult. Since, it is not practical to measure all the states of high order systems, therefore, estimator based optimal control has been shown to be an effective choice for the TRMS and similar system [96].

8.2 Suggestions for future work

In this research the SISO control design has been investigated, an obvious extension is therefore, the MIMO LQG controller design. A 2 DOF autopilot to control pitch and the yaw plane would involve the decoupling objective of the $u1 \rightarrow y1$ channel. It should be fairly straight forward to accomplish this design.

Further work on the nonlinear modelling of a 2 DOF TRMS would be useful. In particular for the *u1* → *y2* channel, which exhibits nonlinear behaviour. As pointed out earlier, this would aid in contoller performance evaluation for this channel.

An interesting development of this work would be to study the roll control of the TRMS. This will necessitate modification of the TRMS rig to provide an additional degree of freedom for the roll movement. The modified TRMS would then mimic the hover mode for a vertical take off and landing (VTOL) type aircraft. This is a non trivial problem and has attracted considerable attention [32,78,81]. The design objectives would then be roll as well as pitch and yaw control.

In order to control a physical system, a plant model is often required and the modelling invariably involves approximation of the real system. Also, the real system undergoes degradation leading to parameter variations and the system is also acted upon by environmental disturbances. Recent robust control design methods, such as H-∞ and μ-synthesis, are capable of tolerating such levels of uncertainty. Robust control methods address the issue of robustness explicitly in the design formulation. Since, the TRMS is very sensitive to external disturbances, robust control could be an attractive alternate proposition.

Reconfiguration is highly desirable in many advanced systems such as advanced tactical fighters, adaptive structures and autonomous robots. The main motivation of reconfiguration is greater survivability and controllability, attained through the ability of the feedback system to reorganise itself in the presence of actuator/sensor failures and surface damage. Two main approaches can be distinguished for plant control reconfiguration. The first is based on the concept of failure detection and identification. This approach works well in restricted cases, but suffers from significant drawbacks. As the number of failures grows, it becomes increasingly difficult and time consuming to carry out the detection and classification. The second consists of identifying the dynamic behaviour of the system in real-time and designing a controller automatically. Because such an approach does not rely on failure classification, it is expected that the resulting system would tolerate a larger class of failures. Adaptive control such as Model Reference Adaptive Control (MRAC), both indirect and direct methods, can be used for reconfiguring control. The TRMS rig is an ideal platform upon which the reconfigurable control strategies can be tested.

Appendix 1

A.1 Description of the toolbox functions

All functions desired for communication between the RTK and Matlab environment have the following general form:

ReturnValue = hl_call(FunctionName, [Argument])

where:

ReturnValue- value returned by the function,

hl_call- name of the DLL library responsible for the communication,

FunctionName- name of the desired operation, string format.

Argument- argument passed to the *hl_call* function (optional).

GetBaseAddress

Purpose: Get the base address of the PCL-812 board.

Synopsis: *BaseAddr = hl_call('GetBaseAddress').*

Description: The function is called to obtain the base address of PCL-812 interface board. If the based address of PCL-812 board is set to zero the RTK generates dummy data. This mode is useful to test communication between the RTK and Matlab without using external hardware.

GetSampleTime

Purpose: Get the basic sampling time.

Synopsis: *SamplT = hl_call('GetSampleTime').*

Description: The function returns the period of the basic RTK clock. The period is given in seconds.

SetSampleTime

Purpose: Set the basic clock.

Synopsis: *hl_call('SetSampleTime', Period).*

Description: The function sets the basic clock of RTK. The sampling period of A/D converter is set by this function. The controller output rate (D/A) can be equal to or greater than the basic clock frequency. The *Period* parameter must be in the range from 0.001s to 32.767s. The lower bound depends on the hardware configurations. The resolution is 0.001s.

GetHistory

Purpose: Get content of the internal RTK buffer.

Synopsis: *hl_call('GetHistory').*

Description: The function returns the *Hist* matrix containing the history of an experiment and set the buffer to zero. *Hist* matrix contains various input-ouput measurements.

References

[1] http://fourier.vuse.vanderbilt.edu/cim/projects/flying.htm.

[2] Harvey B (1997). Micro unmanned aerial vehicles. Intelligent Automation Inc. USA.

[3] Warwick G (2000). Agents for change. Flight International, UK, July, pp. 151-153.

[4] Long M E (1999). Mars on earth. National geographic, USA, July, pp. 36-51.

[5] http:// www. aerosonde. com.

[6] Ting T (1999). Bridging the gap between the theory and practice of control: Aerospace perspective. IEEE Control Systems, Vol. 19, No.6, pp.45-48.

[7] http://avdil.gtri.gatech.edu/RCM/RCM/DroneProject.html.

[8] Freewing aerial robotics corp. (1997). Company R & D history. College station, Texas, USA. www.freewing.com.

[9] Howard R M and Kaminer I (1995). Survey of unmanned air vehicles. In *Proc. American Control Conference*, Seattle, Washington, USA, pp. 2950-2953.

[10] Tokhi M O and Azad A K M (1995). Active vibration suppression of flexible manipulator system open-loop control methods. *International Journal of Active Control, 1, (1)*, pp. 15-43.

[11] Poerwanto H (1998). *Dynamic simulation and control of flexible manipulators systems*, Ph.D thesis, Department of Automatic Control and Systems Engineering, The University of Sheffield, UK.

[12] Singer N C and Seering W P (1990). Preshaping command inputs to reduce system vibration. ASME *Journal of Dynamics Systems, Measurement, and Control,* vol 112, pp. 76-81.

[13] Dimitry G and Vukovich G (1998). Nonlinear input shaping control of flexible spacecraft reorientation maneuver. *Journal of Guidance, Control, and Dynamics,* Vol. 21, No. 2, pp.264-269.

[14] Suk J, Kim Y and Bang H (1998). Experimental evaluation of the torque-shaping method for slew maneuver of flexible space structures. *Journal of Guidance, Control, and Dynamics,* Vol. 21, No. 6, pp.817-822.

[15] Teague E H, How J P, and Parkinson B W (1998). Control of flexible structures using GPS : methods and experimental results. *Journal of Guidance, Control, and Dynamics,* Vol. 21, No. 5, pp.673-683.

[16] Livet T, Kubica F and Magni J F (1995). Robust flight control design with respect to delays, control efficiencies and flexible modes. *Control Engineering Practice,* Vol. 3, No.10, pp.1373-1384.

[17] Livet T, Fath D and Kubica F (1996). Robust autopilot design for a highly flexible aircraft. *IFAC'96,* San Francisco, CA, USA. Preprints, Vol. P, pp 279-284.

[18] Karkoub M, Balas G, Tamma K and Donath M (2000). Robust control of flexible manipulators via μ-synthesis . *Control Engineering Practice,* Vol. 8, pp. 725-734.

[19] Grewal A and Modi V J (2000). Multibody dynamics and robust control of flexible spacecraft. *IEEE Trans. on Aerospace and Electronics Systems,* Vol. 36, No. 2, pp. 491-500.

[20] George K K and Bhat M S (1998). Two-degree-of-freedom H-∞ robust controller for a flexible missile. *Journal of Guidance, Control, and Dynamics,* Vol. 21, No. 3, pp.518-520.

[21] Feedback Instruments Ltd (1996). Twin rotor MIMO system. Manual 33-007-0. Sussex, UK.

[22] Patton R, Miles M and Taylor P (1993). Design and application of test signals for helicopter model validation in the frequency domain. In Godfrey, K. (Ed.), Perturbation Signals For System Identification. Prentice Hall, UK, pp 298-320.

[23] AGARD (1974). *Methods for aircraft state and parameter identification* : AGARD, NASA Research centre, Hampton, Virginia, U.S.A.

[24] Bruce P D, Silva J E and Kellet F M G (1998). Maximum likelihood identification of linear aircraft dynamics using a hybrid genetic algorithm. *In Proceedings of AIAA 36th Aerospaec Sciences Conference,* Reno, Nevada, USA.

[25] Kaminer I Pascoal, A Hallberg E and Silvestre C (1998). Trajectory tracking for autonomous vehicles: an integrated approach to guidance and control. *AIAA, Journal of Guidance, Control, and Dynamics,* 1998, vol 21, 29-38.

[26] Hallberg E, Kaminer I and Pascoal A (1999). Development of a flight test system for unmanned air vehicles. *IEEE Control Systems,* vol.19, No.1, pp. 55-65.

[27] Atkins E M, Miller R H, Pelt T V, Shaw K D, Ribbens W B, Washabaugh P D and Bernstein D S (1998). SOLUS: An autonomous aircraft for flight control and trajectory planning research. *In proceedings of the American Control Conference*, Philadelphia, USA, pp. 689-693.

[28] Linehan R D, Burnham K J and James D J G (1996). 4-Dimensional control of a remotely piloted vehicle. *In Proceedings of United Kingdom Automatic Control Conferenece*, Exeter, UK, pp. 770-775.

[29] Van Nieuwstadt M J and Murray R M (1998). Rapid hover-to-forward-flight transitions for a thrust-vectored aircraft. *AIAA, Journal of Guidance, Control, and Dynamics,* vol. 21, 93-100.

[30] Morris J C, Van Nieuwstadt M J and Pascale B (1994). Identification and control of a model helicopter in hover. *In proceedings of the American Control Conference,* Baltimore, vol. 2, pp.1238-1242.

[31] Houston S S (1998). Identification of autogyro longitudinal stability and control characteristics. *AIAA, Journal of Guidance, Control, and Dynamics,* vol. 21, 391-399.

[32] Werner H and Meister T (1999). Robust control of a laboratory aircraft model via fast output sampling. *Control Engineering Practice,* vol. 7, 305-313.

[33] Blythe P W and Chamitoff G (1995). Estimation of aircrafts aerodynamic coefficients using recurrent neural networks. *In Proc. Second Pacific International Conference on Aerospace Science and Technology*, Australia.

[34] Haley P and Soloway D (1997). Generalized predictive control for active flutter suppression. *IEEE Control Systems*, pp. 64-70.

[35] Ljung L (1987). System identification : theory for the user. Prentice Hall International.

[36] Wellstead P E and Zarrop M B (1991). Self-tuning systems: control and signal processing. John Wiley & Sons.UK. pp.126-128.

[37] Soderstrom T and Stoica P (1989). System identification. Prentice Hall.

[38] Bendat J S and Piersol, A. G. (1980). Engineering application of correlation and spectral analysis. John-Wiley & Sons, 83-84.

[39] Ljung L (1991). System Identification Toolbox. The Math Works Inc, NJ, USA.

[40] Nishimura H and Kojima A (1999). Seismic isolation control for a building like structure.

IEEE Control Systems, vol.19, No.6, pp. 38-44.

[41] Agarwala R, Selahattin O and Mohammed F (2000). Active vibration control of a multi-degree -of-freedom structure by the use of direct model reference adaptive control. *In Proceedings of the American Control Conference,* Chicago, Illinois, USA.

[42] Aspinwall D M (1980). Acceleration profiles for minimising residual response. *ASME Journal of Dynamic Systems, Measurement and Control,* **102**, (1), pp. 3-6.

[43] Suk J Y, Kim, and Bang H (1998). Experimental evaluation of the torque-shaping method for slew maneuver of flexible space structures. *Journal of Guidance, Control, and Dynamics,* Vol. 21, No. 6, pp.817-822.

[44] Meckl P H and Seering W P (1990). Experimental evaluation of shaped inputs to reduce vibration of a cartesian robot. *Trans. of the ASME Journal of Dynamic Systems, Measurement and Control,* Vol. 112, No. 6, pp. 159-165.

[45] Singer N C and Seering W P (1990). Preshaping command inputs to reduce system vibration. ASME *Journal of Dynamics Systems, Measurement, and Control,* vol 112, pp 76-81.

[46] Watkins J and Yurkovich S (1992). Input shaping controllers for slewing flexible structures. *In Proceedings of the first conference on Control Applications,* Dayton, Ohio, USA, pp. 188-193.

[47] Tzes A. and Yurkovich S (1993). An adaptive input shaping control scheme for vibration suppression in slewing flexible structures. *The IEEE Transactions on Control Systems Technology*, **1**, (2), pp. 114-121.

[48] Banerjee A K and Singhose W E (1998). Command shaping in tracking control of a two-link flexible robot. *Journal of Guidance, Control, and Dynamics,* Vol. 21, No. 6, pp.1012-1015.

[49] Gorinevvsky D and Vukovich G (1996). Control of flexible spacecraft nonlinear approximation of input shape dependence on reorientation maneuver parameters. In *IFAC'96,* San Francisco, CA, USA, Preprints, Vol. P, pp. 285-290.

[50] Tokhi M O, Shaheed M H and Poerwanto H (2000). Adaptive neuro-inverse-dynamic active vibration control of a flexible manipulator. In *Proceedings of the Mechatronics-2000,* Atlanta, USA.

[51] Williams C S (1986). Designing digital filters. Prentice Hall, NJ, USA.

[52] Dwight H B (1957). Tables and integrals and other mathematical data, 3rd Ed., Macmillan, New York.

[53] Kim B S and Calise A J (1998). Nonlinear flight control using neural networks. *Journal of Guidance, Control, and Dynamics,* Vol. 20, No. 1, pp.26-33.

[54] Lyshevski S E (2000). Identification of nonlinear flight dynamics: theory and practice. *IEEE Trans. on Aerospace and Electronics Systems,* Vol. 36, No. 2, pp.383-392.

[55] Bruce P D and Kellet M G (2000). Modelling and identification of non-linear aerodynamic functions using b-splines. In *Proc. Instn. of Mech. Engrs.* Vol 214, Part G, pp. 27-40.

[56] Billings S A and Voon W S F (1986). Correlation based validity tests for nonlinear models. *Int. Journal of Control,* Vol. 44, No. 1, pp. 235-244.

[57] Leontaritis I J and Billings S A (1985). Input-output parametric models for nonlinear systems part 1: deterministic nonlinear systems. *Int. Journal of Control* 41(2), pp. 303-328.

[58] Chen S, Cowan C F N and Grant P M (1991). Orthogonal least squares learning algorithm for radial basis function networks. *IEEE Trans. on Neural Networks,* Vol.2, No. 2, pp. 302-309.

[59] Bishop C M (1995). Neural networks for pattern recognition. Clarendon press, Oxford.

[60] M. T Hagan, Demuth H B and Beale M (1993). The Neural Networks Toolbox, Mathworks Inc. USA.

[61] Dougherty H, Tompetrini K, Levinthal J and Nurre G (1982). Space telescope pointing control system. *Journal of Guidance, Control, and Dynamics,* Vol. 5, No. 4, pp. 403-409, 1982.

[62] Franklin G F, Powell J D and Emami-Naeini A (1988). Feedback control of dynamic systems. Addison-Wesley, USA, pp. 447-473.

[63] Azad, A K M (1994). *Analysis and design of control mechanisms for flexible manipulator systems,* PhD thesis, Department of Automatic Control and Systems Engineering, The University of Sheffield, UK.

[64] Ozimina C D, Tayman S K and Chaplin H E (1995). Flight control system design for a small unmanned aircraft. In *Proc. American Control Conference*, Seattle, Washington, USA, pp 2964-2969.

[65] Hansen T, Kahn A, Kannan S, Peon R and Tapia F (1997). Georgia Tech entry for the 1997 international aerial robotics competition. *In Proc. AUVSI 97.*

[66] Teague E H, How J P, and Parkinson B W (1998). Control of flexible structures using gps: methods and experimental results. *Journal of Guidance, Control, and Dynamics,* Vol. 21, No. 5, pp.673-683.

[67] Blight J D, Dailey R L and Gangsaas D (1996). Practical control law design for aircraft using multivariable techniques. In Tischler M.B (Ed.), Advances in Aircraft Flight Control, pp 231-267.

[68] Boyle D P and Chamitoff G E (1999). Automous maneuver tracking for self-piloted vehicles. *Journal of Guidance, Control, and Dynamics,* Vol. 22, No. 1, pp. 58-67.

[69] Bossi J A and Langehough M A (1988). Multivariable autopilot designs for a bank-to-turn missile. In *Proc. American Control Conference*, Atlanta, Georgia, USA, pp 567-572.

[70] Henrichfreise H, Moritz W and Siemensmeyer H (1987). Control of a light, elastic manipulation device. In *Proc. of the Conference on Applied Motion Control,* Minneapolis, USA.

[71] Kosut R L, Salzwedel H and Emami-Naeini A (1983). Robust control of flexible spacecraft. *Journal of Guidance, Control, and Dynamics,* Vol. 6, No. 2, pp. 104-111.

[72] Langehough M A and Simons F E (1988). 6 DOF simulation analysis for a digital bank-to-turn autopilot. In *Proc. American Control Conference*, Atlanta, Georgia, USA, pp.573-578

[73] Lin C F (1994). Advanced control systems design. Prentice Hall Inc. USA.

[74] Rubio F R and Aracil J (1997). Designed of a combined tracking control systems. *Control Engineering Practice,* Vol. 5, No. 1 pp.23-31.

[75] Sheperd C L and Valavani L (1988).Autopilot design for bank-to-turn missiles using LQG/LTR methodology. In *Proc. American Control Conference*, Atlanta, Georgia, USA Vol. 1.

[76] Sutton R P, Halikias G D, Plummer A R and Wilson D A (1999). Modelling and H-∞ control of a single-link flexible manipulator. In *Proc. Instn. Mech Engrs,* Vol 213 Part I, pp. 85-102.

[77] Hyde R and Glover K (1993). The application of scheduled H-∞ controllers to a VSTOL aircraft. *IEEE Transactions on Automatic Control,* Vol 38, pp. 1021-1039.

[78] Sivashankar N, Kaminer I and Kuechenmeister D (1994). Design, analysis and hardware-in-the-loop simulation of MIMO controller for a VTOL unmanned aerial vehicle using synthesis. In *Proc. American Control Conference*, Baltimoore, Maryland, USA, pp 2506-2510.

[79] Schumacher C and Khargonekar P (1998). Stability analysis of a missile control system with a dynamic inversion controller. *Journal of Guidance, Control, and Dynamics,* Vol. 21, No. 3, pp. 508-515.

[80] Littleboy D M and Smith P R (1998). Using bifurcation methods to aid nonlinear dynamic inversion control law design. *Journal of Guidance, Control, and Dynamics,* Vol. 21, No. 4, pp. 632-638.

[81] Kantner M, Bodenheimer B, Bendotti P and Murray R M (1995). An experimental comparison of controllers for a vecored thrust, ducted fan engine. In *Proc. American Control Conference*, Seattle, Washington, USA.

[82] Doyle J C and Stein G (1981). Multivariable feedback design: concepts for a classical /modern synthesis. *IEEE Transactions on Automatic Control*, Vol 26, No. 1, pp. 4-16.

[83] Skogestad S and Postlethwaite I (1996). Multivariable feedback control, analysis and design. Wiley, UK.

[84] Ogata K (1995). Discrete-time control systems. Prentice Hall, NJ, USA.

[85] Franklin G, Powell J D and Workman M (1998). Digital control of dynamic systems. Addison-Wesley, USA.

[86] Friedland B (1987). Control system design, McGraw-Hill. N.Y., USA.

[87] Bryson A E and Ho Y C (1975). Applied optimal control. Halsted Press, USA.

[88] Craig I K and Henning R G D (2000). Evaluation of advanced industrial control projects: a framework for determining economic benefits. *Control Engineering Practice,* Vol. 5, pp.769-780.

[89] Pelegrin M J (1987). A new complement for air and spacecraft: a man/a computer. In *Proc. of IFAC Congress on Automatic Control*, Munich, Germany.

[90] Ahmad S M, Chipperfield A J and Tokhi M O (1999). System identification of a one degree-of-freedom twin rotor Multi-Input Multi-Output system. In *International Conference on Computer and Information Technology (ICCIT' 99)*. SUST, Sylhet, Bangladesh, 3-5 Dec., pp 94-98.

[91] Ahmad S M, Chipperfield A J and Tokhi M O (2000). Parametric modelling and dynamic characterisation of a 2-dof twin rotor MIMO system. IMechE, *Journal of Aerospace Eng.* (to appear).

[92] Ahmad S M, Chipperfield A J and Tokhi M O (2000). Dynamic modelling of a two degree-of-freedom twin rotor Multi-Input Multi-output system. In *Proc. IEE United Kingdom Automatic Control Conference (UKACC '2000)*, Cambridge, UK.

[93] Ahmad S M, Chipperfield A J and Tokhi M O (2000). Nonlinear modelling of a twin rotor MIMO system using Radial Basis Function Networks. In *Proc. IEEE National Aerospace and Electronics Conference (NAECON'2000)*, Dayton, Ohio, USA, 10-12 Oct., pp 313-320.

[94] Ahmad S M, Chipperfield A J and Tokhi M O (2000). Modelling and control of a twin rotor Multi-Input Multi-output system. In *Proc. American Control Conference*, Chicago, IL, USA, pp 1720-1724.

[95] Ahmad S M, Chipperfield A J and Tokhi M O (2000). Dynamic modelling and control of a 2 dof twin rotor Multi-Input Multi-Output system. In *Proc. IEEE Industrial Electronics, Control and Instrumentation Conference (IECON'2000), Nagoya*, Japan, 22-28 Oct. pp 1451-1456.

[96] Ahmad S M, Chipperfield A J and Tokhi M O (2000). Dynamic modelling and optimal control of a twin rotor MIMO system. In *Proc. IEEE National Aerospace and Electronics Conference (NAECON'2000)*, Dayton, Ohio, USA, 10-12 Oct. pp 391-398.